The effect of thermal heat treatment on the corrosion performance of some commercial and advanced magnesium alloys.

Addepalli, Sri Naga Pavan

Swansea University
Prifysgol Abertawe

THE EFFECT OF THERMAL HEAT TREATMENT ON THE CORROSION PERFORMANCE OF SOME COMMERCIAL AND ADVANCED MAGNESIUM ALLOYS

Sri Naga Pavan Addepalli

Supervisors

Dr. Amit Das
Lecturer, MRC
College of Engineering
Swansea University

Dr. Geraint Williams
Lecturer, MRC
College of Engineering
Swansea University

Submitted to the University of Wales
in fulfilment of the requirements for the
Degree of Master of Philosophy

SWANSEA UNIVERSITY

2011

ProQuest LLC.
789 East Eisenhower Parkway
P.O. Box 1346
Ann Arbor, MI 48106 – 1346

ABSTRACT

The research titled "The effect of thermal heat treatment on the corrosion performance of some commercial and advanced magnesium alloys" deals with the use of heat treatment to change the characteristics of some commercial magnesium alloys. The alloys were first subjected to homogeneous solution treatment and quenched in cold water in order to retain the homogeneous state of the material. Then the samples were aged at temperatures as suggested in the literature for different time periods. Their corrosion performance was then assessed using Time lapse photography, Hydrogen evolution experiment and Scanning Vibrating Electrode Technique (SVET). The data obtained from the time lapse photography was assessed using Sigma plot to characterize the corroded rate in terms of area (m^2) over a period of time. The bulk corrosion rates by the amount of hydrogen released was estimated volumetrically over a period of time. Finally the data obtained form the SVET analysis was assessed using Surfer to acquire the local current density rates due to corrosion. From the current density data, the approximate loss of material during SVET was estimated quantitatively. This thesis compares three different magnesium alloys, AZ31, AZ91 and Elektron 21 (E21). It was noticed that heat treatment changed the microstructural characteristics of the alloys which in turn affected the corrosion performance of those alloys. The results show that solution treatment was preferred for AZ31 and Elektron 21 alloy and age hardening for AZ91 alloy. It was also noticed that all the results obtained using various experimental techniques were similar to each other.

DECLARATION

This work has not previously been accepted in substance for any degree and is not being concurrently submitted in candidature for any degree.

Signed .. .. (candidate)

Date ..... 10TH OCTOBER 2011 .....

STATEMENT 1

This thesis is the result of my own investigations, except where otherwise stated. Where correction services have been used, the extent and nature of the correction is clearly marked in a footnote(s).

Other sources are acknowledged by footnotes giving explicit references. A bibliography is appended.

Signed ..... (candidate)

Date ..... 10TH OCTOBER 2011 .....

STATEMENT 2

I hereby give consent for my thesis, if accepted, to be available for photocopying and for inter-library loan, and for the title and summary to be made available to outside organisations.

Signed .... (candidate)

Date ..... 10TH OCTOBER 2011 .....

NB: *Candidates on whose behalf a bar on access has been approved by the University (see Note 7), should use the following version of Statement 2:*

I hereby give consent for my thesis, if accepted, to be available for photocopying and for inter-library loans **after expiry of a bar on access approved by the Swansea University.**

Signed .. .. (candidate)

Date ..... 10TH OCTOBER 2011 .....

CONTENTS

LIST OF FIGURES

LIST OF TABLES

ACKNOWLEDGEMENTS

First of all I would like to thank my supervisor Dr. Amit Das for helping me in completing this thesis. I am greatly indebted to him for all his extensive help, support and patience without which this thesis would not have been possible. He has been my guide and philosopher who supported me during difficult times during my time at Swansea University.

I would like to thank my co-supervisor Dr. Geraint Williams for his help in making me understanding the basic concepts of corrosion. His academic knowledge, inspiration and enthusiasm have helped me solve various academic issues during my time at Swansea. This thesis has been possible because of his supervision and I am grateful for his help during my research studies.

I would like to thank my colleague Richard Grace for his help and support during the early stages of my research studies.

I would also like to thank all my friends and colleagues at Swansea University who have been supportive at all times.

I am grateful to all the Administrators, Secretaries, and Technicians of Materials Research Centre for assisting me in different ways to enable the smooth running of my research.

Lastly, I wish to dedicate this work to my parents. Their never ending love, support, encouragement, and advice during various stages of life have helped me grow up to what I am today.

1. INTRODUCTION

Materials engineering has gained more importance in the last century with development of new range of materials including ceramic and refectory materials, high end light alloys, refined plastics, synthetic fibres and composite materials. Magnesium (Mg), being one of the lightest available metals, has found its place due to its low density and mechanical characteristics. [1] After *Steel* (127.5 million tonnes[1]) and *Aluminium (Al)* (80 million tonnes[1]), Magnesium (700,000 tonnes approx.[1]) is most commonly used in metal structures. It should be noted that magnesium is the seventh most abundant element on Earth's crust (by mass). [2] However the greatest limitation to the use of magnesium is its reactivity with moisture and hence cannot be obtained in its pure form. It corrodes quite readily in certain types of water. With the development of different alloys, there has been tremendous improvement in the mechanical and corrosion properties of magnesium alloys.

1.1 HISTORY OF MAGNESIUM

In 1808 *Sir Humphry Davy* isolated Magnesium. He did electrolysis of a mixture of magnesia and mercuric oxide. It was in 1831 *Antoine Bussy* obtained magnesium in a coherent form. [3] It was only in 1857 that commercial production of magnesium was possible. It was first commercially produced near Paris by *Rousseau.* [1] The principle ores of magnesium are *Dolomite, Magnesite, Brucite,* and *Carnallite.*

Magnesium is a strong reducing agent and has a very high affinity to oxygen. Hence magnesium cannot be extracted by chemical reduction method. Rather it is extracted by electrolysis. Some of the processes which were used to extract magnesium are, [1][3]

- Electrolysis of *Magnesium chloride ($MgCl_2$)* and *Magnesium oxide (MgO)* in salts
- Electrolysis of oxide in a solution form with molten *fluorides*

[1] Source: www.steelonthenet.com/production.html, www.world-aluminium.org/cache/fl0000422.pdf, www.indexmundi.com/en/commodities/minerals/magnesium/magnesium_t8.html

- Reduced directly from oxide form by carbon in an electric arc furnace with *hydrogen (H_2)* atmosphere and redistilled in an inert atmosphere.
- Direct chlorination of *Magnesium oxide*
- The I. G. – MEL Process developed at *Magnesium Elektron Ltd.* in 1936 – an electrolytic process which reuses chlorine in the chlorination stage before electrolysis. The exhaust gas evolved during chlorination is then used to make magnesium chloride solution.
- The *Dow Process* – another electrolytic process where the magnesium chloride solution is the precipitate obtained from agitating magnesium hydroxide with calcium oxide.

Furthering the advancement in technology over the years, there have been considerable changes in the extraction processes with different electrolysis and thermal reduction processes. [3]

Magnesium in the elemental form is highly reactive. It tarnishes quickly on exposure to air. However, it forms a thin oxide layer on its surface and prevents it from tarnishing the metal completely. It can also be noticed that when it is submerged in water, hydrogen bubbles are formed. In the powdered form it is even more reactive and the reaction is much faster with rising temperature. Due to its highly reactive nature both, magnesium and its alloys are highly flammable. [1][3] It burns easily in the powdered form and it becomes very difficult to extinguish the fire as it reacts with *nitrogen (N)* as well as with *carbon di-oxide (CO_2).*

1.2 RECENT DEVELOPMENTS

The 21st century innovation and technologies have made way for material scientists across the globe to look into the properties of light weight magnesium alloys like *AZ31, AZ91, WE43, Elektron21* etc which contain aluminium, zinc, rare earth materials etc. These alloys are primarily used in the transport industry both automotive and aerospace industry due to their low density and light weight. Rare earth materials in small proportions have increased the performance characteristics of these light weight alloys. There has been considerable amount of work carried on a large scale to determine the adaptability of such high end light alloys. However there

still seems to be limitations as these alloys seem to show poor mechanical and corrosion characteristics at higher working temperatures.

1.2.1 IMPACT OF ALLOYING ELEMENTS

Aluminium has been the principle alloying element in a majority of magnesium alloys produced. However the discovery and characterization of rare earth materials, there has been a tremendous change in the characteristics of magnesium alloys. *Zirconium (Zr)* acts as a very good grain refining element [3]. It can be seen that most of the aluminium based magnesium alloys have a few tenths in percentage of *manganese (Mn)*. The presence of manganese in such a combination enhances the corrosion performance of the alloy itself. Zirconium on the other hand helps in maintaining the resistance to loss of tensile properties at room temperature. Cast alloys can be heat treated to obtain attractive tensile properties but show a tendency towards microporosity (small cavities of gases during casting). And the wrought forms are limited to cold formability but are readily hot worked in various ways.

1.2.2 NEW ASSESSMENT TECHNIQUES

Innovations like electron microscopy have helped materials scientist to study the properties of these alloys at microstructural level. Incorporating heat treatment techniques including solution treatment, precipitation hardening (ageing) etc., and comparing the changes in the microstructural properties together with corrosion performance of such alloys helps in studying the behaviour and performance of commercial magnesium alloys at different conditions. There has been considerable amount of work of late to prove that the mechanical and performance characteristics of light magnesium alloys have improved significantly. *Kielbus* [5-6] demonstrates the effect of heat treatment on the microstructure and corrosion properties of Elektron21. Similar works have been reported to bring refinement in other magnesium alloys. With the use of newer technologies like *Scanning Vibrating Electrode Technique (SVET)* (a new electrochemical scanning technique also known as current density scanning) the corrosion performance of these magnesium alloys with various treatments and can be studied further (Refer section 3.4). Thus any significant change due to heat treatment, microstructure and corrosion performance can be monitored more effectively.

1.3 CHARACTERISTICS OF MAGNESIUM ALLOYS

Some interesting facts to be noticed as to why magnesium alloys are preferred to aluminium alloys are as follows

- The low strength to weight ratio of magnesium alloys
- Zirconium based cast/wrought alloys are more preferred in aircraft and missile parts
- Outstanding machinability is a characteristic of magnesium alloys and is welded by inert gas shielded Arc welding.
- With the presence of *thorium (Th)* and other rare earth materials, it is suitable in both short term working and long term working at temperatures exceeding 300°C. This is why they are used in manufacturing aerospace and car engine parts. However care is taken when thorium is being used in the process as it is classified as a radioactive metallic element.
- It can also be noticed that at working temperatures exceeding 300°C and the presence of rare earth materials, the resistivity of the alloy to properties such as pressure, tightness and creep increases.

Thus characteristics such as light weight, higher strength, ductility and ability to be cast make *Magnesium (Mg)* a preferred engineering material in modern Aerospace and Automotive applications. Magnesium alloys with rare earth (RE) materials are specifically being developed for high temperature applications which possess creep resistance in special automotive applications such as powertrain equipments, engine blocks etc [9]. Literature shows the application of thorium rich alloys in the manufacture of missiles & spacecrafts [10]. Some of the direct applications of magnesium alloys in the automobile industry are gear boxes, engine blocks, transmission housing, car seat frames, clutch and brake pedals etc. [10]

1.4 CURRENT RESEARCH

The current research focuses on the corrosion performance of three magnesium alloys, AZ31, AZ91 & Elektron21 under various heat treatment conditions. It has been proved that heat treatment improves the mechanical properties of magnesium

alloys and also helps in preparing the alloy for specific fabrication conditions. In this study, the corrosion performance of the above mentioned alloys is determined under three different conditions, as received, solution treated and aging treatment (See section 2.4). Solution treatment improves the strength of the material imparting maximum toughness and shock resistance. Aging, after solution treatment, increases the hardness & yield strength of the alloy and decreases the toughness acquired from solution treatment. The treatment regimes are dependent on the alloy composition of independent alloys. These heat treatments in turn change the microstructural characteristics and literature (refer section 2.4) suggests that this has an impact on the corrosion performance of the alloys.

There have been several studies relating to the corrosion performance due to the effects of heat treatment on magnesium alloys. *Ravi Kumar et al* [7] says that microstructural changes occur in the material when they are subjected to high temperature production processes such as extrusion in case of AZ91. These microstructural changes due to heat treatment refining the grain structure and thus the alloying elements (Aluminium in this case) precipitates at the grain boundary [8] thereby improving the corrosion performance of magnesium alloy.

Song [11] in his review says that magnesium alloys have an excellent strength – to – weight ratio and have poor corrosion properties. This poor corrosion performance is the alloy's major limitation. Song *et al* in their review paper [12] describe in detail the corrosion mechanisms which the magnesium alloys are likely to undergo. They say that when the alloy is exposed to corrosive environment, a thin oxide layer is formed initially which acts as a protective layer. For longer exposure times, the corrosion seems to be following a localized corrosion centres corroding the surface of the exposed alloy. The research further suggests that this corrosion behaviour is due to the presence of secondary phases and or impurities and the formation of an oxide rich surface film on exposure to corrosive environments. Research publication by Song *et al* [13] at a later date suggests a clear layout of the different activities that constitute magnesium corrosion. They suggest that there are various factors which influence the corrosion behaviour of magnesium alloys in general which results in localized corrosion, galvanic corrosion, stress corrosion cracking, negative difference effect etc of the alloy. It was also noticed that the alloying elements and impurities govern the

corrosion activity of the alloy which can be understood from the results obtained in the research by Song *et al.*

Though magnesium alloys outweigh the mechanical properties of aluminium alloys, it is the problem of corrosion performance that limits the usage of magnesium alloys. This research primarily focuses on the performance of three magnesium rich alloys AZ31, AZ91 & Elektron21. Experimental techniques such as time lapse photography, hydrogen evolution and scanning vibrating electrode technique (SVET) etc are used to evaluate the corrosion properties of the above mentioned alloys under various heat treatment conditions to determine the optimum performance of those alloys. Subjective analysis, overall corrosion performance and localized corrosion behaviour of the alloys were carried out in this research to determine the corrosion performance of the alloys.

2. LITERATURE REVIEW

2.1 PROPERTIES OF MAGNESIUM

Magnesium crystals are highly ductile and can be extruded up to three times its original length without fracture at 225°C. According to *Schmid* [1][3], deformation at or above 225°C is due to the slip on 12 planes (pyramidal) next to the basal planes. These planes have a very dense packing. And it was observed that at 300°C, the metal expanded 9 times its original length with reference to its basal plane due to slip. [1][3]

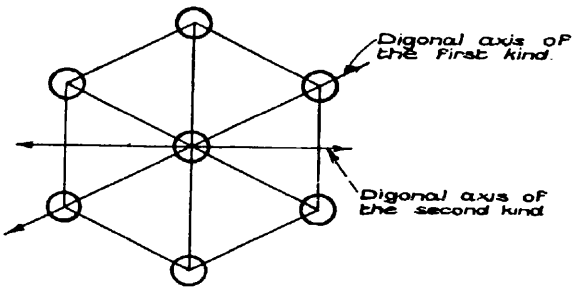

Figure 2.1 The basal plane of a magnesium crystal [1]

However deformation occurs in a single crystal of magnesium because of twinning, which is nothing but the interchange of atomic positions without appreciable change of lattice structure characteristics. Patterns from extruded materials reveal that at lower temperatures, the direction of flow of the material is parallel to the diagonal axis of the second kind. It is seen that the basal plane is parallel to the direction of flow but arranged in all possible orientations about its axis of rotation. It can be seen that the grain pattern appears to be different in extrusion when compared with forged material. This difference of grain structure is not because of the mechanism of glide but is based on the method of working. Again at higher temperatures, the direction of slip is parallel to the diagonal axis of the first kind and does not determine the plane of slip. Most of these tests were carried out on *zinc (Zn)* crystal which has a similar structure when compared to magnesium as they belong to the same family of alkali metals. [1]

It has been seen that the temperature at which a sheet of magnesium is rolled and or finished may exert a profound effect on its mechanical properties. Cold rolling done at temperatures ranging from 190°C to 300°C might actually decrease the ductility of

the sheet. It is also quite hard to finish a sheet at such low temperatures and if the finishing temperature is even low then there is a huge risk of the material being ruined. A control on the finishing temperatures can actually aid in obtaining the exact degree of hardness.

2.2 MAGNESIUM ALLOYS

There are a lot of alloying elements which are commercially available. But before these elements are being studied, the following observations should be taken into considerations,

- Metals with hexagonal crystal structure undergo solid solution stage continuously. E.g., zinc, beryllium, cadmium, titanium, zirconium etc. [3]
- As magnesium has an electron ratio of 2, it can only combine with elements having a valency electron ratios of 3 : 2, 21 : 13, 7 : 4 etc.
- Compound formation of magnesium is only possible with less electropositive metals as magnesium itself is electropositive.
- There is restriction of atomic size of the alloying metal/element as it cannot be greater than 15 percent of that of magnesium. This is because of the fact that the extensive solid solution formation of Magnesium crystal is restricted by atomic size of the element. This is was illustrated by *Carapella* [3] in the following diagram.(Figure 2.2)

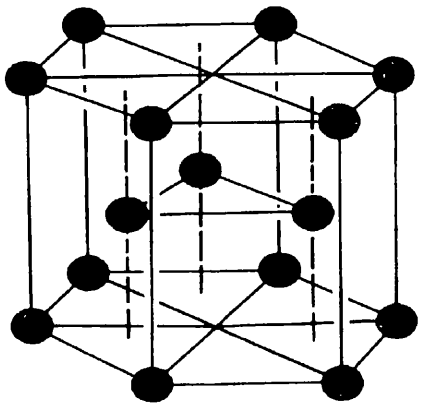

Figure 2.2 The hexagonal lattice structure of magnesium crystal [3]

It can be shown by Figure 2.3 [3] that the maximum solid solution characteristic is restricted with increase in atomic number. This is because of the non-movement of the valency electron from 2 as the solute exhibits a stronger characteristic at lower valency states [3]. The Figure 2.3 [3] shows the various materials that have factors favourable for solubility in magnesium

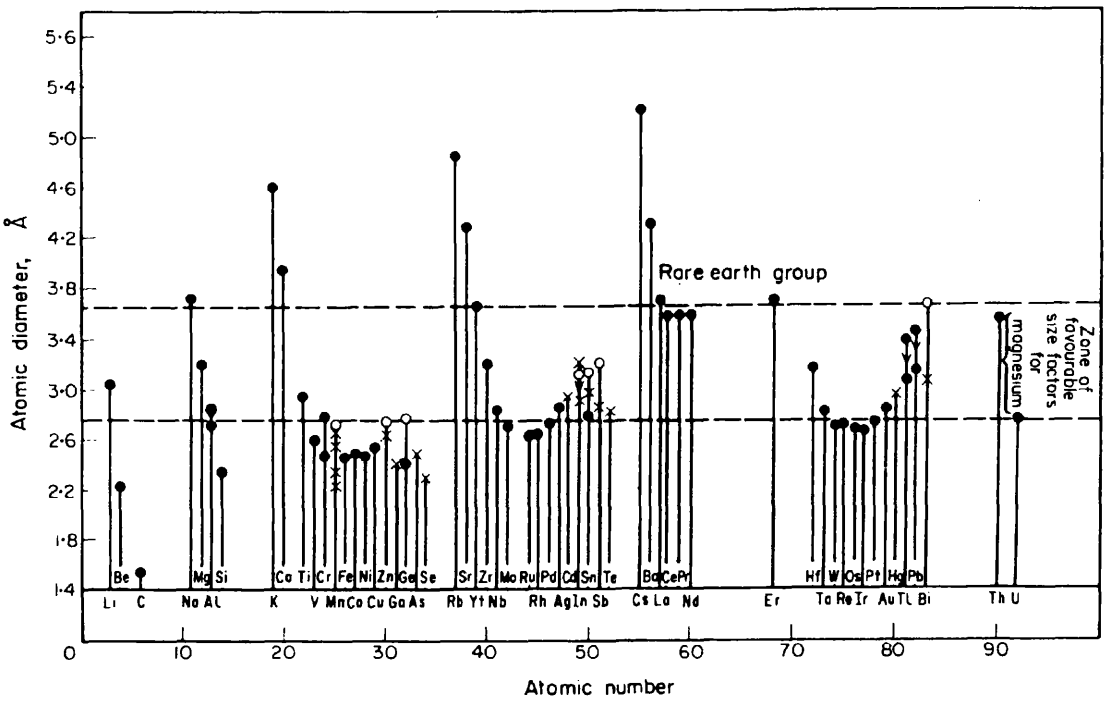

● Interatomic distance where all close neighbours equidistant; or distance of approach in basal plane of close packed hexagonal crystals.
× Closest approach where sets of neighbours are at different distances.
○ Goldschmidt atomic diameters.

Figure 2.3 A plot of atomic diameter of elements with the zone of favourable size factors [3]

The following periodic table[1] (Figure 2.4) illustrates the general solubility of various elements/metals in liquid magnesium.

[1] Emley E. F., "Principles of Magnesium Technology", 1966, pg.229

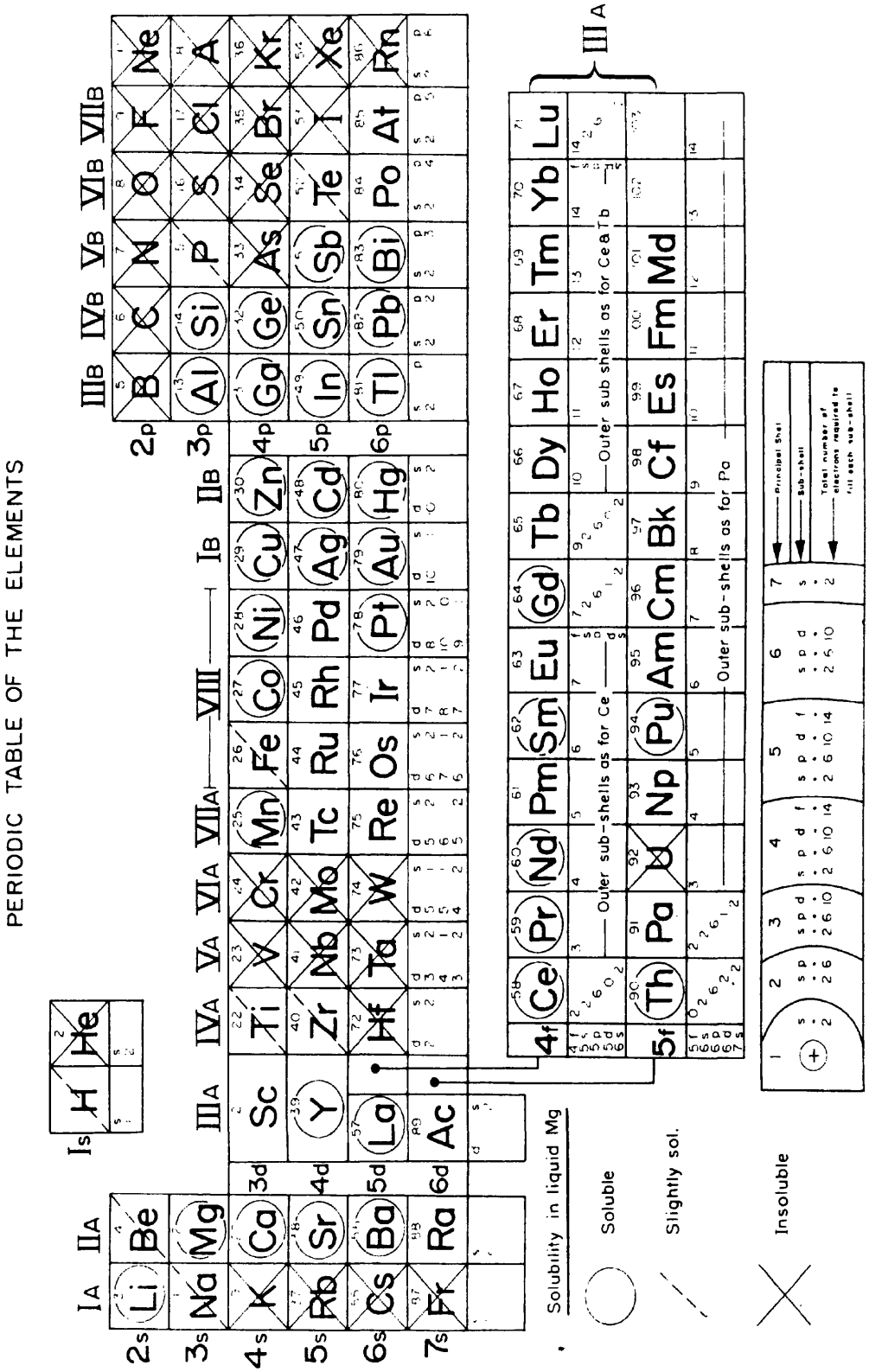

Figure 2.4 Solubility of Magnesium with various elements of a periodic table [3]

2.2.1 CLASSIFICATION OF MAGNESIUM ALLOYS

Elements exhibiting considerable solubility in magnesium within the binary system can be grouped as follows [3],

a) *"Continuous Solid Solution – Cadmium (Cd)"*

b) *"Peritectic System – Indium (In), Manganese (Mn), Zirconium (Zr)"*

c) *"Eutectic system (Solid solubility exceeding 1 percent) – Lead (Pb), Thallium (Tl), Silver (Ag), Tin (Sn), Aluminium (Al), Bismuth (Bi), Zinc (Zn), Gallium (Ga), Lithium (Li), Osmium (Os), Thorium (Th), Mercury (Hg), Neodymium (Nd), Praseodymium (Pr)"*

d) *"Eutectic Systems (Solid solubility up to 1 percent)*
Alloy Composition > 5 percent : Gold (Au), Antimony (Sb), Copper (Cu), Nickel (Ni), Cerium (Ce), Strontium (Sr), Calcium (Ca), Barium (Ba), Lanthanum (La)
Alloy Composition ≤ 5 percent : Cobalt (Co), Germanium (Ge), Iron (Fe), Silicon (Si)"

e) *"Eutectic system with liquid miscibility – Sodium (Na)"*

2.2.2 EFFECTS OF COMMERCIALLY IMPORTANT ALLOYING ELEMENTS

It gives a good insight on the behaviour of the alloy systems based on the alloying element. The following are some of the commercially important alloys and their influence on magnesium,

Aluminium –

It is the base of age old heat treatable alloy systems. On superheating, the strength of the alloy increases and refined the cast structure. However there is a tendency for microporosity to occur.[3]

Manganese –

Good for corrosion resistance but does not have much strength. It was the base for old Magnesium – Manganese wrought alloys.[3]

Zinc –

Addition of zinc helps in grain refinement of the alloy there by increasing the strength of the alloy itself. They are heat treatable alloys. However they exhibit some brittleness on heat treatment and an addition of zirconium could refine the alloy characteristics considerably. They also exhibit microporosity to some degree.[3]

Zirconium –

There is a very high degree of grain refinement observed in the alloy due to addition of Zirconium also increasing the ductility of the alloy. But there is no much increase in the strength of the alloy. It works like a scavenging element by removing elements like iron, aluminium, silicon etc., at very low levels resulting in the production of high purity alloys.[3]

Rare Earth Metals –

Long term creep resistance for temperatures less than 250°C, reduction in microporosity, reduces brittleness caused by the presence of zinc form the characteristics of rare earth metals. However, grain refinement is effective on addition of zirconium, and does not contribute to good ductility. In the absence of zirconium, these elements have weak tensile properties in cast alloy systems. Overall basis they exhibit good corrosion resistance for some combinations.[3]

Thorium –

The creep resistance is conferred to the alloy for temperatures up to 350°C. It is good in reducing microporosity and brittleness and there by increases ductility of the alloy system.[3]

Silver –

The presence of silver with other rare earth metals improves the response to heat treatment as they are completely treatable. However they form a decent heat treatable alloy system (eutectic) with good solid solubility.[3]

2.2.3 EFEECTS OF SOME IMPURITIES

Presence of impurities such as iron, copper, sodium etc., adversely affects the mechanical properties of the alloy system making them totally unstable. Also there is deterioration in the corrosion resistivity of the alloy. Issues like microporosity also crop up.

Iron –

It affects the corrosion resistance of Magnesium – Aluminium alloy system adversely. This can be controlled by addition of few tenths in percent of manganese.

Nickel and Cobalt –

It has adverse effect on corrosion property to a high degree.

Copper (Cu) –

It affects the corrosion resistivity of the magnesium alloy system when present in higher percentages.

Sodium (Na), Potassium (K) and Barium (Ba) –

Their presence leads to embrittlement of the alloy system but are highly unlikely to be present during the conventional process. However they could appear during salt reduction process during alloying element addition.

Hydrogen –

It reduces the ultimate tensile strength of the alloy system and the elongation values due to the induction of microporosity during the alloying process.

2.3 ALLOY SYSTEMS OF INTEREST

2.3.1 MAGNESIUM – ALUMINIUM – ZINC ALLOY SYSTEM

2.3.1.1 EFFECT OF ALUMINIUM

There has been considerable amount of study on the effect of aluminium on the tensile properties of the magnesium alloy system. These results were studies in the form of micrographs / microstructures obtained from microscopy techniques. Again

the manufacturing techniques, i.e., wrought alloy or a cast alloy changed the tensile properties significantly. A number of studies on the binary Magnesium – Aluminium system showed that depending on the particles of β – phase formed as a result of different cooling rates, about 2 percent of aluminium appeared in the structure and about 8 percent of aluminium was in the form of an incomplete / degenerative eutectic system around the grain boundaries [3]. The β particles represent the alloying elements forming the secondary phase. Thus the presence of inter-dendrite like particles in the β – phase with strong layering and or coring of aluminium was noticed which further suggested that refinement of the grain structure of the alloy was essential. It was also noticed that on completion of full heat treatment and quenched by water, the microstructure had "equiaxed structures with smooth grain boundaries". [3]

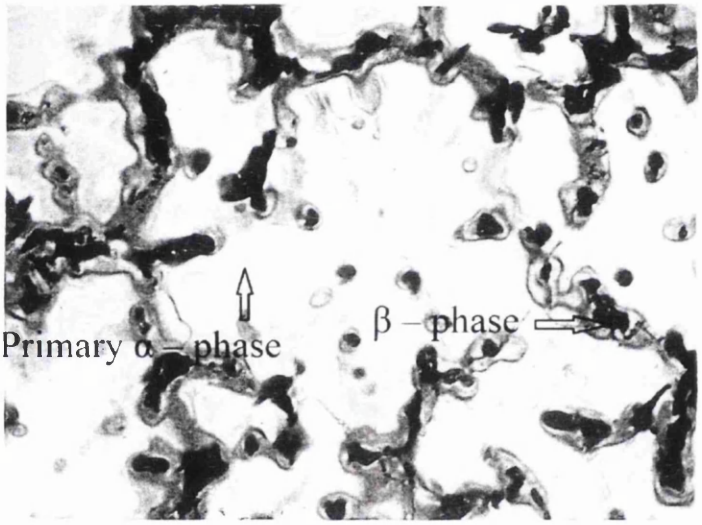

Figure 2.5 Microstructure of chill cast A8 (Mg, Al – 8%, Zn –0.5%, Mn – 0.25%) (×250) [3]

2.3.1.2 EFFECT OF ZINC

It was seen that the Magnesium – Aluminium alloy system had a higher percentage of optimal aluminium content to be heat treated. And it was also noticed that the addition of zinc in all three states (as cast, solution treated, fully heat treated) resulted in an increase in proof stress (P.S.) of the alloy, and more significantly during full heat treatment. Figure 2.6 [3] given below shows the effect of different precipitation treatments on a fully solutionized alloy AZ91.

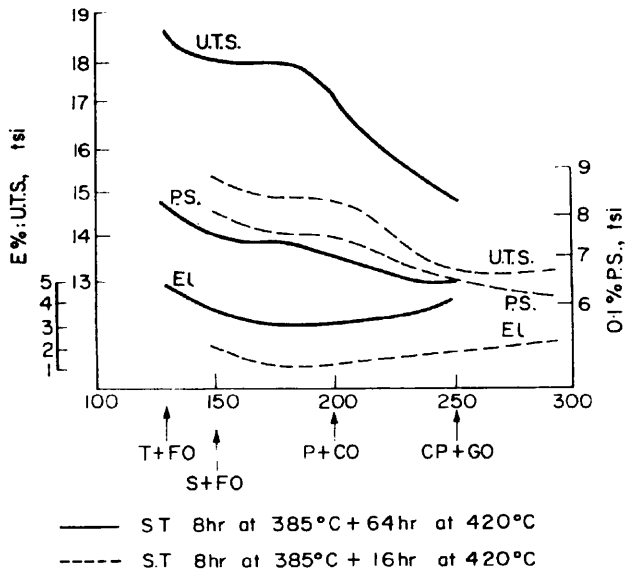

Figure 2.6 The "effect of precipitation temperature on the tensile properties of AZ91 solution treated and precipitation treated to maximum hardness (after Fox)" [3]

The following figures (Figure 2.7 (a) – (c)) show the test results by Fox[2]. [3] It was noticed that the values of proof stress increased from 6.5tsi[3] (on cast alloy for a 10% Al and 2% Zn) to 8tsi (for the same composition) on complete heat treatment. It was also inferred that this particular alloy did not perform well during the solution treatment as the proof stress reduced by about 1tsi for the same composition.

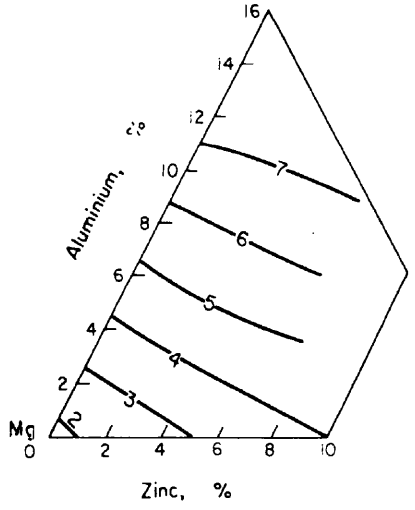

Figure 2.7 (a) '0.1% P.S., as cast'.[3]

[2] F. A. Fox, J. Inst. Met., 1945, 71,415 [3]

[3] tsi or tonns force per square inch is a non-metric unit to measure pressure applied on the material

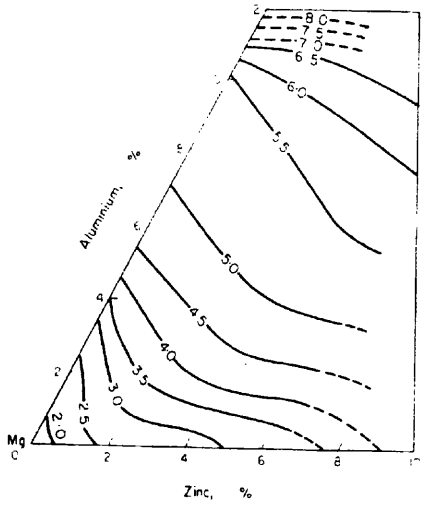

Figure 2.7 (b) '0.1% P.S., solution heat treated'

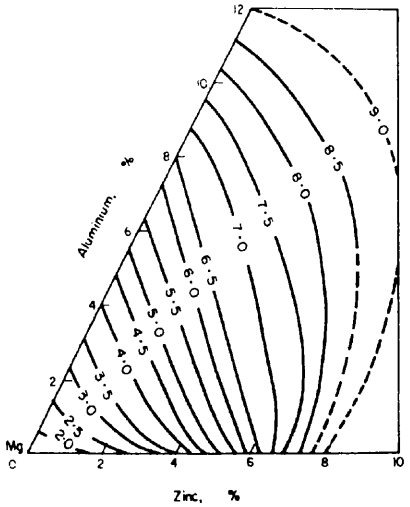

Figure 2.7 (c) '0.1% P.S., fully heat treated'

Figure 2.7 (a) – (c) The change in tensile properties of Mg-Al-Zn alloy systems due to alloy composition and heat treatment on British sand cast test bars (after Fox) [3]

It could be seen from the above (Figure 2.7 (a) – (c)) that a 3 percent addition of zinc increased the proof stress by 1.5tsi with a 3 percent elongation. Thus addition of zinc improved the tensile properties of the alloy with a minimal loss in ductility of the alloy. It was also found that water quenching of such alloy system resulted in a "discontinuous precipitation" [3] increasing both the strength and ductility of the alloy. (Refer to Figure 2.8)

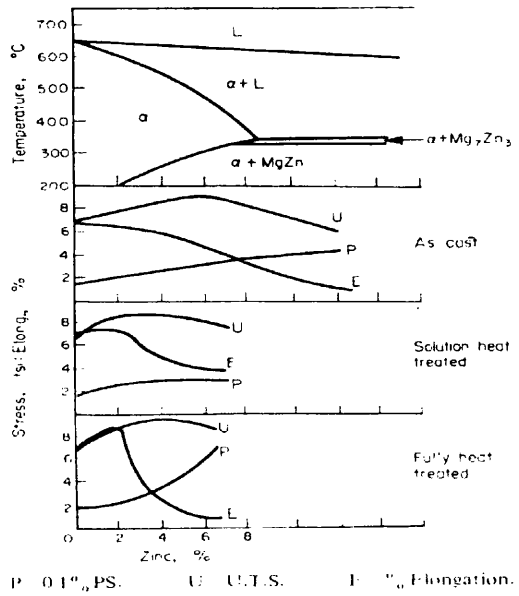

Figure 2.8 The change in tensile properties of Mg-Zn alloy systems due to alloy composition and heat treatment on British sand cast test bars (after Fox) [3]

The addition of zinc also improved corrosion resistance of the alloy system especially after heat treatment. However, there is always limitation to the amount of zinc that can be added and or present in the Magnesium – Aluminium system. It was seen that increase and improper addition of zinc during casting resulted in an increase in microporosity.

2.3.1.3 DISADVANTAGES OF Mg – Al – Zn ALLOY SYSTEM

Even though the magnesium – aluminium – zinc alloy system exhibits better properties than its previous counterparts, it still has disadvantages.

- Tendency towards microporosity
- Low ductility on heat treatment for improvement of proof stress. [3]

2.3.2 MAGNESIUM – RARE EARTH METAL – ZIRCONIUM ALLOY SYSTEM

{Note: The work described under this sub-title is adapted from Emley's "Principles of Magnesium Technology" [3] published in 1966. As the development in the magnesium – rare earth metal zirconium alloy took place during later years; it has been elaborated in the recent advancements in section 2.7.[4]}

The characteristics of this alloy system haven't been identified prior to 1966. There had been very little work carried out on alloys with rare earth metals as the maximum solubility was left unaffected due to zirconium addition. Murphy and Payne[5], [3] the pioneer in this alloy system, proved that grain refinement by zirconium addition was possible and the alloy met the commercial standards. This was later demonstrated by Meier [3] using ASTM bars which were sand casted which can be inferred from the figure below. (Figure 2.9)

[4] Refer to page number 25

[5] A. J. Murphy and R. J. M. Payne, J. Inst. Met. 1947, 73, 105 [3]

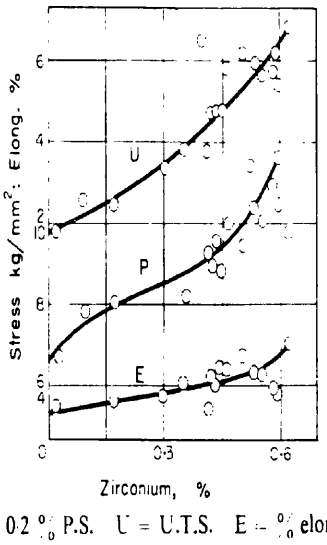

Figure 2.9 The change in tensile properties of sand cast Mg – Re 3% - Zr alloy ASTM bars (Meier) [3]

A low-zirconium alloy (EK30) (RE – 3%, Zn – 0.25%), which needed a high temperature solution treatment (565°C), was introduced in U. S. A. However failure to show acceptable tensile properties at room temperature led to the use of zinc based quaternary alloy ZER1 (EZ33) (Mg, RE – 2.75%, Zn – 2.25%,Zr – 0.7%).

It has been proved that, with full grain refinement the 'inter-dendritic β-phase' does not appear, and at some period of time exhibits a true eutectic appearance[††].

2.4 HEAT TREATMENT

Heat treatment is a process of alternate heating and cooling a material in its solid state in order to obtain the material with desirable properties [14][15][16][17]. Predominantly, there are three important methods in heat treatment.

a) Cold working – processes where plastic deformation is caused on the material below its re-crystallization temperature. Some examples include, rolling, drawing, pressing etc [16].

b) Solution strengthening – process where the material is heated close to re-crystallization temperature so that the alloying elements of the material give a homogeneous phase. The sample is then rapidly cooled (or Quenching) in

either water or oil in order to retain the homogeneous phase of the material [14][17].

c) Precipitation hardening – process where the material is heated for at elevated temperatures much less than the re-crystallization temperature of the material over a period of time and then cooled rapidly in order to retain the precipitate of the alloying material [17].

Cold working and solution strengthening process have been carried out since ancient times. However, the process of Precipitation hardening or Age hardening was observed by Alfred Wilm [17] during his experiments (1906 – 1909) in Germany. The search for an aluminium alloy which could be hardened by heat treatment similar to that of steel is what made Wilm conduct experiments. Experiments on "Duralumin" (Copper – 4%, Magnesium – 0.5%, small amount of Manganese) revealed that the hardness of the alloy improved with heat treatment and quenching over a period of time. Though Wilm did not understand the fundamental principle of "Ageing", it was Merica *et al* [17] who published a paper in 1919 demonstrating the decrease in copper solubility in aluminium with decrease in temperature over a period of time. They suggested that the precipitation of a second phase due to ageing and quenching is what increased the hardness of Duralumin and they referred the precipitate as "submicroscopic dispersion" [17]. From then on, age hardening of alloys has been carried out in most of the emerging and developed alloys either on its own or with a combination of solution treatment and precipitation hardening.

In order to understand the process of hardening more clearly, it is necessary to understand the thermodynamics and phase transformations of the material. According to Porter *et al* [18], a phase can be defined as a part of a system exhibiting homogenous properties and composition and are different from the rest of the system. The phase composition can be got from different amounts of elements or components constituting the system. Thus phase transformations deals with the change in the phases of the alloy system in order to acquire desired properties for the material. Porter *et al* [18] says that the reason behind transformation is because of the instability of the alloy from its initial to its final state. Thus the most fundamental concept which controls phase transformation is by diffusion of atoms.

Precipitation predominantly occurs due to diffusion of atoms. This diffusion of atoms could either be

a) *Substitutional* atoms [18] which diffuse due to vacancies present in the crystal structure and

b) *Interstitial* atoms [18] which move by force making way between larger atoms.

The diffusion coefficient can be defined from Fick's equation [17] [18] as,

$$J = -D\frac{dc}{dx} \quad mol/sec$$

where J – is mass flowing per unit time (mol/sec)
D – diffusion coefficient or diffusivity (m^2/sec)
c – concentration of the diffusing mass (mol/m^3)
x – distance measured (m)

Now concentration 'c' of vacancies in the inter-atomic structure at a given temperature 'T' can be written as

$$c = exp\ (S_f / k)\ exp\ (-E_f / kT)\ [16]$$

where S_f & E_f – entropy and activation energy for vacancy formation
k – Boltzmann's constant

In the above equation the expression for entropy ($exp\ (S_f / k)$) is considered a constant between 1 and 10. This shows that with increase in temperature, equivalent number of vacancies are formed in order to obtain the equilibrium forcing the diffusion of atoms from higher energy to lower energy in accordance with Gibbs free energy *(G)* [17] [18] where,

$$G = U + PV - TS$$

where U – total internal energy of the system (*Joules*)
P – pressure (*Pascal*)
V – volume (m^3)

T – absolute temperature of the system (K)

S – entropy of the system ($Joules / K$)

Thus it can be seen that movement of atoms create changes in the grain of the material giving it typical grain structure referred to as microstructure of the material. A general methodology for precipitation hardening or age hardening can be carried out in the following steps [14],

1. Heating the alloy close to its re-crystallization temperature to acquire a homogeneous solid solution. (Solution treatment)
2. Quenching the solution treated alloy in order to retain the solid solution structure at room temperature.
3. Heating the alloy to a slightly elevated temperature over a period of time to harden the material artificially.

It has been noticed in various studies that continuous ageing gives a precipitate. In other words, coarse grain particles of the second phase appear all over the alloy from the homogeneous state. This can be seen and understood from the following phase diagram showing Magnesium – Aluminium ($Mg - Al$) with all its phase concentrations over a range of temperatures.

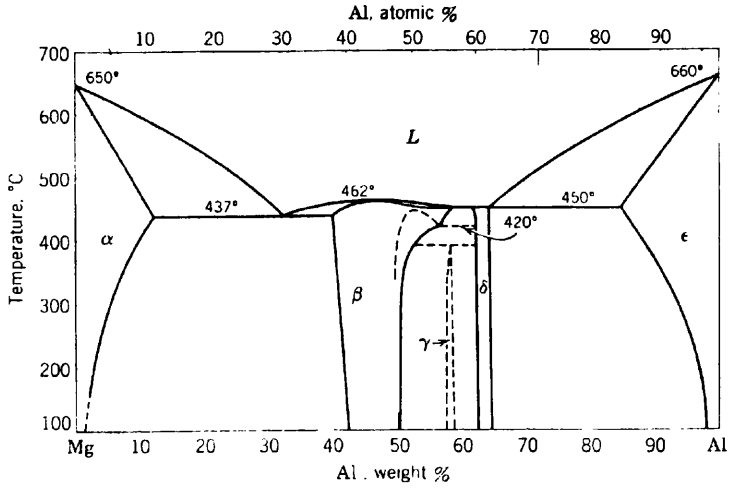

Figure 2.10 Phase diagram of $Mg - Al$ alloy system [19]

The $Mg - Al$ phase diagram (Figure 2.10) shows the composition of Magnesium and Aluminium in terms of atomic weight along the X axis and temperature along Y axis.

The solid solution state which is Magnesium rich is represented by α followed by solute phases β, γ, δ, and ε [19]. The molten alloy state is represented by notation L. It should be noted that only single phase notations are used in the phase diagram for better understanding of the phase diagram. Thus for a typical AZ31 alloy, the typical solution treatment temperature will be under 437°C (refer Figure 2.10), the ageing treatment will be around 200°C at the boundary of the solidus curve.

2.5 METALLOGRAPHY

Cochran[6] defines Metallography as "the study of the internal or surface structure of materials whether by optical, electron, x-ray, microprobe, field-ion or emission analysis" [20]. The image thus acquired showing the surface material structure is referred to as Microstructure. The scanning electron microscope (SEM) is probably the most exciting instrument used by metallurgists to determine the structure of new and existing materials [21].

2.6 CORROSION

Mattsson [22] defines as "a physicochemical reaction between the material and its environment and leads to changes in the properties of the material". He further says that this "Corrosion Effect" is detrimental to the material and at times be useful as well. Thus corrosion is nothing but the disintegration of the material which in turn affects the reliability of the structure leading to the failure of the system.

2.6.1 MAGNESIUM'S ANODIC BEHAVIOUR

The standard electrode potential of Magnesium is –2.40 v [3][8][19][22]. Since the electrode potential is very low, Magnesium falls under the "base metal" category of the "noble metals" list [22]. This is also one of the reasons why magnesium used as a sacrificial anode [8][19]. It has been noticed by Roberts [19] that when magnesium alloy is exposed to an aqueous solution a thin film of magnesium hydroxide is formed. As the $Mg(OH)_2$ is strongly basic, it resists the reaction of alkaline regions.

[6] Cochran F. L., Metallography 1, #1, (1968), p. vii [20]

Thus corrosion of Magnesium in a aqueous solution is mainly a cathodic reaction in which hydrogen evolves [19]. With the supply of oxygen through electrolyte, the electrical resistance of the alloy is increased permitting local cathodic reaction. This oxygen reduction together with hydrogen evolution is termed as "negative difference effect" [11][12][13][19] and occurs primarily in base metals.

The corrosion reaction can be understood from the following equations [8],

Anodic Reaction:

$$Mg \rightarrow Mg^{2+} + 2\ e^-$$

Cathodic reaction:

$$2H_2O + 2\ e^- \rightarrow 2H_2 \uparrow + 2\ OH^-$$

The total reaction:

$$Mg^{2+} + 2H_2O = Mg(OH)_2 + 2H_2 \uparrow$$

where Mg^{2+} – Magnesium ions

e^- – Electrons released

H_2O – Water

OH^- – Hydroxide ions

$2H_2$ – Hydrogen

$Mg(OH)_2$ – Magnesium hydroxide

It can be seen from the above equations that, Magnesium releases 2 electrons on reaction with water. These excess electrons split the water molecule into hydrogen and hydroxide ions. Now the hydroxide ions react with the electropositive magnesium ions to form magnesium hydroxide.

2.6.2 CORROSION EFFECT DUE TO ALLOYING ELEMENTS

During the early days of magnesium alloy development, it was noticed that the alloying materials and various heat treatments affected the corrosion properties of the alloy. It was Hanawalt *et al* [3][19] who demonstrated that addition of iron, copper and nickel in portions of 170, 1300 & 5 ppm, the corrosion rate of "pure" magnesium increased rapidly. It was later found that the iron had a huge influence on the

corrosion characteristics of pure magnesium. Thus the amount of these three impurities or "tolerance limits" [19], as the researchers called it, controls the corrosion performance of the alloy. The following are some of the generalisation results seen by investigators over a period of time,

- Alloying element reduces electrode activity of pure magnesium alloy decreasing the rate of corrosion [19]
- The tolerance limits change with the introduction of metals like Aluminium reducing the impact of iron.
- Addition of Manganese and Zinc to Mg-Al alloy system reduced the corrosion rate considerably.

It has been seen that chloride solutions corrode magnesium readily. An immersion test in a chloride solution affects the corrosion performance of magnesium alloys considerably. It was noticed that when the alloy was heat treated, a fine "sub-microscopic" [3] structure was formed accompanied by an increase in corrosion rate.

Thus Zeng et al [8] in their review paper say that the poor corrosion performance of magnesium alloy is due to

- "The oxide films forming on the surface are not perfect and protective"
- "Galvanic or bi-metallic corrosion can be caused by impurities and second phases"

2.6.3 TYPES OF CORROSION

The following are the common types of corrosion mechanisms which magnesium alloys are susceptible. This section is from Zeng *et al*'s review paper [8] on corrosion of magnesium alloys.

1. Galvanic corrosion – or bi-metallic corrosion occurs due to the presence of different materials in an electrolyte. In case of magnesium alloys, this can be interpreted as material substrate and a secondary phase. It has been seen that magnesium behaves as an anode and the alloying elements behave as a cathode thereby completing the electrochemical process of corrosion.

2. Pitting corrosion – occurs in magnesium due to the presence of "chloride ions in a non-oxidizing medium". It was noticed that pits were formed due to corrosion activity initiated due to flaws adjacent to the secondary phases.

3. Intergranular corrosion – occurs predominantly due to the precipitates at the grain boundaries. Maker et al [8] said that the corrosion occurred next to the grains as the grains were supposed to be cathodic. However, recent studies showed that intergranular corrosion occurred at the grain boundary and not as suggested previously. It was also noticed that during the initial stages of corrosion, localized corrosion activity seemed to take place along the grain boundary at the interface of the cathodic precipitates. It was also noticed that ageing of AZ80 led to the decrease in the concentration of aluminium content in the α matrix [8]. This prevented the formation of protective oxide layer increasing the rate of corrosion.

4. Filiform corrosion – occurs on the surface of the alloys by active galvanic cells. Investigations revealed that pitting and filiform characteristics were noticed in the early stages of corrosion activity on AZ91 alloy.

5. Crevice corrosion – occurs due to the presence of moisture in narrow gaps of the material. Though initial investigations revealed that magnesium alloys do not undergo crevice corrosion, recent studies point out that there is possibility for this type of corrosion to occur as filiform corrosion does occur in magnesium. And filiform corrosion is special type of crevice corrosion.

6. Stress corrosion cracking – occurs in heavy engineering equipments where a crack is formed leading to a continuous or discontinuous multiple cracks leading to the failure of the equipment. Air, distilled water and chloride solutions usually enhance this type of corrosion cracking in service equipments in engineering industries.

7. Corrosion fatigue – occurs over a period of time and compliments to fatigue of the structure. It has been noticed over years that fatigue strength of the material increases with increase in grain size of the material. Studies also revealed that exposure of magnesium to chloride solutions affect the fatigue life of the structure significantly.

2.7 RECENT ADVANCEMENTS

Though heat treatment processes have been around for a long time now, there have been various studies carried out on the effective heat treatment methodologies for existing and emerging magnesium alloys. Recent advancements can be found in this section which explains the need to identify a treatment process best suited for acquiring better corrosion performance characteristics.

There have been many studies relating heat treatment to change in microstructural features in turn leading to change in mechanical properties of the material. Cáceres *et al* [23] investigated the effects of various solidification rates and heat treatments on the mechanical properties of AZ91 alloy. They measured the secondary dendritic arm spacing of the cast alloys with all treatments and saw that the spacing decreased with increase in solute. They tried to relate this change with the tensile properties of the material and concluded that these characteristics were a result of the secondary phase's incomplete dissolution. Further the ageing treatment increased the hardness of the alloy. However, the important factors relating microstructure and mechanical properties were not completely understood.

Studies on the effect of heat treatment on corrosion performance of AZ91D material [24] showed that solution treatment at 420°C dissolved the β-phase completely and ageing at 200°C cause the precipitate to appear along the grain boundaries. It was noticed that homogeneous solution state had better corrosion performance in comparison with the aged alloy when the precipitates started appearing along the grain boundaries.

Ravi Kumar *et al* [7] processed AZ91 alloy thermo-mechanical extrusion to refine the alloys microstructure. They concluded that the secondary β-phase did not affect the torsion behaviour corresponding to different grain sizes. Their study also supported the idea of fine-scale microstructures.

The superplastic condition of magnesium alloys was investigated by Vesling *et al* [25]. It was seen that homogeneous solution treatment, quenching followed by artificial ageing lead to the formation of fine grains upon hot pressing. They established that the grain size depended on the ageing time and showed good

superplastic characteristics due to the alloys fine grain structure obtained as a result of heat treatment.

Strengthening studies by Zhao *et al* [26] showed that homogenized annealing of AZ91 alloy at 683 K increased the strength of the alloy. It was noticed that there was no obvious loss of corrosion characteristics due to the single step homogenized annealing. Further it was noticed that the tensile strength and the elongation of the AZ91 alloy increased due to the heat treatment.

Bialobrzeski *et al* [27] suggested through his review paper that with the use of light weight alloys, the problems relating to the corrosion performance of those alloys need to be addressed. Problems relating to solubility of the alloying element, formation of intermetallic phases and segregation problems associated with alloy need to be studied in detail with respect to corrosion.

There have been various studies investigating the use of coatings as an option to prevent corrosion of magnesium alloys. Shigematsu *et al* [28] suggested a surface treatment process by diffusion coating on AZ91D alloy. Aluminium and Zirconia powder were used for the diffusion coating of the alloy. Though the thickness of the alloy increased, the hardness of the material remained the same.

Gray *et al* [29] discusses various surface coating methods such as electrochemical plating, conversion coating, anodizing, gas-phase coating, organic coating, etc., which are currently in use. He says that till date there is no single coating technology that has been developed to tackle the problems relating to magnesium corrosion.

It was seen by Fan *et al* [30] that heat treatment enhanced the mechanical properties of the alloy. The investigation involved comparison of as received AZ91D alloy and a Rheo-diecast AZ91 alloy which was developed for the production of alloys with high technical integrity. Various characteristics such as solidification processes, microstructural changes and heat treatment were considered in the research. It could be inferred that heat treatment did change the characteristics of the alloy there by suggesting that there is a possibility of corrosion characteristics of the alloy to change as well.

There have been reports that the influence of rare-earth materials changed the characteristics of the alloy. It was seen by Stanford *et al* [31] that the microstructural

properties changed during the extrusion process of AZ31 and suggested that this was because of the alloying material. Moreover the influence of neodymium (Nd) resulted in the "Particle-stimulated nucleation (PSN) of recrystallization". It was also noticed in the investigation that this PSN characteristic attributed to the larger particles in both AZ31 and ME10 alloys and yet the texture of the alloys differed from each other.

Investigations were carried out by Dobrzanski *et al* [32] to determine the influence of characteristics such as chemical composition and precipitation on the microstructure and in turn the mechanical characteristics of magnesium alloys. It was noticed that there were changes in the microstructure in the as cast, solution treated and age hardened samples. They also estimated the chemical composition of the alloy under various heat treatment conditions using EDS. They reported that different heat treatment processes definitely changed the mechanical characteristics of the alloy.

Studies on solid mould casting of AZ91D alloy were carried out [33]. It was reported that casting and mould preheating temperatures had minor changes in the microstructural and mechanical properties of the cast alloy. It was noticed that the casting process in itself influenced the mechanical properties with the top fill showing tendency to the formation of microporosity where as the bottom fill showed better tensile and yield strengths.

In another investigation by Han *et al* [34], microstructural changes due to heat treatment were studied and was related to the mechanical properties. A nano-scale hardness evaluation was carried out using Berkovich's nano-indentation technique. Both die-cast and permanent mold cast alloys were subjected to heat treatment and all the different secondary and ternary phases were studied and compared with the mechanical properties of those alloys. The results showed that age hardening increased the mechanical performance with increase in hardness of the alloy.

El-Amoush [35] assessed Mg-Al alloys with 5, 15 and 30% aluminium content by casting the alloys in the mentioned concentrations using a cold die cast injection moulding. It was reported that the increase in aluminium content in the alloy resulted in the increase in appearance of aluminium in the hydrogenation process which in turn resulted in increasing the hardness of the material.

Lindemann *et al* [36] determined the density values for AZ91 and AM60 alloys at temperature range 30-500°C. Other thermo-mechanical properties were also evaluated and compared with the DSC signal curves for each of the alloys. The problems associated with the evaluation process were also discussed in the results.

Kubota *et al* [37] in their review paper suggest that small grain sizes were desirable as they produced alloys with high strength and ductility at room temperatures. They also suggest that with grain refinement, magnesium alloys exhibit a superplastic behaviour. It was reported that thermal treatments greatly influenced change in grain size and structure producing alloys with better mechanical properties.

Lyon et al [38] in their paper discuss the elemental composition of Elektron 21 alloy in detail and compare the characteristics with that of aluminium containing alloys. They were reports on the corrosion behaviour of E21 in comparison with AZ91D alloy and suggested that Nickel contributed significantly to the corrosion behaviour of E21 where as aluminium was the key element determining the corrosion behaviour of AZ91D alloy.

Kielbus [5][6] examined the effects of solution treatment and age hardening of Elektron 21. However primitive methods were used to analyse the amount of material loss by weighing the alloy before and after corrosion. This is the closest research found to date comparing the microstructural, mechanical and corrosion properties of E21 alloy.

There have however been DSC investigation studies of Elektron 21. Riontino *et al* [39] report that isothermal heat treatment at 300°C producing a hardening response had a strong correlation with the characteristics of the secondary phase obtained due to annealing. This case has been found similar to other alloys containing rare-earth metals. The DSC signal evolution from heat treated samples supported that there were changes in characteristics in of the material due to thermal treatment.

Guadarrama-Munoz *et al* [40] studies the electrochemical behaviour of magnesium anodic rods with different efficiencies by testing with two different aqueous soloutions, Sodium chloride (NaCl) and Calcium sulphate – magnesium hydroxide ($CaSO_4$–$Mg(OH)_2$) solutions. It was reported that the electrochemical behaviour of each of the samples differed due to their chemical composition. It was found that the

anodic current density differed with each sample producing different electrode potentials suggesting that the composition of the sample played a major role in governing the characteristics of the magnesium samples. It was also reported that the main corrosion product formed as a result of the electrochemical reaction between the sample and 3% NaCl solution was identified as magnesium hydroxide ($Mg(OH)_2$).

Studies indicate that the alloying elements play a major role in governing the corrosion process of magnesium alloys [41]. It has been reported that addition of rare earth materials improves the corrosion resistance of magnesium alloys. Heat treatment of such alloys with rare earth have helped in acquiring alloys with less corrosion activity thereby increasing the corrosion performance of magnesium.

Bobby Kannan *et al* [42] conducted "slow strain rate test method" (SSRT) in air, distilled water and 0.5wt.% NaCl solution on rare-earth magnesium alloys ZE41, QE22 and Elektron 21 to determine the stress corrosion cracking of the alloys. It was reported that of the three alloys Elektron 21 had a high corrosion cracking resistance in both distilled water and 0.5wt.% NaCl solution.

Investigation on ageing of AZ91D for ageing times exceeding 45 hours have been carried out by Song *et al* [43]. It has been noticed that the initial ageing at 160°C improved the corrosion resistance of the alloy. However when the ageing was carried out for over 45 hours, the corrosion rates increased suggesting that the presence of aluminium in the β-phase appearing during early ageing prevented corrosion. As the ageing time increased, the aluminium content in the α-Mg matrix reduced considerable there by increasing the rate of corrosion of the alloy.

Recent developments in the corrosion studies of magnesium alloys have been reviewed by Song [11]. Various special corrosion phenomena such as "'spacer effect', 'passivation effect', alkalization effect, 'poisoning effect', 'short-circuit effect', 'galvanic NDE' [11] have been addressed in his review. Recent concepts such as "anodic dissolution of magnesium", "negative difference effect (NDE)" have also been reviewed. Factors such as rate of corrosion, the general corrosion behaviour of magnesium alloys, effect of alloy composition and microstructure, etc have been discussed by Song [11]. The review suggests that the hydrogen evolved during corrosion process behaves strangely and this is due to the anodic dissolution. This is primarily responsible for the negative difference effect as suggested by Song. Further

the author suggests that a suitable method should employed to measure the amount of hydrogen evolved in order to estimate the rate of corrosion of the alloy, as the corrosion process primarily involves hydrogen evolution.

In a previous publication by Song *et al* [12], the authors discuss the corrosion process, corrosion mechanisms and corrosion thermodynamics of magnesium and its alloys. They also introduce the NDE phenomena [11][12][13][19] due to the irregular anodic dissolution of hydrogen during corrosion of magnesium alloys. They predict that the corrosion mechanism follows four different models. The 1st model [12] is based on the formation of a protective film on the surface of the alloy due to NDE. As the current density increases, the protective film breaks down increasing the rate of corrosion. The 2nd model is the actual break down of magnesium into the "mono-valent magnesium ions". The 3rd model is the "particle undermining model" where in the magnesium matrix particles fall out due to the reactivity of the secondary phases resulting in loss of the alloy. The 4th model deals with the formation of magnesium hydride on the surface of the alloy. The so formed magnesium hydride formed due to corrosion process readily decomposes in water forming magnesium ions and hydrogen [12].

The research further suggests that the alloy composition, alloy phases and microstructure are other factors which influence the rate of corrosion of magnesium and its alloys. Song et al conclude that only on complete understanding of the above factors and electrochemical behaviour of the secondary phases can be predicted which in turn will lead to the development of a new generation of magnesium alloy systems which are corrosion resistant.

In a later publication, Song *et al* [13] establish various corrosion mechanisms supporting the previous models. They establish concepts of NDE, localised corrosion, influence of alloy composition, galvanic corrosion and stress corrosion cracking. They further suggest a way of measuring the amount of hydrogen evolved during the corrosion process estimating the loss of material due to corrosion. The effect of secondary phases in the alloying structure has also been discussed.

Atrens *et al* [44] says that there is a lot of interest in the "negative difference effect for magnesium corrosion". The author tries to establish the concept of 'uni-positive Mg^+ ion' and tries to seek evidence for the possible lifetime of Mg^+ which might exist

between metallic Mg and Mg^{++}. Atrens *et al* [44] suggests that it will be useful to carry out various experiments to determine the anodic corrosion of magnesium alloy in different aqueous solutions measuring characteristics such as loss of magnesium alloy, amount of hydrogen evolved and the quantity of Mg^{++} ions present in the solute at the end of the experiment.

Ghali *et al* [45][46] discusses in detail about the various magnesium alloy systems, their compositions, microstructural properties, casting processes, and corrosion mechanisms. He discusses the impact of the above mentioned factors on the general and localised corrosion mechanisms. They support previous researches suggesting that the poor corrosion performance of magnesium alloys resulted in galvanic corrosion which may have caused due to the secondary phases and impurities present in the alloy. Further factors such as environmental conditions, pH, agitation, oxygenation etc have been discussed in detail and appropriate electrochemical reactions have been suggested. Finally corrosion testing and the impact of measurement in order to design a corrosion resistant magnesium alloy have also been suggested.

A research carried out by Zanotto [10] focussed on the corrosion behaviour and methods to prevent corrosion & surface treatments in AZ31 magnesium alloys. The research describes in detail the corrosion behaviour of AZ31 alloy. The research explored the factors influencing corrosion, various corrosion mechanisms, effect of microstructure and protective coatings. The author concluded that the corrosion resistance of the alloy depended on the casting method as each method resulted in a different distribution and composition of phases. The corrosion reaction, the cathodic behaviour, the anodic behaviour, effects such as the 'Negative Difference Effect (NDE)' [10][11] have been defined in detail to establish the corrosion mechanism of AZ31 alloy. The author speculates that the corrosion behaviour of the AZ31 alloy is dependent on the characteristics of the oxide film layer formed on the surface of the alloy which behaves as a passive layer there by generating localised corrosion centres when exposed to corrosive environment. It was also noticed that when the aluminium content reaches 8% (by mass), the corrosion performance of the alloy improves. It is also highly likely that this presence of aluminium has a strong tendency to form the passive film. As literature suggests, magnesium is a passive metal and hence pitting corrosion is evident. However the presence of secondary

phase is what governs the corrosion behaviour of the alloy. This proves the fact that the principle alloying elements have a huge impact on the corrosion behaviour of AZ31 alloy.

It has been reported that the β-phase of AZ91 alloy acts as a corrosion barrier in one literature [10] where as the contrast also exists. This is dependent on the distribution of the β-phase particles present in the alloy (AZ91). On measurement of the current density of both the α & β phases, the corrosion current density was much lower for the β-phase in comparison with the α-phase. Thus it was noticed that the β-phase acted as a galvanic cathode accelerating the corrosion process when the concentration of the alloying elements in the β-phase was low and acted as an anodic barrier when the concentration of the alloying elements in the β-phase was higher.

Song et al [47] conducted a study on the effect of various treatments including heat treatment on the corrosion characteristics of magnesium alloy AZ31 sheets. As received the AZ31 sheets were found to have poor corrosion characteristics which improved on surface grinding and acid cleaning. However sandblasting deteriorated the corrosion performance. The authors suggest that this could be because of the ferrous impurities present on the surface. Further when the alloy was subjected to heat treatment, the rate of corrosion increased. This performance was influenced by the change in grain size and the presence of inter-metallic particles along the grain boundary.

Research on the effect of solution treatment and ageing of Mg-3Zn magnesium alloy was published by Liu at al [48]. During the solution treatment of Mg-3Zn, the zinc elements completely dissolved in the α-Magnesium matrix and started to reappear as fine layers along the grain boundaries during ageing. Corrosion analysis showed that the solution treatment improved corrosion resistance of the alloy where as the rate of corrosion increased due to ageing. The authors suggest that this deterioration in corrosion performance during ageing is due to the reappearance of zinc particles in the precipitate along the grain boundaries.

In a previous study by Lunder et al [49], corrosion performance of mold-cast AZ91 magnesium alloy was monitored for as received, solution treated and age hardened condition. A standard corrosion analysis by immersing the samples in 5% NaCl solution for 24 hours and then determining the weight loss of material was carried

out. It was seen that the rate of corrosion was slow in the case of artificially aged sample in comparison to the as received and solution treated samples. It was noticed that the aluminium rich cores in the β-precipitate was highly anodic thereby preventing corrosion in those areas. This meant that the magnesium rich α-matrix behaves as a cathode there by corroding readily. This would possibly explain the slow corrosion rate of aged sample in comparison with its counterparts where the β-particles were unevenly distributed in the as received condition and the absence of aluminium rich cores in the homogeneous solution treated condition. The authors concluded that the corrosion resistance seen in the alloy as a result of heat treatment was dependent on the β-phase and magnesium acted as a strong cathode in the presence of aluminium which also added to the poor corrosion resistance of the alloy.

Corrosion studies on magnesium alloy AZ91 were carried out using corrosion maps which represented the 'electrode potential' and 'chlorine concentration' [50]. Wang et al [50] carried out the investigation on the behaviour of AZ91 in dilute NaCl solutions. It was noticed that the corrosion was dominant in the α-phase which was magnesium rich and the intact boundary was composed of β-phase particles. This is because of the more 'negative free corrosion potential' of the primary α-phase particles. It was noted that the corrosion rate could be influenced by the micro-galvanic coupling between the primary and secondary phases. It was also noticed that chlorine ion (Cl^-) had a great tendency to penetrate the hydroxyl film layer thereby influencing the rate of corrosion in turn resulting in the formation of a passivation zone. There was formation of surface films in these passivation zones, which later became local centres of corrosion thereby increasing the overall rate of corrosion. The surface morphology patterns confirmed the presence of various corrosion products in the surface film in the corroded area.

The above literature clearly indicates the need to carry out corrosion studies on light weight alloys to understand the performance characteristics of these modern, light-weight magnesium alloys with the help of modern techniques such as Scanning vibrating electrode technique (SVET) which in turn will help aid effective utilization of these alloys. Reduction in weight will in turn save energy and reduce emissions in the transport industry.

3. EXPERIMENTAL TECHNIQUES

The current research deals with different experimental techniques to study and induce changes in characteristics of commercially available magnesium alloys and monitor the changes effectively by various tools. Similar experimental techniques have been used for the characterization of magnesium alloys AZ31, AZ91 and ELEKTRON 21.

The chemical composition of AZ31 alloy as described by Zhang et al [51] is as follows. (Table 3.1)

Table 3.1 Chemical composition of AZ31 magnesium alloy (wt %) [51]

Al	Zn	Mn	Si	Fe	Cu	Ni	Mg
3.2	0.11	0.30	0.014	0.0015	0.0021	0.0009	Balance

The chemical composition of AZ91 alloy as obtained by Lunder *et al* [49] is as follows (Table 3.2)

Table 3.2 Chemical composition of AZ91 alloy as obtained by spectrographic analysis (wt %) [49]

Al	Zn	Mn	Si	Fe	Cu	Ni	Mg
8.6	0.73	0.17	0.02	0.009	0.001	0.001	Balance

The chemical composition of Elektron21 alloy is as follows (Table 3.3) [5]

Table 3.3 Chemical composition of Elektron 21 alloy (wt %) [5]

Gd	Nd	Zr	Zn	Mn	Fe	Ag	TRE	Mg
1.2	2.7	0.49	0.4	0.001	0.003	0.01	4.2	Balance

Where

Al – Aluminium

Zn – Zinc

Mn – Manganese

Si – Silicon

Fe – Ferrous

Cu – Copper

Ni – Nickel

Mg – Magnesium

Gd – Gadolinium

Nd – Neodymium

Zr – Zirconium

Ag – Silver

TRE – Traces of other rare earth materials

These experimental evaluation techniques have been described in the current chapter.

3.1 MICROSTRUCTURAL EVALUATION

Microstructural evaluation or Metallography forms the first step in the characterization of the alloys. There are two stages involved in evaluating the microstructure of the specimen. They are surface preparation and microscopy analysis.

3.1.1 SURFACE PREPARATION

This research involved the use of samples cut from alloy ingots. The process involved use of sand papers of various grit sizes (265μm, 100μm, 20μm) for coarse to fine grinding of the sample surface. Then the sample was subjected to polishing using polishing wheels. Initially a 5 micron (μm) paste was used to polish until most of the visible scratches disappeared. It was then polished with a 1 micron (μm) paste to get a high quality polish / mirror finish to the surface. Care was taken to use different polishing wheels in order to prevent further scratching on the sample due to particle size of the polishing paste and lubricating oil was used during polishing. The finished sample surface was washed with a detergent to remove any particles which were still stuck to the specimen and was cleaned with ethanol / acetone immediately to remove any water / moisture being left on the surface of the sample. The sample was dried immediately by a blower. This ethanol / acetone wash was done to prevent tarnishing patters appearing on the polished surface as magnesium has a high affinity to moisture and starts tarnishing at a rapid pace. Care was taken not to touch the

polished surface of the sample as fingerprint impression could easily appear on the surface of the sample.

3.1.2 MICORSCOPY

The finished sample was then used to determine the microstructure mainly using Reichert Jung MeF3 optical microscope with Olympus E330 camera. The sample is placed in the aperture of the microscope table with the polished surface facing downwards. This is a unique microscope which used a fine light beam to focus onto the polished surface of the specimen. The Reichert MeF3 microscope has a very low magnification (x2) and also has option to look at the micrograph / microstructure at different viewing modes. The images were captures using an Olympus E330 camera.

3.2 TIME LAPSE PHOTOGRAPHY EXPERIMENT

The time lapse photography gave a good estimation of the corroded area there by giving an insight to the amount of metal loss. A sample with a known, exposed area was immersed in 5 percent Sodium chloride (NaCl) solution[1]. A camera was set above the immersion and photographs were taken on a continuous basis at regular intervals.

The sample was polished as per the details mention in the previous section. (Refer Section 3.1) The sample was then covered with a PVB tape exposing only a small section of 5mm × 5mm (25 mm^2). The sample was firmly attached to a Petri dish and was filled to the top with the 5 percent sodium chloride solution. The Petri dish with sample was placed under a Nikon D70S SLR camera (Figure 3.1). The camera was set to a time lapse mode controlled by the computer and magnified pictures were taken at intervals less than 5 minutes (Figure 3.2).

[1] A 5 percent sodium chloride (NaCl) solution is prepared by dissolving 50 grams of NaCl in 1 litre of distilled water.

Figure 3.1 Experimental setup of time lapse photography with the Petri-dish in the bottom and the camera lens directly over it.

The images obtained from the camera were analysed using Sigma Plot software. The corroded area was highlighted using Photoshop and the highlighted area was calculated using Sigma Plot.

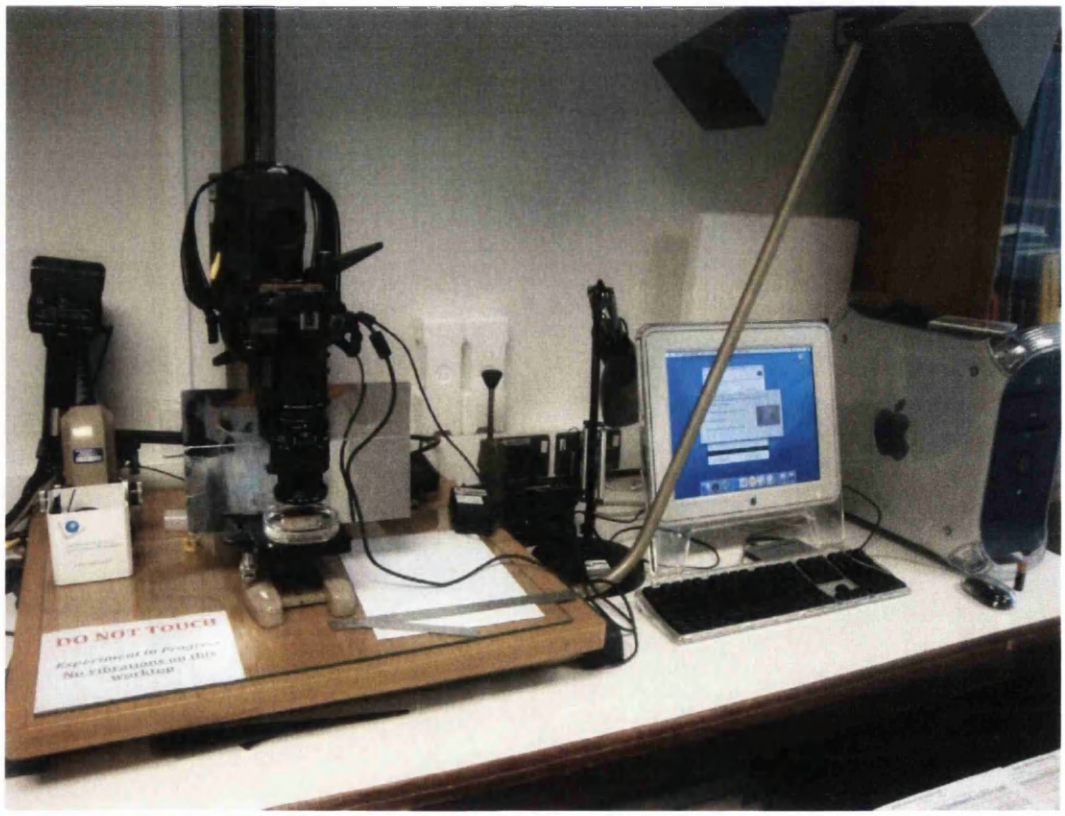

Figure 3.2 The experimental setup of time lapse photography

3.3 HYDROGEN EVOLUTION EXPERIMENT

The hydrogen evolution techniques helped to quantify the amount of hydrogen evolved which in turn was used to estimate the loss of metal. The sample was polished as per section 3.1 and was taped up with the PVB tape. An area of 30mm × 30mm was exposed and the sample was taped in a 250ml beaker. A funnel was placed on top of the sample inside the beaker with the wide mouth of the funnel covering the exposed area and the beaker was filled with 5 percent sodium chloride solution (Figure 3.2). A burette filled with the sodium chloride solution was inverted and placed such that the stem of the funnel was inside the burette opening and was clamped to a stand. An initial reading on the burette was noted. As the surface of the sample broke down, hydrogen evolved in the form of small bubbles. These bubbles rose along the inner walls of the funnel through the stem of the funnel and into the burette. The volume of hydrogen was measures as cubic centimetre over a period of 24 hours. For ELEKTRON 21, since the corrosion rates were slow, a time lapse camera was used to take pictures of the burette reading. The readings were tabulated with respect to time and estimated accordingly.

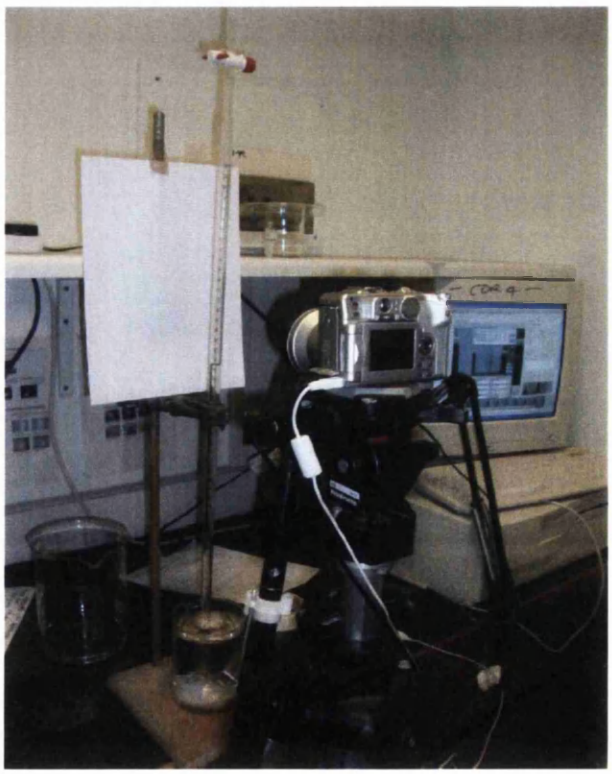

Figure 3.3 The experimental setup for a hydrogen evolution experiment

3.4 SCANNING VIBRATING ELECTRODE TECHNIQUE

As the name suggests the scanning vibrating electrode technique consists of a probe vibrating mechanically moving at a set frequency, height and amplitude over a sample immersed in an electrolyte. The probe senses the current density over the sample surface along the direction of vibration which is generated due to the current flowing in the electrolyte. Thus the amplitude of the vibrating head is directly proportional to the current density in the solution. The SVET has the ability to detect cathodic and anodic currents. The change in current density due to corrosion is picked up by the probe and its comparison with the natural vibrating frequency of the probe gives the actual current density of the corrosion process. This is represented by surface plots in the Surfer 8^{TM} software.

Due to its robust nature SVET has found specific uses including steel, power and aerospace industries for corrosion investigations. Extensive corrosion investigations have been carried out to link microstructural changes [52][53], steels that are coated organically [54][55] with corrosion.

The scanning vibrating electrode technique apparatus consists of the following parts,

1. Motor stage – controlling the movement of the SVET head in all the 3 directions, X, Y and Z. The motor moves at steps of 2.5μm. A trip switch is in place if the motor stage moves to the end of their travelling limit. Care should be taken so that ample travelling distance is provided for the stage head to move.

2. Motor box – is the main source of power to the motor stage and integrates computer control to the motor stage.

3. SVET head – houses the platinum vibrating probe and the speaker. There are two connectors that pass signals to the probe, a 3 way panel plug from the top controlled by the height scan box and tip and SMC converter to the side sending data to the data scan box. A reference electrode is attached to the body of the head and this electrode must be in the electrolyte at all times during the test.

4. SVET tip – is housed in the SVET head and is attached to the push rod from the speaker by a Teflon holder.

5. Amplifier – provides signal from the lockin inorder to vibrate the tip.

6. Data scan box – receives signals from the SVET tip from the SMC connector.

7. Height scan box – is used primarily to do height scans
8. Lockin amplifier – controls the vibration of the SVET tip. It also receives and processes signals from the SVET tip.

The SVET uses a specific software called SVET 3D to operate the apparatus. The sample to be tested is polished as per section 3.1.1. An area of 10 mm × 10 mm is exposed and the remaining sample is taped. This sample is set on to a sample table and is placed in the bath. Now, the sample is levelled and a height scan is performed to check the level of the sample. The software is used to input all the necessary dimensions and number of scans needed in order to carry out the test. Then the prepared 5% NaCl salt solution is introduced into the bath and the experiment is started. As the electrochemical reaction starts, the electrode potential difference at each point on the exposed area of the alloy is measured and stored in the computer in the form of grid files. These grid files are then processed using the calibration data obtained prior to the test.

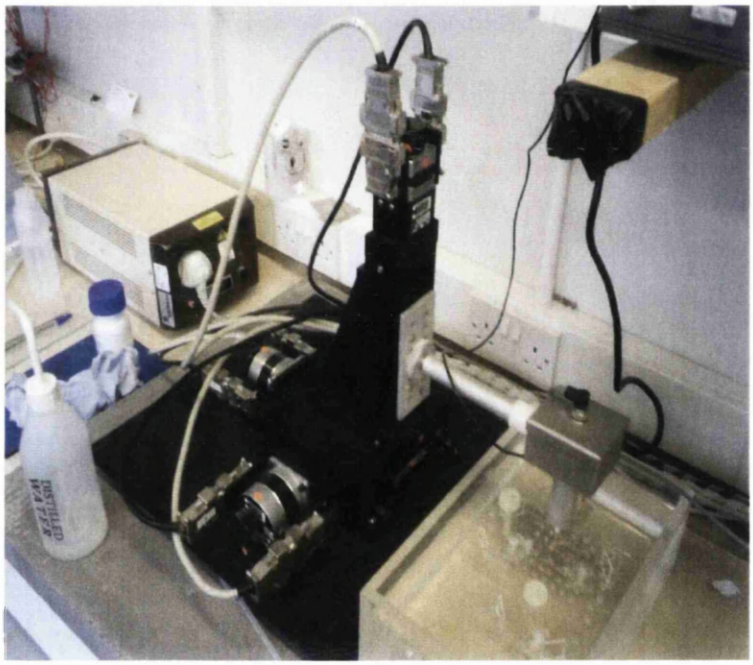

Figure 3.4 The experimental setup of Scanning Vibrating Electrode Technique. Source Swansea University website*.

The sample calibration graph was obtained by running the apparatus with a galvanometer prior to introducing the sample to be tested. This processed data in grid form gives the relative current data plot of the sample. The data is now assessed using Surfer to calculate the anodic summary thereby determining the approximate loss of material in gm/m^2.

The following graph is the calibration graph used to process the SVET data obtained as Grid note files from SVET 3D software.

* Source: www.swan.ac.uk/engineering/materials/research/corrosionandcoatings/scanningelectrochemicaltechniques/

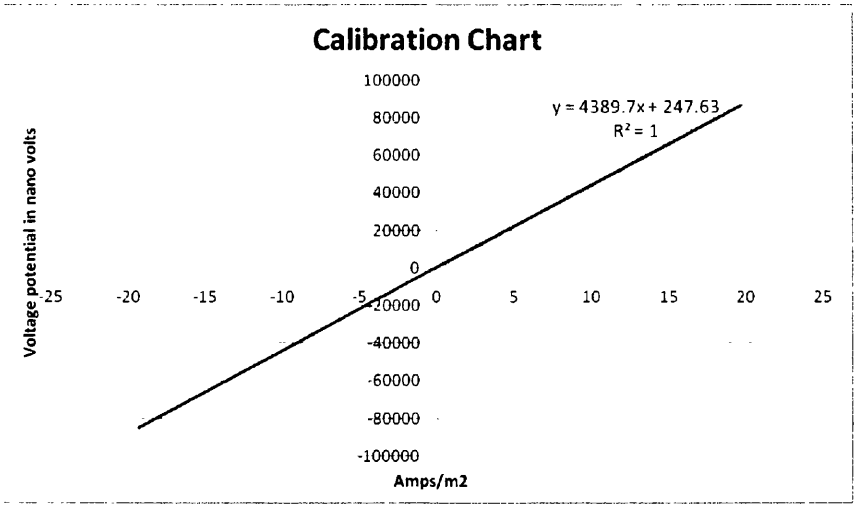

Figure 3.5 Calibration plot for SVET analysis – SVET Tip Frequency : 0.04V RMS

For the analysis of SVET data, the instrument must be calibrated periodically in order to monitor the change in measured voltage before the sample is introduced for testing. In order to check the voltage response of the equipment, controlled applied current densities are compared with the help of a tea pot cell. When there is a flow of current in the electrolyte, a voltage density is picked up by the vibrating tip. Now the positive electrode is connected to the galvanostat and the introduced into the tea pot cell in the elctrolyte bath. The negative electrode is intrduced into the bulk electrolyte. The SVET tip is lowered into the orifice of the spout of the tea pot cell and the tip is made to vibrate at 0.04V RMS. Now the galvanostat is used to increase the current and the voltage response is recorded from the lockin amplifier. The process is repeated after reversing the cathode anode electrode in the electrolyte and tea pot cell and recorded. The obtained is represented in the form of the above graph. The slope of the plot gives the calibration factor which is used to process the data obtained from the SVET analysis with test sample.

The SVET system however has limitations [56]. It should be noted that the data obtained from the SVET is semi-quatitative due to the following assumptions

- The mass loss data is not a directly associated with the sample weight loss as a number of assumptions were made during the integration process[56].
- The corrosion activity is considered to be constant between scans though it is not the case in reality[56].
- The resolution is 1.5 times the scan height of 100μm [56] and will not detect cathodes and anodes less than this stated distance.

3.5 HEAT TREATMENT

Heat treatment both solution treatment and age hardening were performed on all the 3 alloys viz., AZ31, AZ91, ELEKTRON 21. Heat treatment was performed in a high temperature furnace. The samples to be treated were cut into smaller pieces and were placed in a ceramic crucible at the centre of the furnace. As the solution treatment temperatures were high, the samples were covered with carbon black powder in order to prevent oxidation tracks and pits appearing on the surface of the metal. The AZ31 and AZ91 were subjected to solution treatment at 395°C (as per ASTM handbook) [57] for about 20 hours until the β-phase completed disappeared. This was checked using the Reichert Jung MeF3 imaging microscope after polishing the sample as described in earlier sections. The corrosion tests, viz., Time lapse photography, Hydrogen evolution experiment and SVET surface maps were performed on the solution treated alloys. Then the solutionized samples were aged for about 48 hours at a temperature of about 175°C. The microstructural investigation and corrosion analysis was repeated on the aged alloys as mentioned in the previous sections.

ELEKTRON 21, due to its rare earth – zirconium combination was solutionized at about 520°C [6][7] for about 12 hours to dissolve the eutectic phase of the alloy structure (β-phase). And the age hardening process was carried out at about 200°C at two different time periods. One was continuous ageing for 16 hours to attain peak ageing condition and the second was a continuous ageing for 48 hours for attaining over-aged condition [6][7]. Both the ageing processes are carried out so that the precipitates reappear in the grain structure and then allowed to grow. Rapid quenching thus helps in restricting the scarcely distributed precipitates along the grain boundaries which will help identify an appropriate treatment process for better corrosion properties of the alloy. The treated alloys were subjected to both Microstructural evaluation and corrosion investigation similar to the AZ31 and AZ91 alloys.

It should be noted that all the alloys after different heat treatments were quenched in cold water immediately in order to retain the microstructural features at respective temperatures preventing the appearance of β-phase.

4. RESULTS AND ANALYSIS

This chapter deals with the results obtained as a result of various experiments performed on magnesium alloys AZ31, AZ91 and ELEKTRON 21

4.1 MAGNESIUM ALLOY AZ31

Magnesium alloy AZ31 is made up of 4.52% Al, 0.24% Zn, and the remaining being magnesium. This data was obtained from Energy Dispersive X-ray spectroscopy analysis to determine the composition of the alloy. The following spectrum (Figure 4.1) obtained from EDX spectroscopy using JOEL 35C SEM

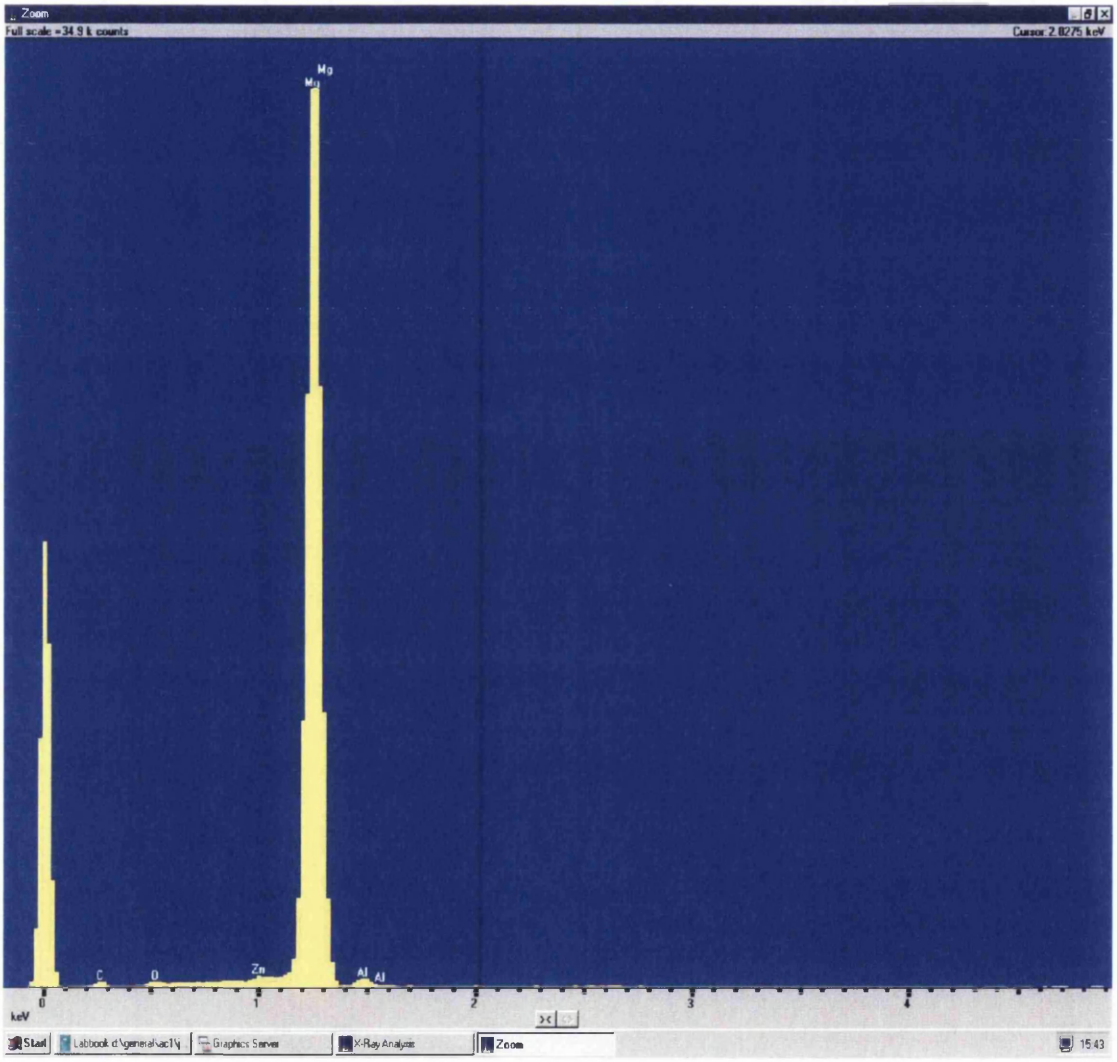

Figure 4.1 EDX Spectrum of AZ31 alloy (as received) at a magnification of ×1000

The EDX spectrum shows the peaks in accordance with the composition with maximum peak as Magnesium (Mg). It can also be seen that Aluminium and Zinc are present in smaller portions thus confirming the composition of AZ31 alloy. The following is the data generated from the EDX system,

==========

SEMQuant results. Listed at 15:04:20 on 04/02/10
Operator: Peter Davies
Client: EDX analysis
Job: Job number 47 - Dec09
Spectrum label: AZ31 x1kma medium area
System resolution = 61 eV
Quantitative method: ZAF (3 iterations).

Analysed all elements and normalised results. 3 peaks possibly omitted: 0.00, 0.26, 0.52 keV

Standards :

Mg K	MgO 01/12/93
Al K	Al2O3 23/11/93
Zn K	Zn 01/12/93

Elmt	Element %	Atomic %
Mg K	94.38	95.23
Al K	4.97	4.52
Zn K	0.65	0.24
Total	100.00	100.00

* = <2 Sigma

It should be noted that the data obtained from the EDX is in comparison with the element with the highest atomic number and is merely a qualitative representation of the elemental configuration. It does not give the exact chemical composition of the material under study.

4.1.1 MICROSTRUCTURAL EVALUTION

Fig. 4.2 shows the micrograph of AZ31 obtained by Watanabe *et al* [58]. The microstructure of AZ31 is made up of recrystallized grains with equal axial length of the crystals.

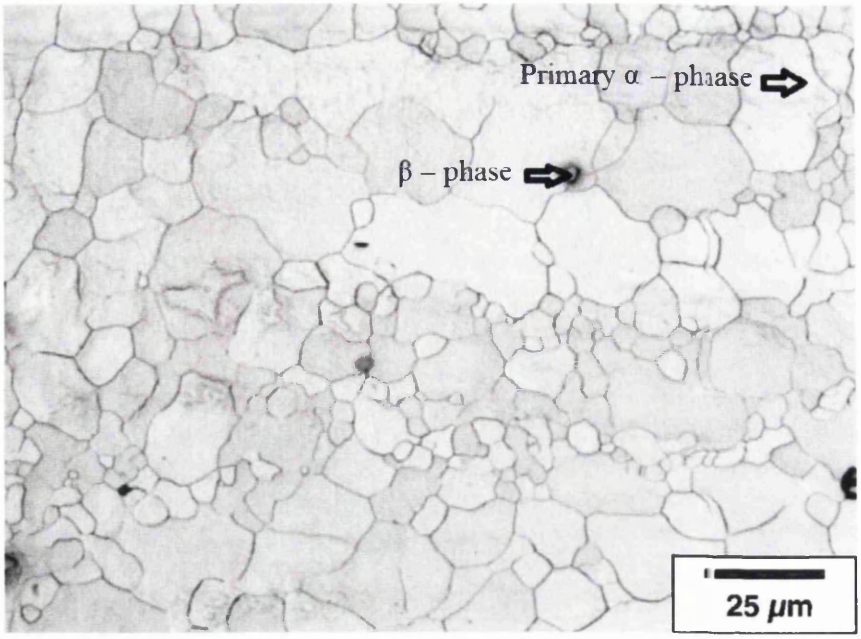

Figure 4.2 The micrograph of as received AZ31 without heeat treatment.

Source: *Watanabe et al* [58]

It was noticed that the β-phase particles were distributed along tthe grain boundaries. This meant that the lower performance of the alloy, the mechaanical characteristics would be poor. This could be because of such inter-dendritic acccumulation of the β-phase along the grain boundaries of the alloy.

4.1.2 TIME LAPSE PHOTOGRAPHY EXPERIMENT

The time lapse photography for AZ31 alloy without any heat treeatment was initiated. The following are the pictures (Figure 4.3 (a) – (f)) of AZ31 without any heat treatment. The sample with an exposed area of 25 mm^2 (5mm × 5mm) was placed in a Petri-dish and filled with 5% NaCl salt solution.

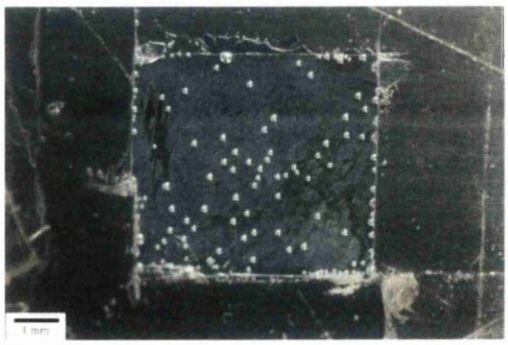

Figure 4.3 (a) At Time = 0 minutes

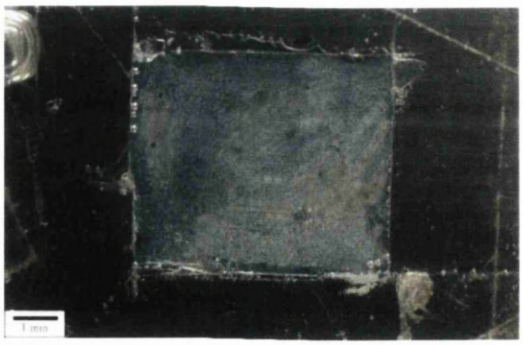

Figure 4.3 (b) At Time = 5 minutes

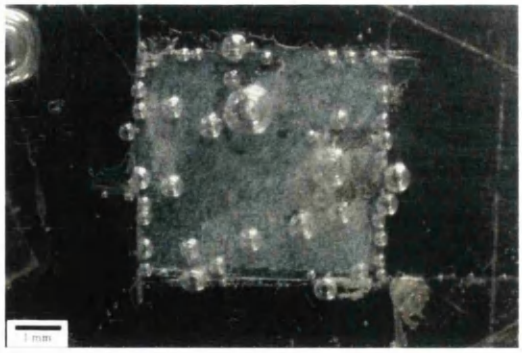

Figure 4.3 (c) At Time = 30 minutes

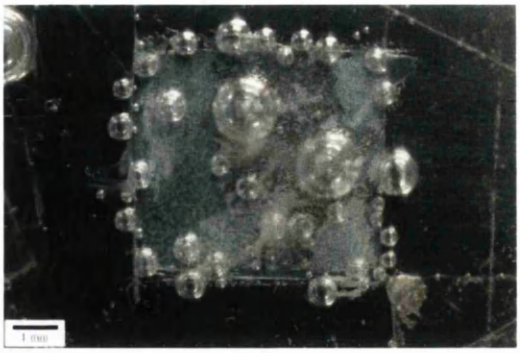

Figure 4.3 (d) At Time = 1 hour

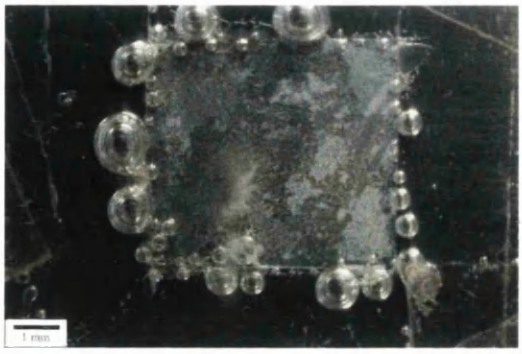

Figure 4.3 (e) At Time = 2 hours

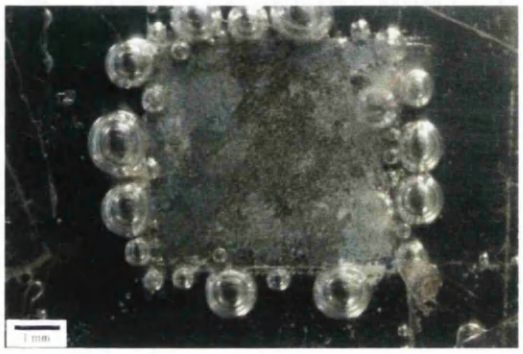

Figure 4.3 (f) At Time = 3 hours

Figure 4.3 (a) – (f) Time lapse experimental data of as received AZ31 alloy.

Figure 4.3 (a) is the picture taken at the start of the time lapse experiment. It can be inferred from the figure 4.3 (b) that a thin white oxide layer has been formed. A magnified picture of figure 4.3 (b) revealed that there was a distinctive pattern of the white layer which could be interpreted as oxide layer formed due to the electrochemical reaction. It was also noticed that the appearance of the oxide layer was instantaneous within 5 minutes from the start of the experiment.

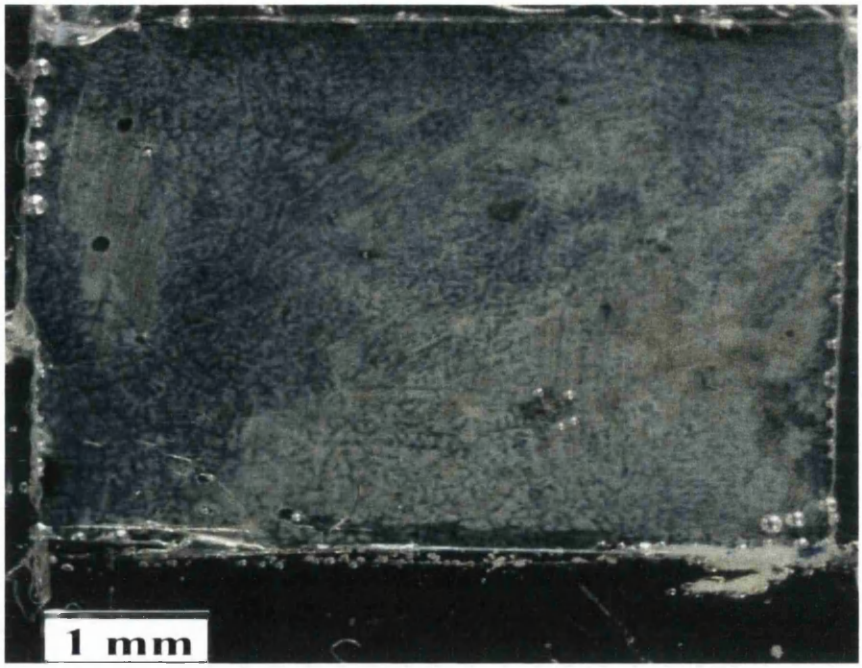

Figure 4.4 The magnified picture of Figure 4.3 (b)

Further it was noticed that the surface breakdown was instant and the rate of corrosion was rapid within the first 30 minutes of the start of the experiment. This was inferred from Figure 4.3 (c). From then onwards, there was formation of localized corrosion centres which followed the pattern along the surface area of the exposed sample. These localized corrosion centres could be seen in the form of big bubbles formed as a result of a stream of small bubbles on the surface of the alloy. These bubbles are due to the electrochemical reaction of the salt solution and the alloy. It was noticed that the corroded part stayed dormant for a while and then started corroding again on further formation of oxide layer. (Refer to Figure 4.3 (e) and Figure 4.3 (f)).

The time lapse experiment was repeated for solution treated and a fully aged AZ31 alloy. The following are the images obtained for the solution treated and age hardened samples of AZ31 alloy.

SOLUTION TREATED AZ31

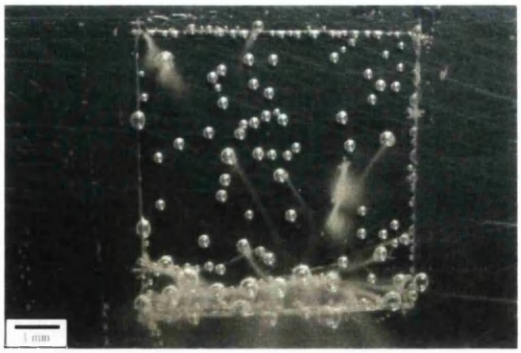

Figure 4.5 (a) At Time = 0 minutes

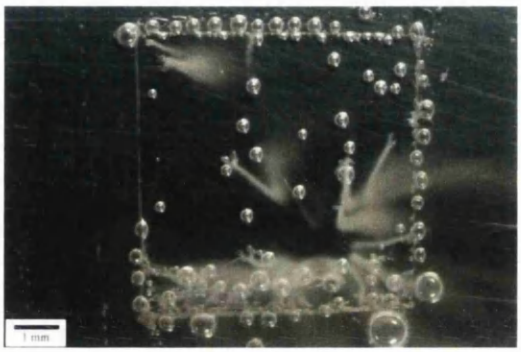

Figure 4.5 (b) At Time = 2 minutes

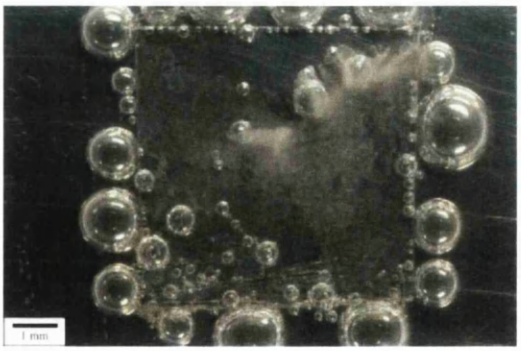

Figure 4.5 (c) At Time = 1 hour

AGE HARDENED AZ31

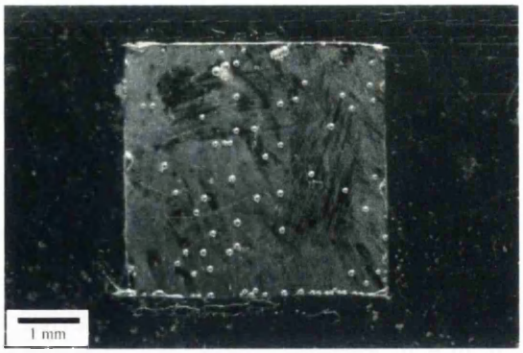

Figure 4.6 (a) At Time = 0 minutes

Figure 4.6 (b) At Time = 10 minutes

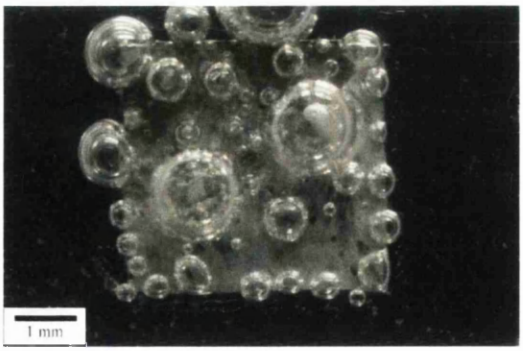

Figure 4.6 (c) At Time = 1 hour

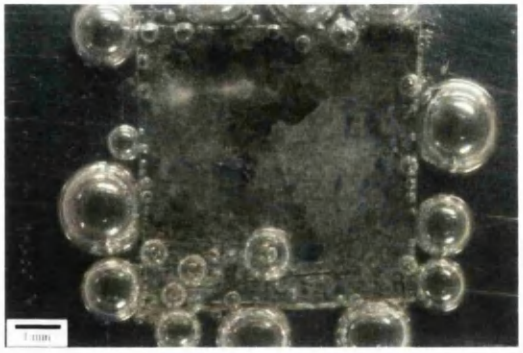

Figure 4.5 (d) At Time = 2 hours

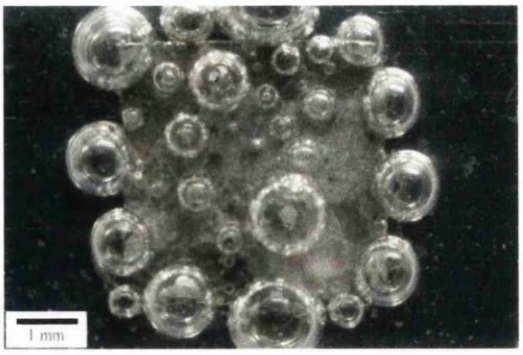

Figure 4.6 (d) At Time = 2 hours

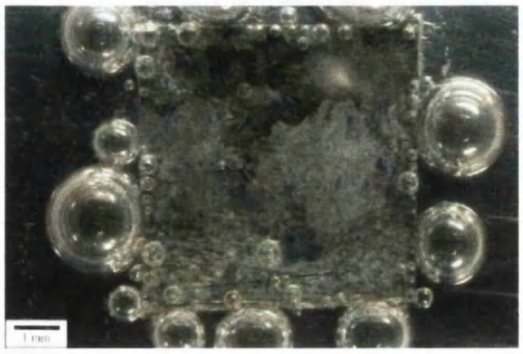

Figure 4.5 (e) AT Time = 3 hours

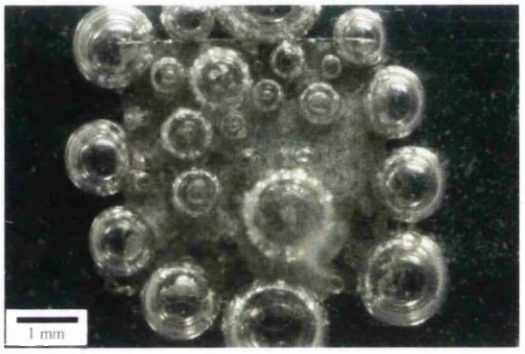

Figure 4.6 (e) At Time = 3 hours

Figure 4.5 (a) – (e) Time lapse images of Solution treated AZ31 alloy
Figure 4.6 (a) – (e) Time lapse images of Fully aged AZ31 alloy

It can be seen in Figure 4.5 (a) the electrochemical reaction between the AZ31 solution treated sample and 5% NaCl solution is initiated immediately. The first visible surface breakdown occurs within 2 minutes of start of the experiment (Fig. 4.5 (b)). On the other side, it takes about 10 minutes for the age hardened AZ31 sample for the surface to breakdown. It should be noted that the solution treated sample reacts quickly and corrodes the area completely within a few hours (Figure 4.5 (a) – (e)). And on the other hand, the age hardened sample corrodes steadily and takes a bit longer to corrode completely (Figure 4.6 (a) – (e)). In both case, it can be seen that formation of localized corrosion spots appear at various parts of the exposed area.

4.1.2.1 SIGMA PLOT ANALYSIS

The images obtained from the time lapse photography was used in determining the approximate corroded area. As mentioned in section 3.2, the corroded area was highlighted using Photoshop. The corroded area of the sample at various time intervals was determined using Sigma plot. The following is the data obtained from Sigma plot.

Table 4.1 The corroded area of AZ31 under different heat treatment conditions over a period of 5 hours evaluated using Sigma plot

Time in hours	Corroded area in $\times 10^{-5}$ m^2		
	AZ31 as received	AZ31 Solution treated	AZ31 Age Hardened
0	0	0	0
0.033		0.137	
0.05	0.0021		
0.25			0.22
1	0.41	1.85	1.68
2	1.22	2.15	2.19
3	1.49	2.01	2.38
4	1.83	2.2	2.36
5	2.05	2.27	2.4

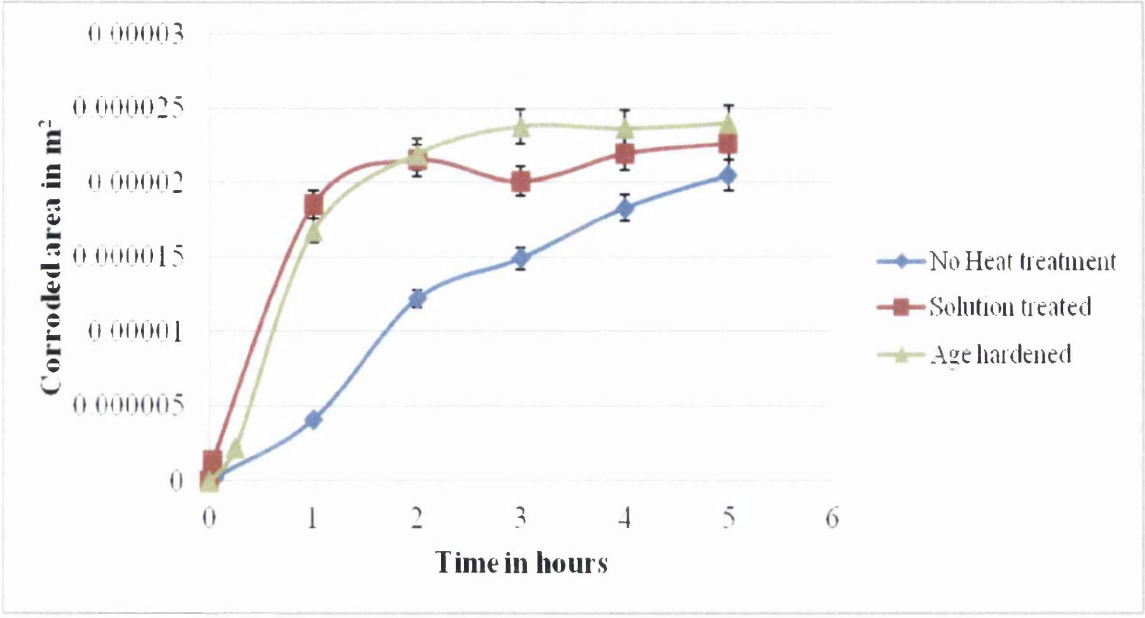

Figure 4.7 – Graph showing rate of corrosion expressed in terms of corroded area evaluated using Sigma Plot

The above graph (Figure 4.7) shows the rate of corrosion for AZ31 alloy with and without heat treatment. It can be seen that the rate of corrosion is quite steady in case of AZ31 without any heat treatment where as the solution treated and the age hardened samples of AZ31 corrode quite quickly.

4.1.3 HYDROGEN EVOLUTION EXPERIMENT

The AZ31 sample was subject to hydrogen evolution experiment. The experiment was set up as per section 3.3 from the previous chapter. An area of 30mm × 30mm was exposed to the 5% NaCl salt solution. The data obtained is in cubic centimetres and is converted into number of moles of hydrogen evolved using the ideal gas law formula.

According to ideal gas law,

$$n = \frac{P \times V}{R \times T} = \frac{1.01325 \times 10^5 \times V \times 10^{-6}}{8.314472 \times 293} = 4.1592 \times 10^{-5} \times V \text{ mol}$$

Where

n – Number of moles of hydrogen evolved (mol)

P – Pressure ($\times 10^5\ N/m^2$)

V – Volume of hydrogen collected in the burette (cm^3)

R – Gas constant ($J/K/mol$)

T – Temperature (K)

On substituting the value of V in cubic centimetres, we get the number of moles of hydrogen evolved. The following table gives the data obtained during the experiment in terms of number of moles of hydrogen evolved.

Table 4.2 Data obtained from hydrogen evolution experiment conducted on AZ31 alloy with and without heat treatment

Time in Hours	Hydrogen Evolved in $\times 10^{-5}$ moles		
	AZ31 as received	AZ31 Solution treated	AZ31 Age hardened
0	0	0	0
1		1.25	5.4
1.58	4.98		
2		4.15	12.04
2.78	11.21		
3		8.72	18.69
3.47	13.29		
4		12.04	22.84
4.75	14.95		
5		14.54	25.75
5.42	15.78		
6		16.4	27.82
6.5	17.03		
7		18.27	30.73
7.58	18.27		
8		19.93	32.81
8.85	19.93		
9		22.01	34.88

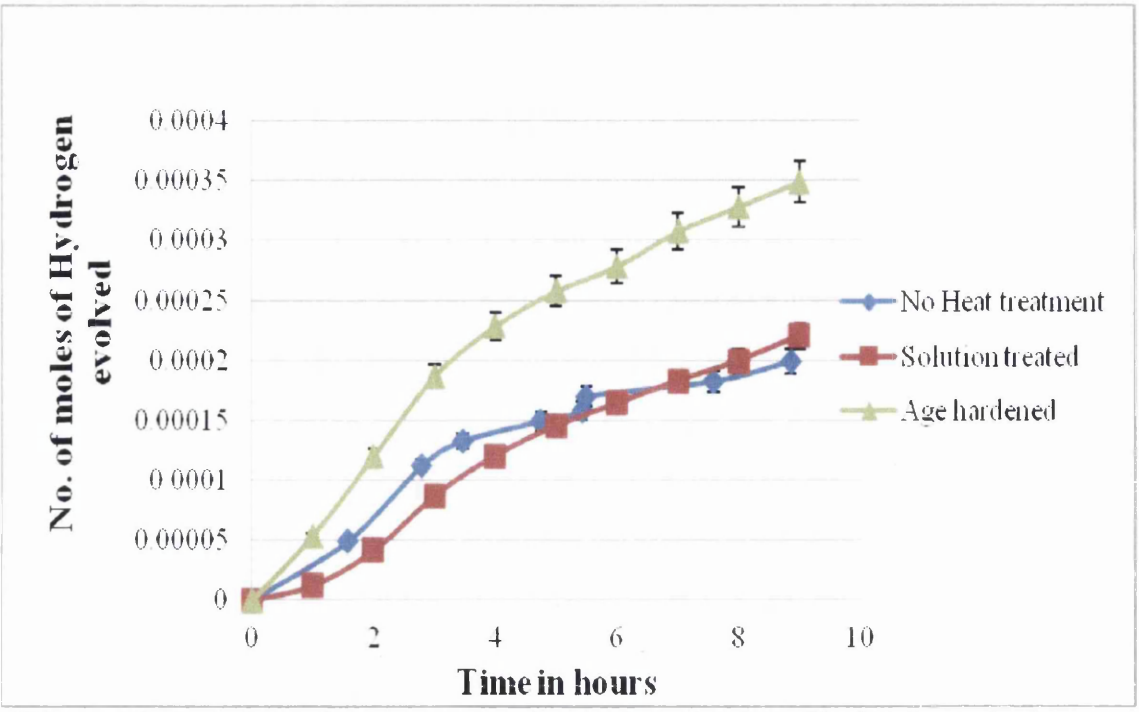

Figure 4.8 A graphical plot representing the number of moles of hydrogen evolved from an AZ31 sample

The tabular column (Table 4.2) and graphical plot (Figure 4.8) represents the amount of hydrogen evolved over a period of 9 hours. It can be seen from the above graph that an age hardened sample evolves more hydrogen than the sample without heat treatment and the sample with solution treatment.

4.1.4 SVET ANALYSIS

As per section 3.1.1, the surface of the sample was polished. A 10mm × 10mm area was exposed to 5 % NaCl solution in the salt bath as described in 3.5. The SVET apparatus was calibrated before the sample was subjected to testing. The experiment is initiated after the height scans were checked as per section 3.5.

Using the grid volume calculator in Surfer, the negative (cut) value was found from the data generated from SVET. This negative value represents the anodic current (in micro amps, μA) picked up by the SVET probe as the scan was initiated.

The loss of magnesium metal over the period of the experiment can be determined as follows,

1. The current per unit area is first determined.

$$MeanJ_a = \frac{J_a \times 1 \times 10^{-6}}{Area} A/m^2$$

Where J_a – is the anodic current value obtained from Surfer (μA)

$Area$ – Area exposed in During the SVET (m^2)

2. Then the average scan time T_{avg} of the experiment is determined using the following formula,

$$T_{avg} = \frac{T}{N} \times 60\ sec$$

Where T – Total time taken to finish the experiment (in minutes)

N – Total no. of scans

3. Now the anodic current is multiplied with the average scan time and divided by Faraday's constant to get loss of metal alloy in mol/m^2,

$$\text{Loss of material} = \frac{MeanJ_a \times T_{avg}}{F}\ mol/m^2$$

Where Mean J_a – Anodic current obtained in (A/m^2)

T_{avg} – is Avg. Scan time (sec)

F – Faraday constant (F = 96,500 $Coul/mol$)

4. Now the loss of magnesium can be determined in g/m^2 by multiplying the loss of material data obtained previously with the relative atomic mass of Magnesium (= 24.3 g/mol). It should also be noted that when the alloy corrodes it produces a Mg^{2+} and hence the value has to be divided by 2.

$$\text{Loss of material in } g/m^2 = \text{Loss of material in } mol/m^2 \times (24.3 / 2)$$

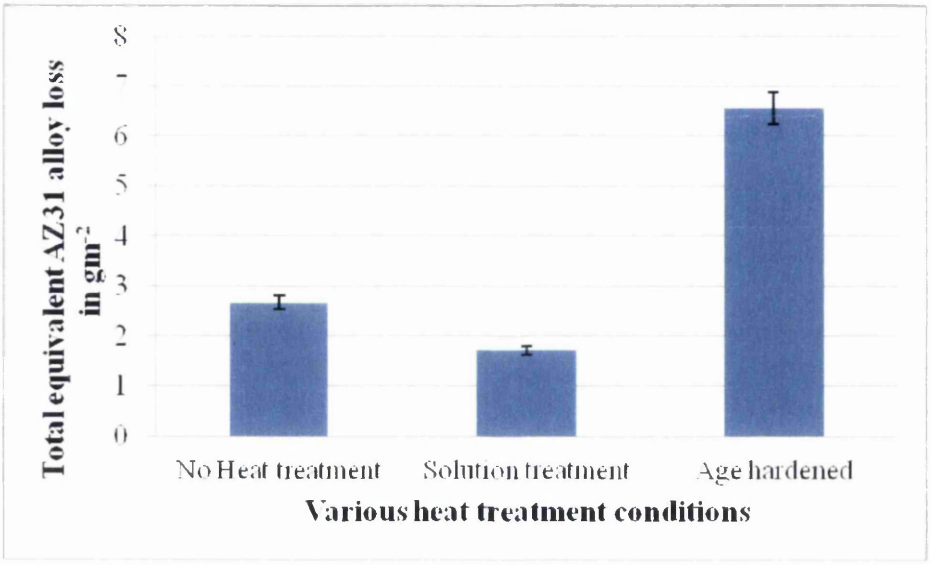

Figure 4.9 A bar chart showing the amount of AZ31 in g/m^2

Table 4.3 The loss of AZ31 under all heat treatment conditions

Heat treatment condition	Loss of AZ31 in g/m^2
No heat treatment	2.68
Solution treatment	1.73
Age hardened	6.56

The above data (Table 4.3) was obtained on processing the data from the SVET experiment. It can be seen that corrosion accelerates on age hardening as the amount of loss of AZ31 is high in comparison with its counterparts. Also the anodic current data from Figure 4.10 shows that the intensity of current generated during the electrochemical reaction is quite high in comparison with its counter parts. This corresponds to the loss of material data and the data from the hydrogen evolution experiment as mentioned in section 4.1.3.

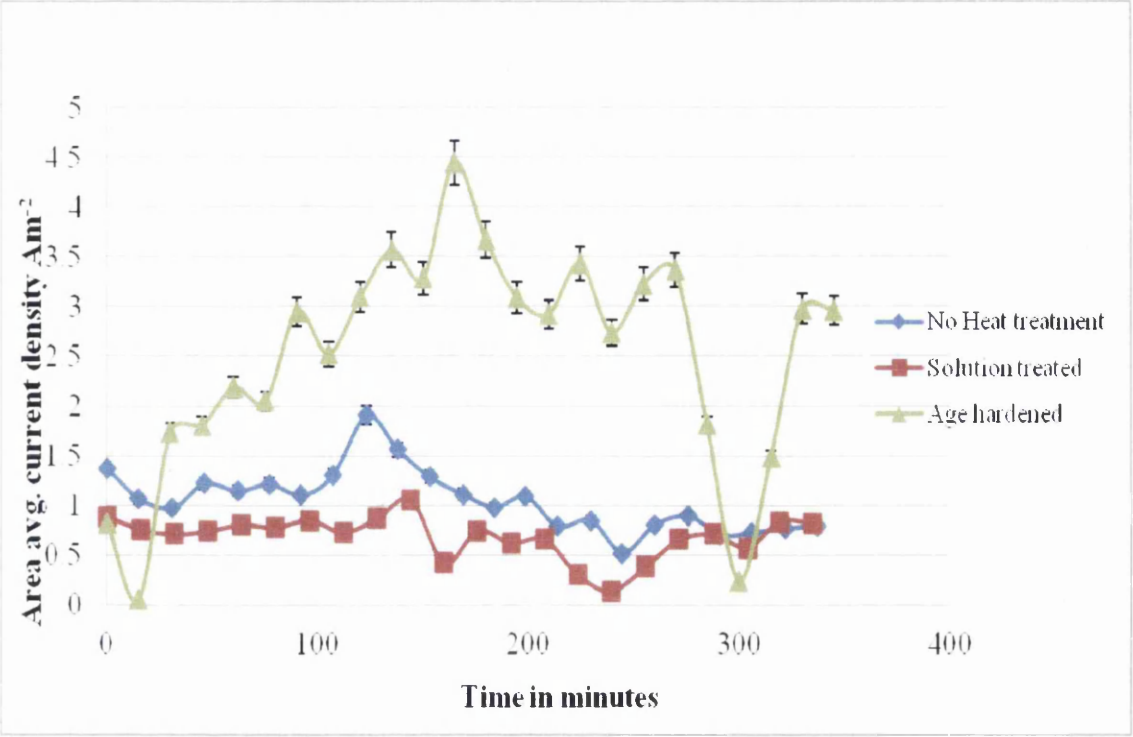

Figure 4.10 A graphical representation of the anodic obtained from SVET data using Surfer for AZ31

The data obtained from SVET can be represented in the form of surface maps.

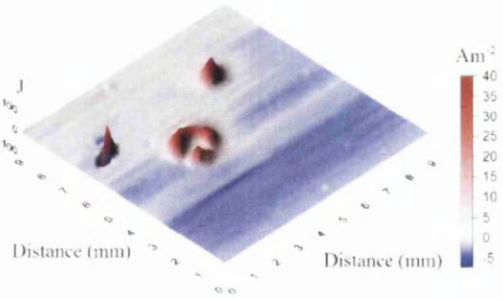

Figure 4.10 (a) At Time = 0 minutes

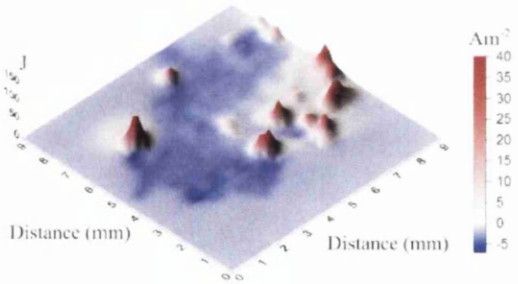

Figure 4.10 (b) At Time = 1 hour

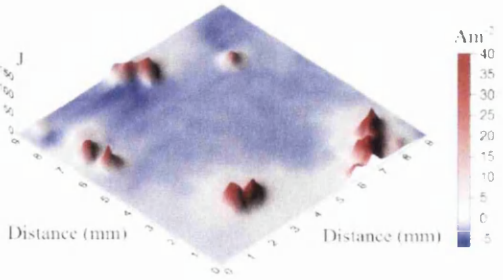

Figure 4.10 (c) At Time = 2 hours

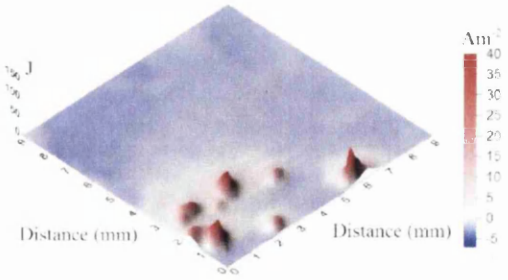

Figure 4.10 (d) At Time = 3hours

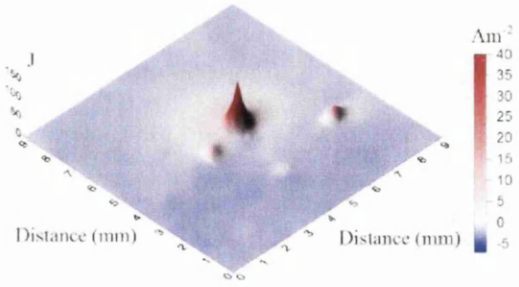

Figure 4.10 (e) At Time = 4 hours

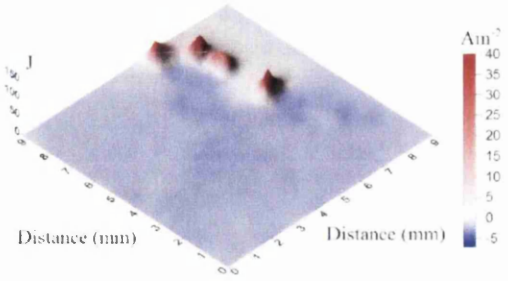

Figure 4.10 (f) At Time = 5 hours

Figure 4.10 (a) – (f) Surface map images of AZ31 from SVET analysis

Figure 4.10 (a) – (f) show surface maps of AZ31 without heat treatment. It can be seen that there are anodic peaks which represent the localized corrosion centres. These peaks are scattered all over the area. The image is colour coded. The peaks with red colour show the anodic reaction and the blue surface represents cathodic reaction. The SVET experiment was conducted on the samples with solution treatment and age hardening and the following images were obtained.

SOLUTION TREATED AZ31

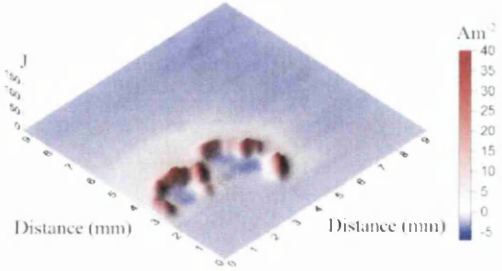

Figure 4.11 (a) At Time = 0 minutes

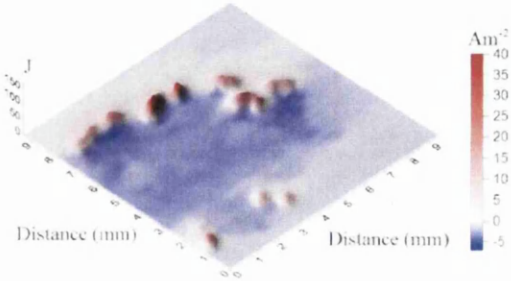

Figure 4.11 (b) At Time = 1 hour

AGE HARDENED AZ31

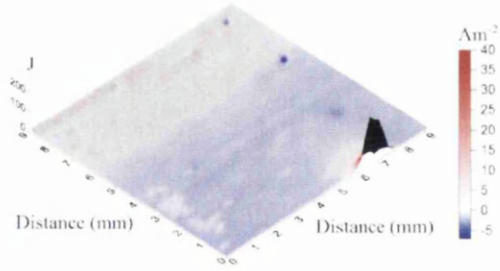

Figure 4.12 (a) At Time = 0 minutes

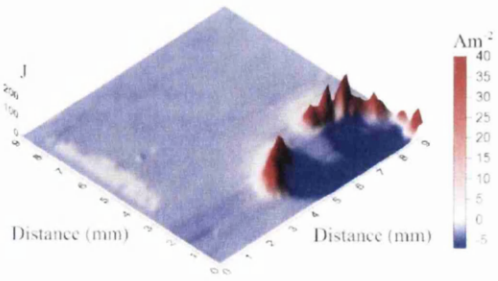

Figure 4.12 (b) At Time = 1 hour

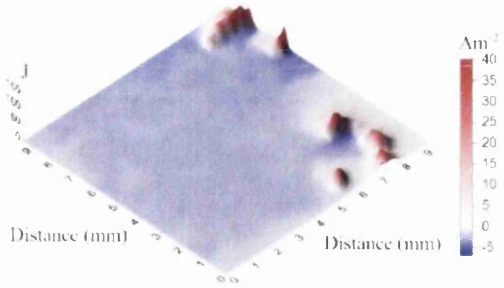

Figure 4.11 (c) At Time = 2 hours

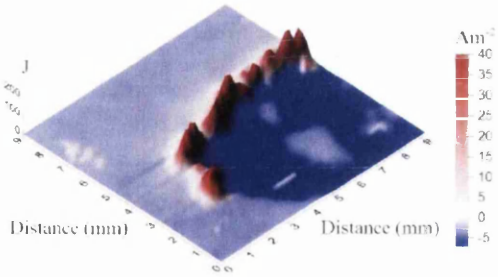

Figure 4.12 (c) At Time = 2 hours

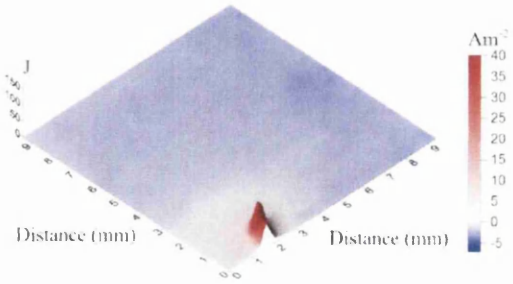

Figure 4.11 (d) At Time = 3 hours

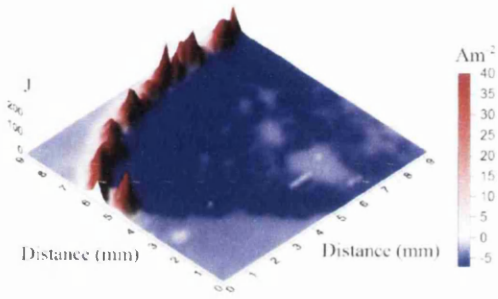

Figure 4.12 (d) At Time = 3 hours

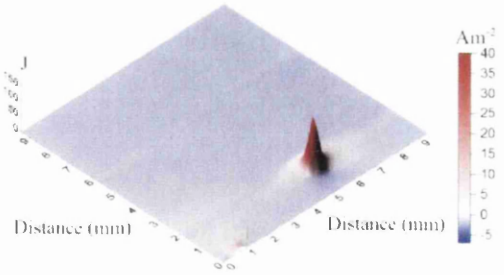

Figure 4.11 (e) At Time = 4 hours

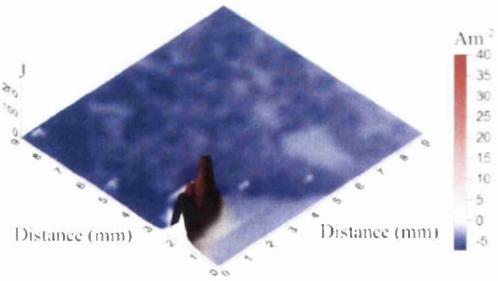

Figure 4.12 (e) At Time = 4 hours

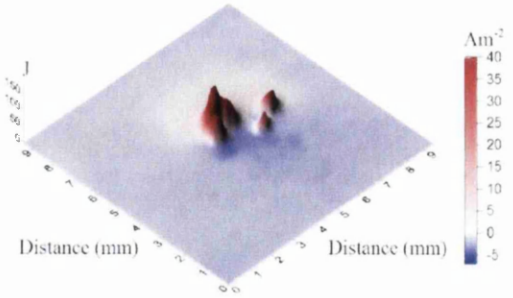

Figure 4.11 (f) At Time = 5 hours

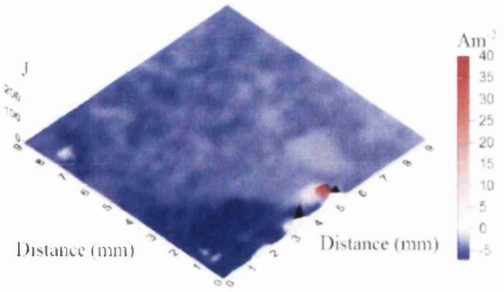

Figure 4.12 (f) At Time = 5 hours

Figure 4.11 (a) – (f) Surface map images of Solution treated AZ31 from SVET data.
Figure 4.12 (a) – (f) Surface map images of Age hardened AZ31 from SVET data.

It can be seen in the SVET images above that there is a huge difference in current intensities due to the heat treatment. It can also be inferred that in the age hardened sample, the electrochemical reaction is prominent and thus corresponds with a higher value of loss of the alloy material.

4.2 MAGNESIUM ALLOY AZ91

Magnesium alloy AZ91 is made up of 10.34% Al, 0.31% Zn, and the remaining being magnesium. This can be seen represented in the form of a spectrum (Figure 4.13) obtained from Energy Dispersive X-ray spectroscopy (EDX) using JOEL 35C SEM

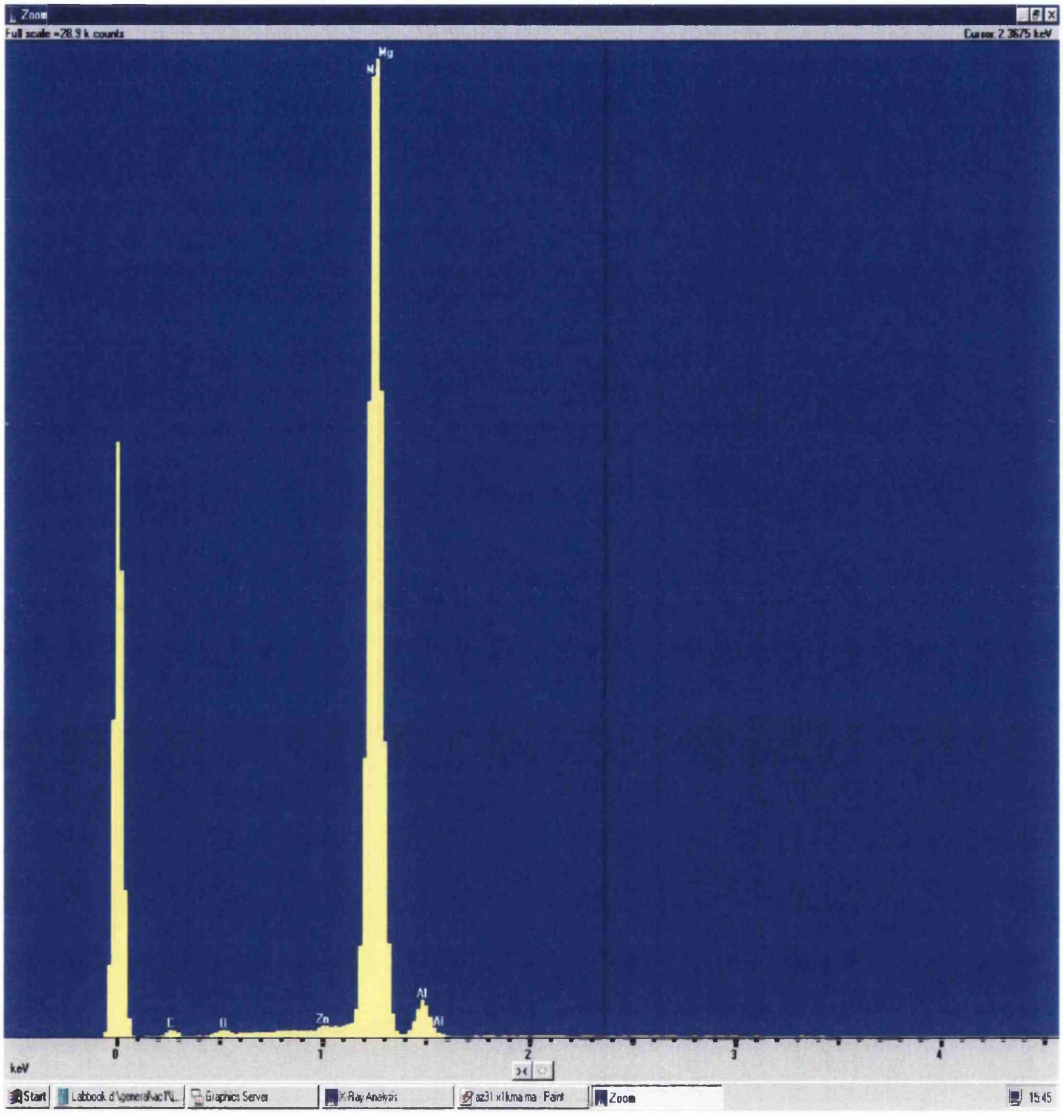

Figure 4.13 EDX Spectrum of AZ91 alloy (as received) at a magnification of ×1000

The above spectrum (Figure 4.13) shows the elemental composition of as received AZ91 alloy taken over an area of 40 μm × 30 μm at a magnification of ×1000. The maximum peak is the Magnesium composition. It can be seen that the amount of aluminium present is about 9% and higher in the spectral image in comparison with

that of AZ31. (See Figure 4.1) The following is the data generated from the EDX system,

==========

SEMQuant results. Listed at 15:21:29 on 04/02/10
Operator: Peter Davies
Client: EDX analysis
Job: Job number 47 - Dec09
Spectrum label: AZ91 x1kma medium area
System resolution = 61 eV
Quantitative method: ZAF (3 iterations).

Analysed all elements and normalised results.

4 peaks possibly omitted: 0.00, 0.26, 0.52, 2.54 keV

Standards :

Mg K MgO 01/12/93

Al K Al2O3 23/11/93

Zn K Zn 01/12/93

Elmt	Element %	Atomic %
Mg K	87.89	89.35
Al K	11.28	10.34
Zn K	0.82	0.31
Total	100.00	100.00

* = <2 Sigma

4.2.1 MICROSTRUCTURAL EVALUTION

Fig. 4.14 shows the micrograph of AZ91 obtained by Lü *et al* [59]. It can be inferred from the microstructure that the AZ91 alloy is made up of α-magnesium matrix and distributed β-precipitation forming the secondary phase along the grain boundary.

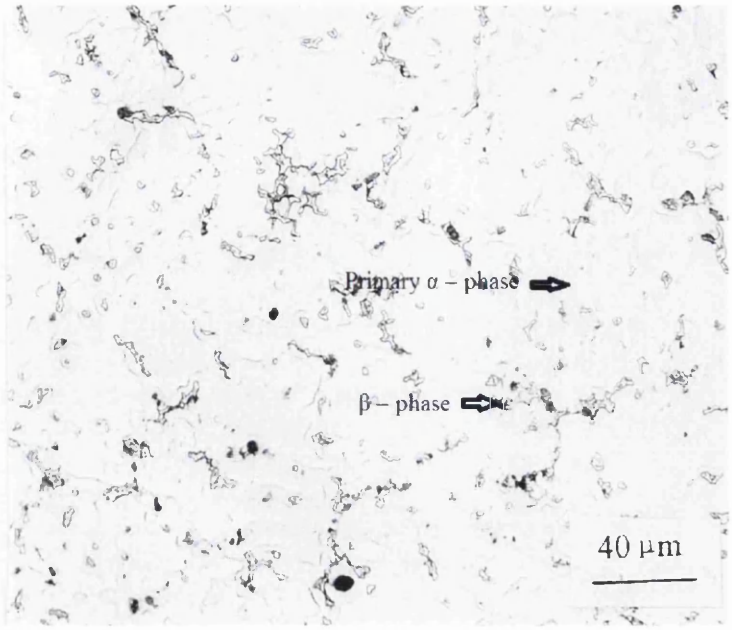

Figure 4.14 Micrograph of AZ91. Source: *Lü et al* [59]

The microstructure for AZ91 shows the distribution of the different phases in the alloy. This distribution governs the mechanical and corrosion characteristics of this alloy.

4.2.2 TIME LAPSE PHOTOGRAPHY

The time lapse photography for AZ91 alloy without any heat treatment was initiated. The following are the pictures (Figure 4.15 (a) – (e)) of AZ91 without any heat treatment. As mentioned in the previous sections (Section 3.2 & 4.1.2) the sample with an exposed area of 25 mm^2 (5mm × 5mm) was placed in a Petri-dish and filled with 5% NaCl salt solution and the camera was started in the time lapse mode. The following are the images obtained at various time intervals.

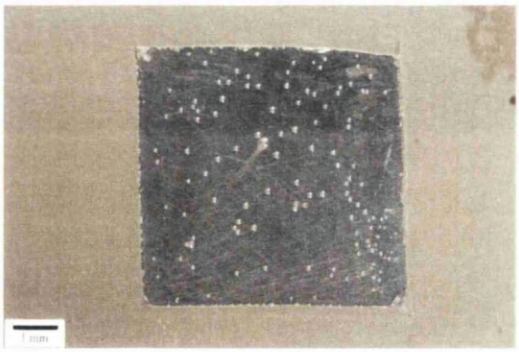

Figure 4.15 (a) At Time = 0 minutes

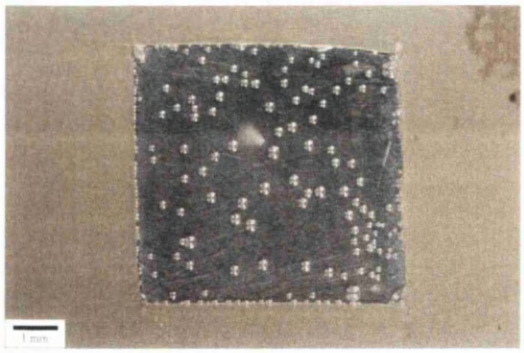

Figure 4.15 (b) At Time = 3 minutes

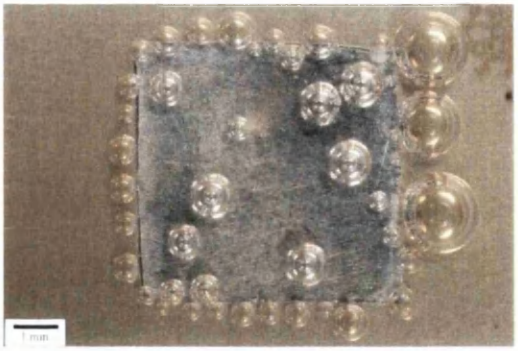

Figure 4.15 (c) At Time = 3 hours

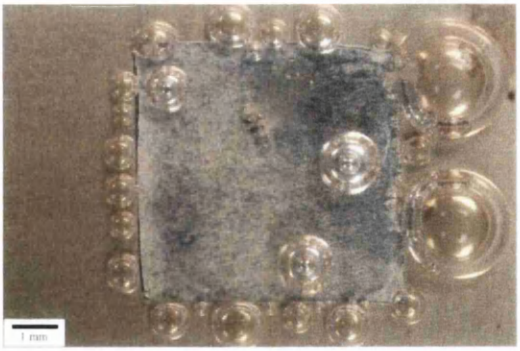

Figure 4.15 (d) At Time = 6 hours

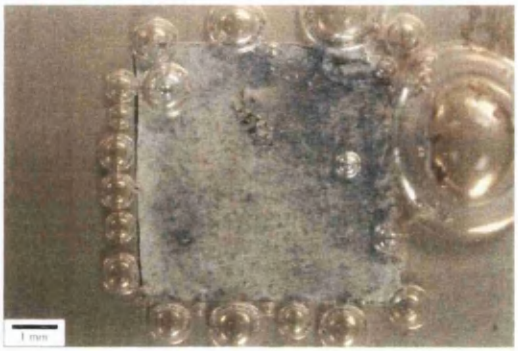

Figure 4.15 (e) At Time = 10 hours

Figure 4.3 (a) – (e) Time lapse experimental data of AZ91 alloy with no heat treatment

It can be seen in the above images that the surface breakdown occurs within 3 minutes of initiating the experiment. However, the rate of corrosion is quite slow which can be interpreted from the corroded area. The time lapse experiment was repeated for the solution treated and fully aged AZ91 alloy and the following images were obtained.

SOLUTION TREATED AZ91

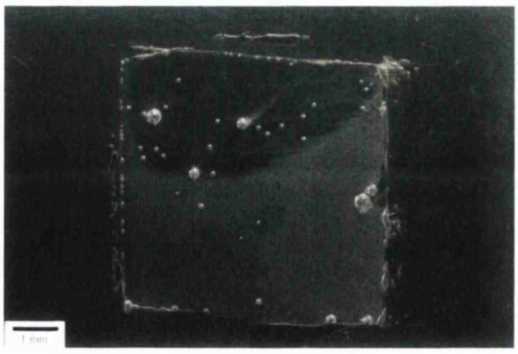

Figure 4.16 (a) At Time = 0 minutes

AGE HARDENED AZ91

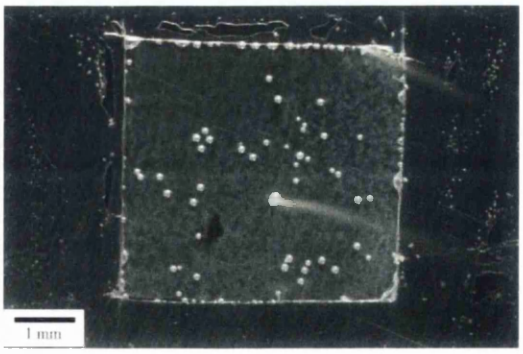

Figure 4.17 (a) At Time = 0 minutes

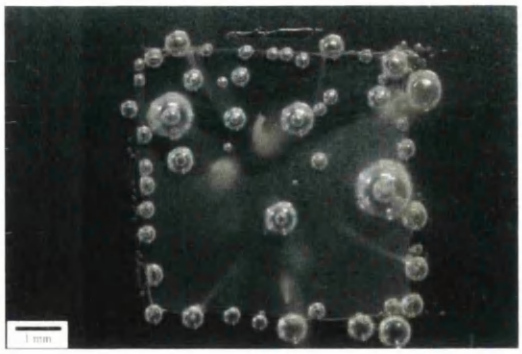

Figure 4.16 (b) At Time = 7 minutes

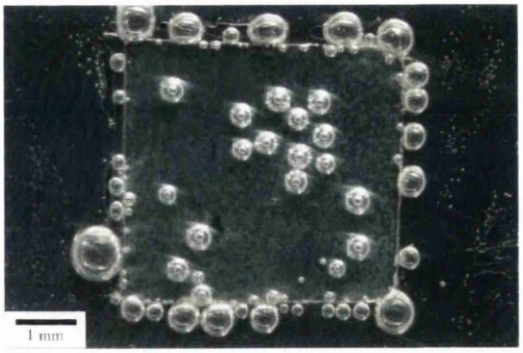

Figure 4.17 (b) At Time = 10 minutes

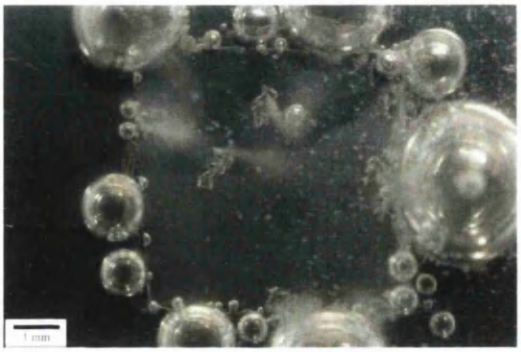

Figure 4.16 (c) At Time = 3 hours

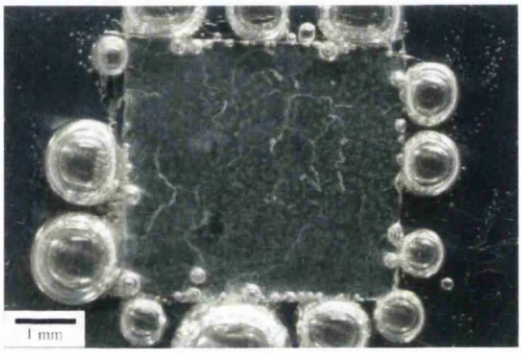

Figure 4.17 (c) At Time = 3 hours

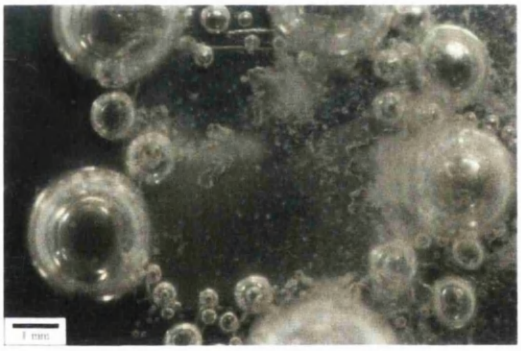

Figure 4.16 (d) At Time = 6 hours

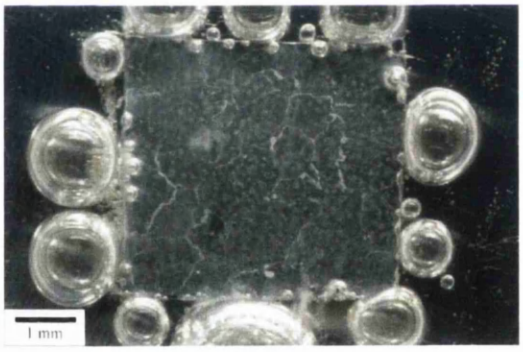

Figure 4.17 (d) At Time = 6 hours

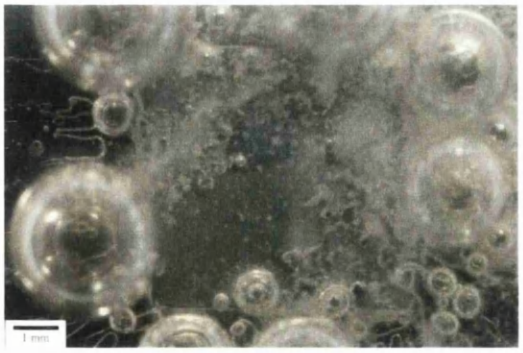

Figure 4.16 (e) At Time = 10 hours

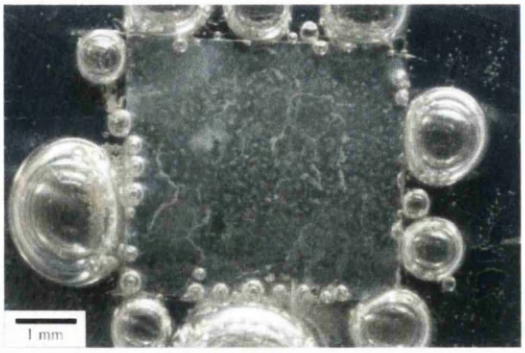

Figure 4.17 (e) At Time = 10 hours

Figure 4.16 (a) – (e) Time lapse images of Solution treated AZ91 alloy

Figure 4.17 (a) – (e) Time lapse images of Fully aged AZ91 alloy

The electrochemical reaction between the 5% NaCl solution and the heat treated alloys starts immediately as soon as the salt solution comes in contact with the alloy samples (Figure 4.16 (a) & Figure 4.17 (a)). The surface breakdown in both the solution treated and the age hardened samples is about 7 minutes (Figure 4.16 (b)) to 10 minutes (Figure 4.17 (b)). It can be seen that in case of the solutionized AZ91 alloy (Figure 4.16 (c) – (e)), the corrosion is quite rapid with the formation of multiple localized corrosion centres whereas the fully aged sample the corrosion rate is very slow.

4.2.2.1 SIGMA PLOT EVALUATION OF AZ91 ALLOY

A sigma plot evaluation of all the AZ91 sample images both with and without heat treatment can be represented graphically as follows,

Table 4.4 The corroded area of AZ 91 with different heat treatments over a period of 10 hours evaluated using Sigma plot

Time in hours	Corroded area in $\times 10^{-6}$ m^2		
	AZ91 as received	AZ91 Solution treated	AZ91 Age hardened
0	0	0	0
0.05	0.09		
0.12		0.2	
0.17			0.05
1	1.15	1.13	0.57
2	2.54	3.52	1.63
3	4.24	4.15	2.11
4	5.04	4.96	2.68
5	6.1	5.74	2.87
6	6.87	6.57	3.22
7	7.45	8.72	3.51
8	9.59	9.72	3.79
9	10.86	1.11	3.96
10	13.49	1.27	4.29

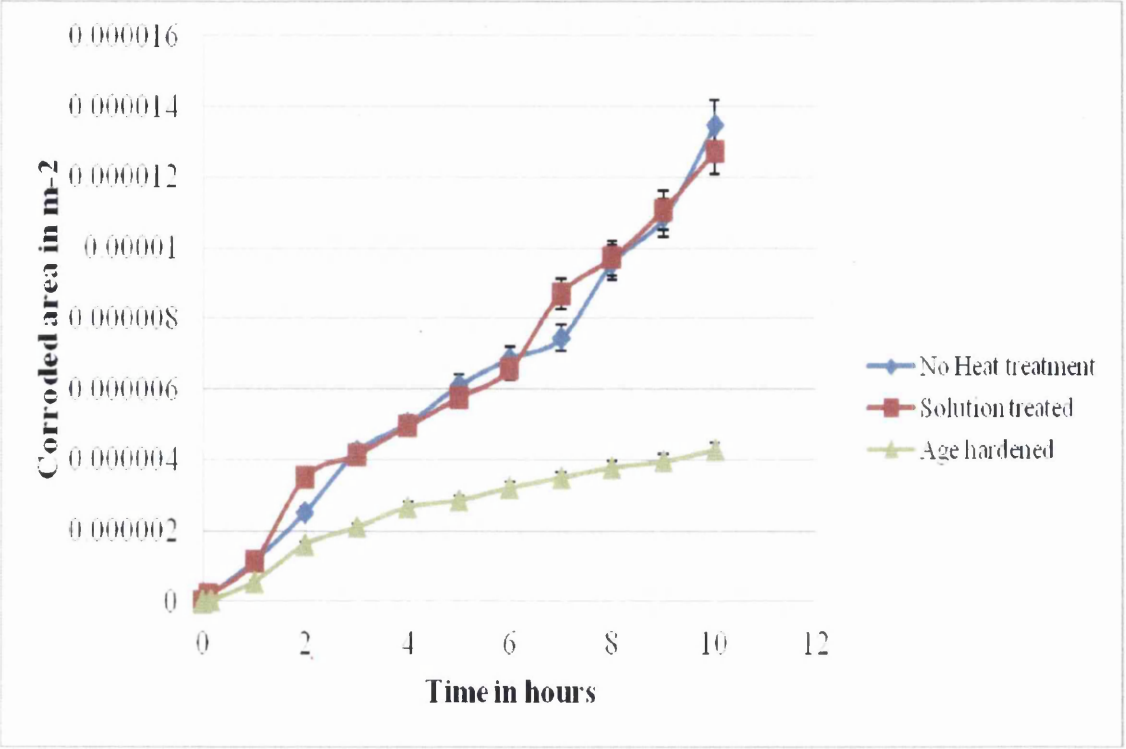

Figure 4.18 – Graph showing rate of corrosion expressed in terms of corroded area of AZ 91 alloy under different heat treatment conditions evaluated using Sigma plot.

It can be seen from the above graph (Figure 4.18) that the area of AZ91 alloy corroded is less in case of fully aged sample where as the sample without any heat treatment and the sample with solution treatment behave in a similar way and were found to be much higher that the fully ages AZ91 alloy sample.

4.2.3 HYDROGEN EVOLUTION EXPERIMENT

A hydrogen evolution experiment was conducted on all samples of AZ91 alloy. The experiment was set up as per section 3.3 from the previous chapter and assessed as mentioned in section 4.1.3. An area of 30mm × 30mm was exposed to the 5% NaCl salt solution. The data obtained is in cubic centimetres and is converted into number of moles of hydrogen evolved using the ideal gas law formula. The following is the data obtained from the experiment which represents the number of moles of hydrogen evolved.

Table 4.5 Data obtained from hydrogen evolution experiment conducted on AZ91 alloy with and without heat treatment

Time in Hours	Hydrogen evolved in $\times 10^{-5}$ moles		
	AZ91 as received	AZ91 Solution treated	AZ91 Age hardened
0	0	0	0
1	0.42	3.12	0.83
2	1.04	5.40	1.45
3	1.66	7.48	1.87
4	2.49	10.8	2.49
5	3.32	14.95	3.32
6	4.15	19.1	3.74
7	4.78	23.26	4.36
8	5.4	27.82	4.57
9	6.23	32.81	4.98
10	6.85	37.38	5.4
11	7.48	42.98	5.81
12	8.31	48.17	6.02
13	9.14	53.57	6.23
14	9.97	58.14	6.44
15	10.59	63.12	6.65
16	11.21	68.32	7.06
17	12.04	73.1	7.28
18	12.87	78.08	7.48
19	13.5	83.06	7.89
20	14.33	92.4	8.72

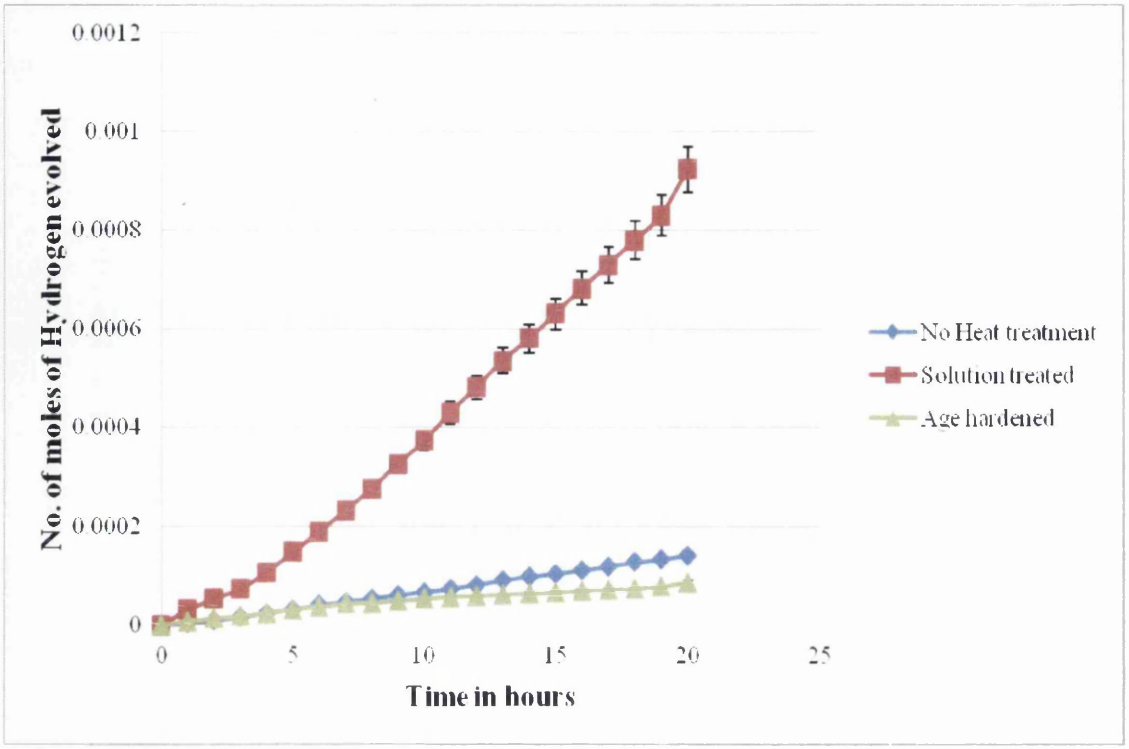

Figure 4.19 A graphical plot representing the number of moles of hydrogen evolved from an AZ91 sample

The above graph clearly shows that the amount of hydrogen evolved from the solution treated AZ91 is high in comparison with the fully aged sample. This shows that the corrosion performance of aged AZ91 sample is better than its counterparts. The time lapse experiment images also show that the reaction rate of salt solution and the solutionized AZ91 sample is much faster than the fully aged sample.

4.2.4 SVET ANALYSIS

As per section 3.1.1 and 4.1.4, the surface of the sample was polished and a 10mm × 10mm area was exposed to 5 % NaCl solution. Using the grid volume calculator in Surfer, the cut value was found from the data generated from SVET. The loss of magnesium metal over the period of the experiment was determined as mentioned in section 4.1.4 and following are the results obtained from the experiment for all heat treatment and non-treatment conditions of AZ91 sample.

It can be inferred from the following data (Figure 4.20 & Table 4.6) that the electrochemical reaction is quite slow and of lower intensity in case of a fully aged sample of AZ91.

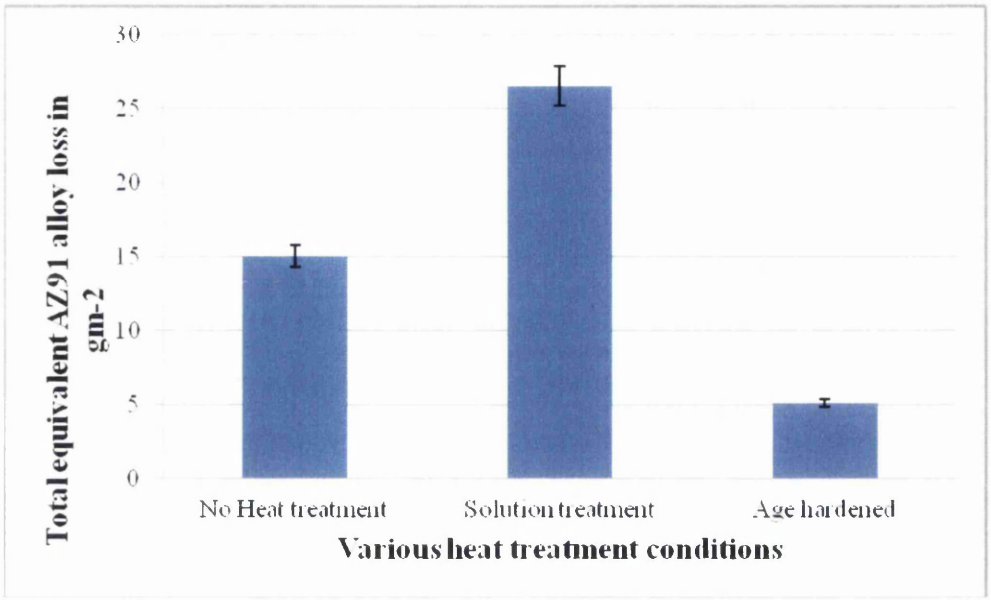

Figure 4.20 A bar chart showing the amount of AZ91 in g/m^2

Table 4.6 The loss of AZ91 under all heat treatment conditions

Heat treatment condition	Loss of AZ91 in g/m^2
No heat treatment	15.05
Solution treatment	26.55
Age hardened	5.11

It can also be seen that the solution treatment increases the corrosion activity of the AZ91 alloy. The characteristics of the non-heat treated alloy remains in between the solution treated and age hardened sample. The anodic activity of the alloy under different heat treatment conditions was also evaluated using Surfer and the following result was obtained, (Figure 4.21).

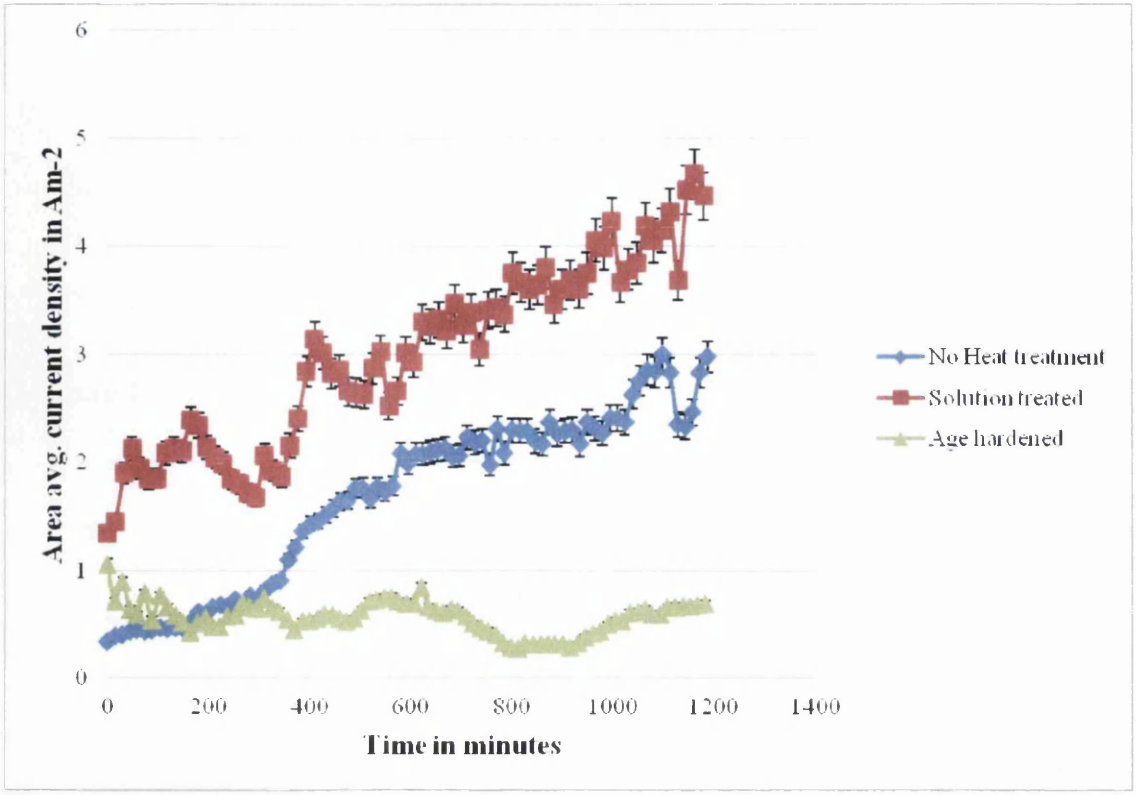

Figure 4.21 A graphical data of the anodic summary of AZ91 alloy under various heat treatment conditions obtained from SVET data evaluated using Surfer

The data obtained from SVET can be represented in the form of surface colour maps showing the anodic and cathodic activity using Surfer.

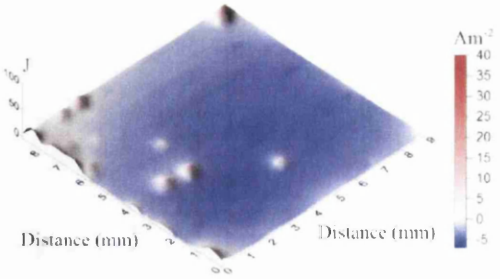

Figure 4.22 (a) At Time = 0 minutes

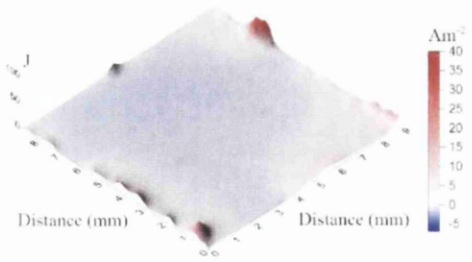

Figure 4.22 (b) At Time = 3 hours

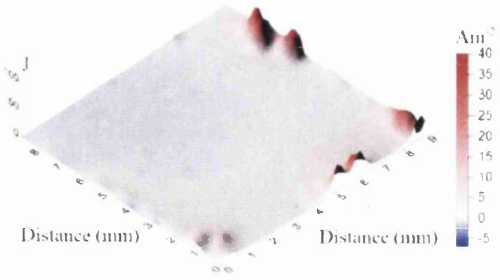

Figure 4.22 (c) At Time = 6 hours

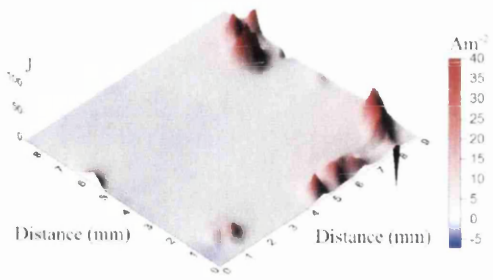

Figure 4.22 (d) At Time = 10 hours

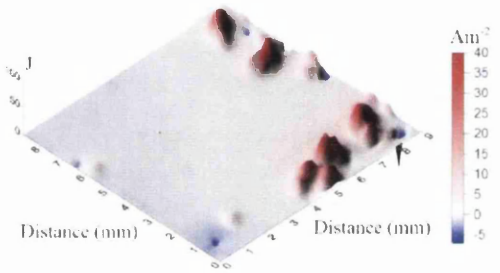

Figure 4.22 (e) At Time = 14 hours

Figure 4.22 (a) – (e) Surface maps of AZ91 alloy without any heat treatment evaluated from the data obtained from SVET experiment

The SVET experiment which was repeated for the AZ91 alloy samples with solution and ageing treatments can also be represented as surface maps as follows,

SOLUTION TREATED AZ91

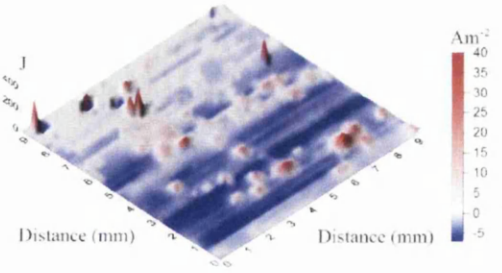

Figure 4.23 (a) At Time = 0 minutes

AGE HARDENED AZ91

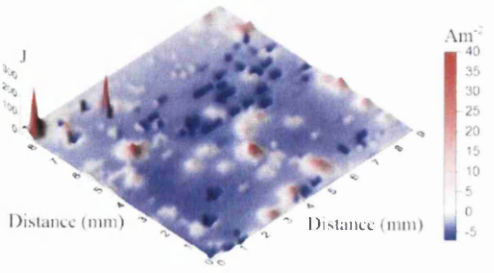

Figure 4.24 (a) At Time = 0 minutes

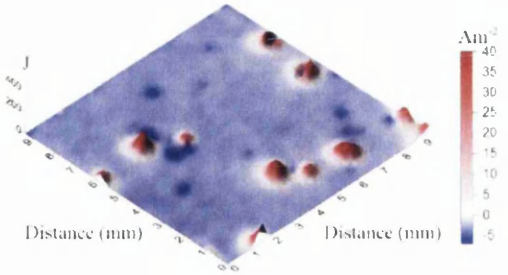

Figure 4.23 (b) At Time = 3 hours

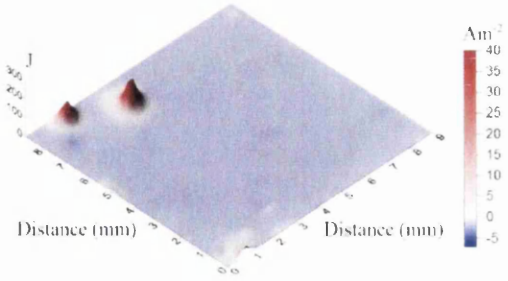

Figure 4.24 (b) At Time = 3 hours

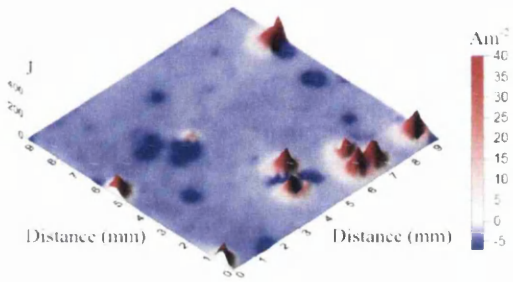

Figure 4.23 (c) At Time = 6 hours

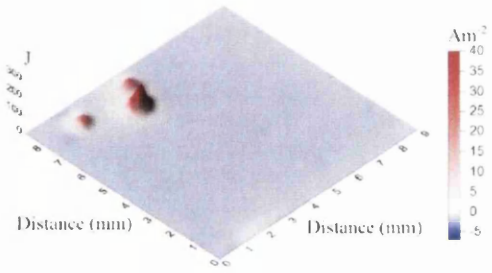

Figure 4.24 (c) At Time = 6 hours

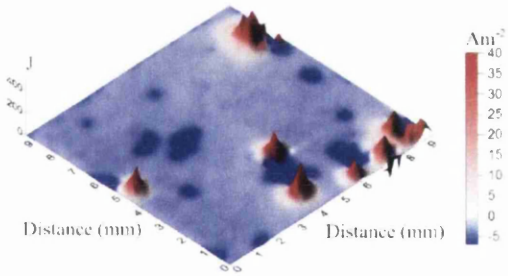

Figure 4.23 (d) At Time = 10 hours

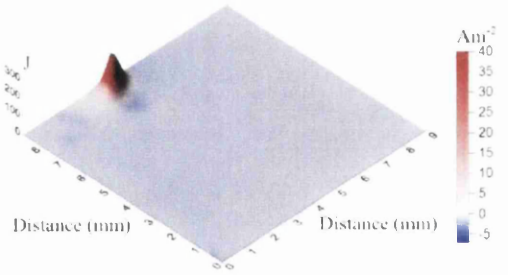

Figure 4.24 (d) At Time = 10 hours

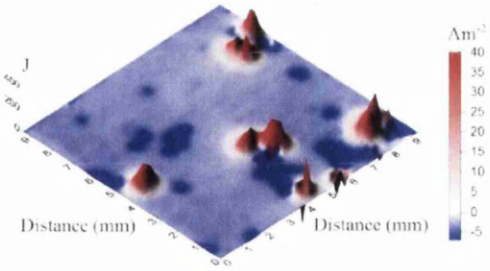

Figure 4.23 (e) At Time = 14 hours

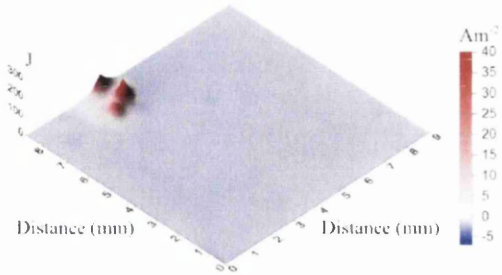

Figure 4.24 (e) At Time = 14 hours

Figure 4.23 (a) – (e) Surface images of solution treated AZ91 alloy from SVET data
Figure 4.24 (a) – (e) Surface images of a fully aged AZ91 alloy from SVET data

It can be seen in the above images that the solution treated AZ91 alloy exhibits higher anodic activity in comparison with the age hardened one. Also the cathodic activity is very low in for the fully aged sample in comparison with the solution treated alloy sample. Further analysis and discussion of the results is mentioned in the next chapter. (Chapter 5)

4.3 MAGNESIUM ALLOY ELEKTRON 21

ELEKTRON 21's composition obtained from JOEL 35C SEM consists of Mg – 96.68%, Zn – 0.30%, Nd – 2.30%, Gd – 0.71% and reserve of Zr. The following spectrum (Figure 4.25) is the data for the general alloy obtained from the EDX scan using a JOEL 35C SEM.

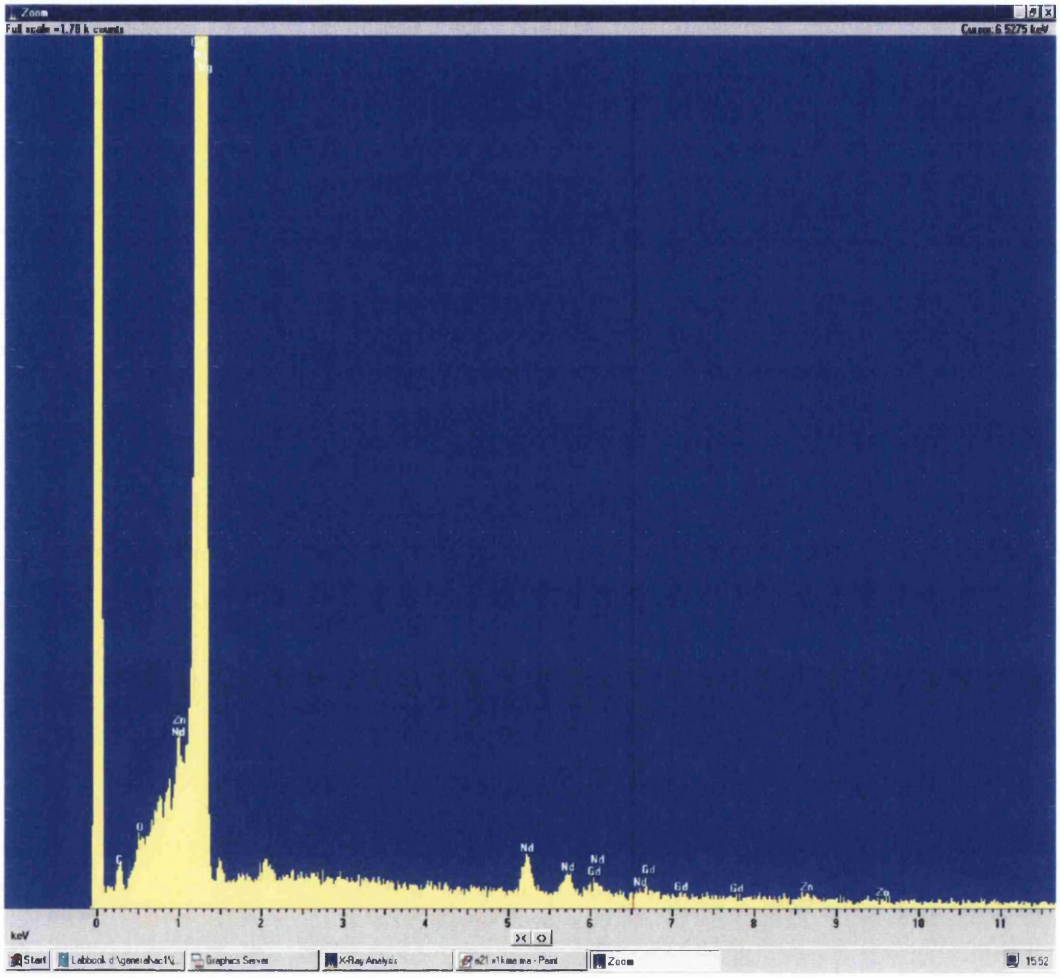

Figure 4.25 EDX Spectrum of Elektron21 alloy (as received) at ×1000 magnification

In the above spectrum (Figure 4.25), the maximum peak represents the Magnesium (*Mg*) content. It can be inferred from the above composition that neodymium (*Nd*), gadolinium (*Gd*) and zinc (*Zn*) are present is smaller proportions. This EDX analysis spectrum was obtained from an area of 40 μm × 30 μm of the sample at a magnification of x1000. The following is the data obtained from the EDX system,

==========

SEMQuant results. Listed at 15:34:21 on 04/02/10
Operator: Peter Davies
Client: EDX analysis
Job: Job number 47 - Dec09
Spectrum label: elektron21 x1kma medium area
System resolution = 61 eV
Quantitative method: ZAF (4 iterations).

Analysed all elements and normalised results.
3 peaks possibly omitted: 0.00, 0.26, 0.50 keV

Standards :

Mg K	MgO 01/12/93
Zn K	Zn 01/12/93
Zr L	Zr 01/12/93
Nd L	NdF3 01/12/93
Gd L	GdF3 01/12/93
Th M	ThO2 01/12/93

Elmt	Element %	Atomic %
Mg K	94.94	98.90
Zn K	0.62	0.24
Zr L	1.03	0.29
Nd L	2.47	0.43
Gd L	0.79	0.13
Th M	0.16*	0.02*
Total	100.00	100.00

* = <2 Sigma

4.3.1 MICROSTRUCTURAL ANALYSIS

The following is the microstructure of Elektron 21 without any heat treatment. It can be seen that the alloying elements are concentrated at the grain boundary represented

by the eutectic phase. This image is obtained following procedures as described in Section 3.1.1 and section 4.1.1.

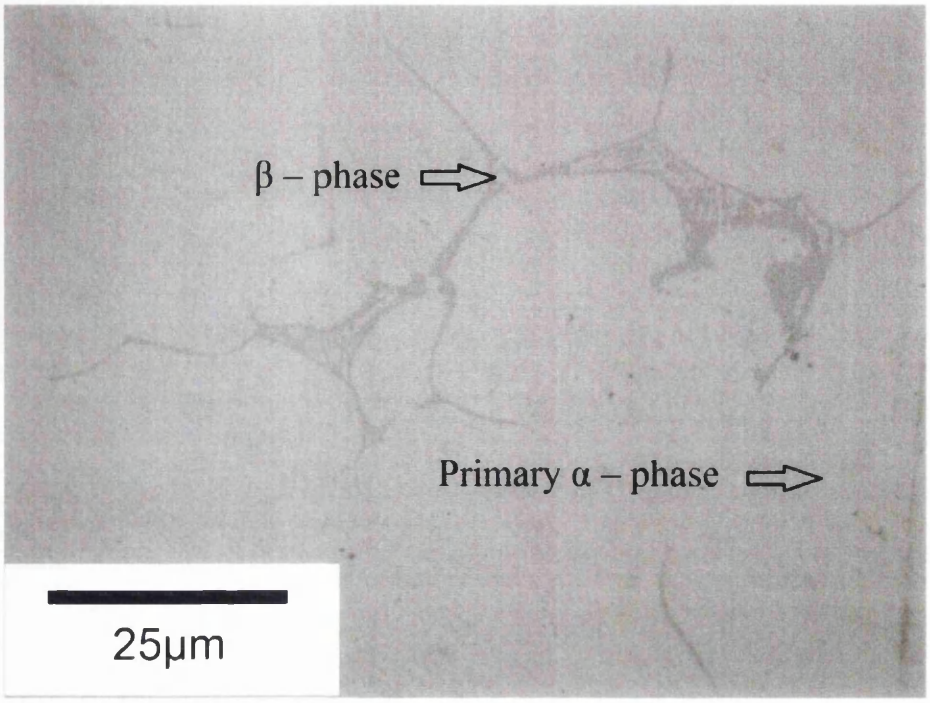

Fig 4.26 The microstructure of Elektron 21 at ×500 magnification using a Reichert Jung MeF3 microscope.

4.3.2 TIME LAPSE PHOTOGRAPHY

The time lapse photography experiment was conducted on a sample of Elecktron 21 without any heat treatment in accordance with procedure mentioned in section 3.2 and the following images were obtained.

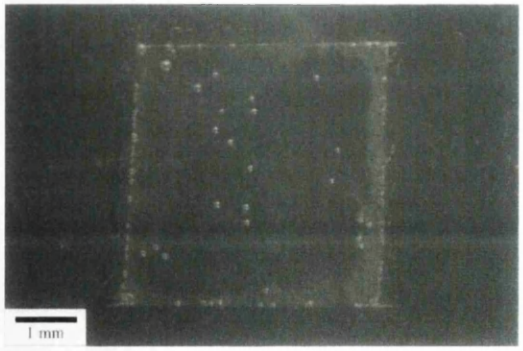

Figure 4.27 (a) At Time = 0 minutes

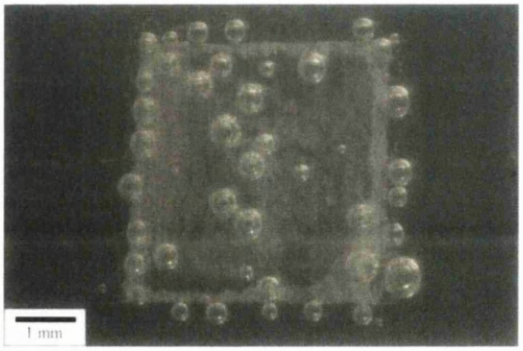

Figure 4.27 (b) At Time = 30 minutes

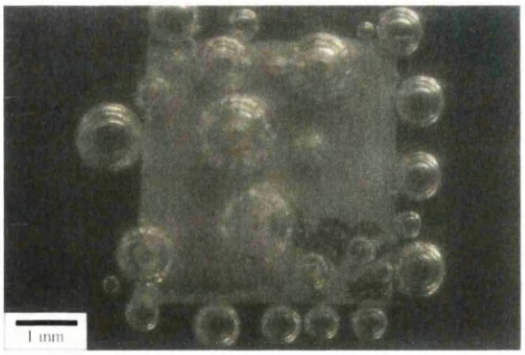

Figure 4.27 (c) At Time = 3 hours

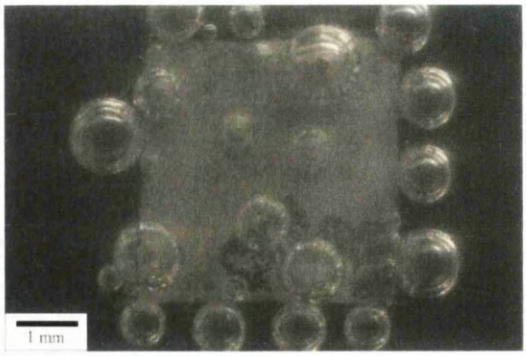

Figure 4.27 (d) At Time = 6 hours

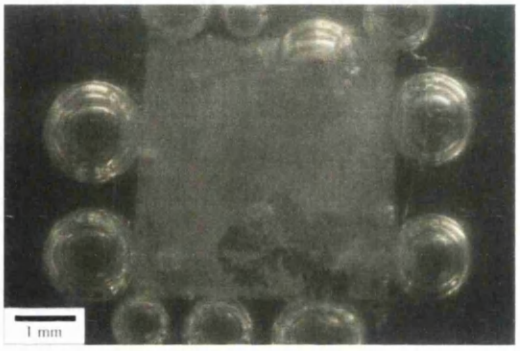

Figure 4.27 (e) At Time = 10 hours

Figure 4.27 (a) – (e) Time lapse photography images of Elektron 21 with no heat treatment

It can be seen from Figure 4.27(b) that the surface breakdown occurs at about 30 minutes from the start of the experiment. From then on, the electrochemical reaction leads to the corrosion of the alloy in the form of a dendrite with corrosion following the microstructural pattern of the alloy. A thin oxide film is also seen in the image.

The Elektron 21 alloy was then subjected to heat treatment. First the samples were Solution treated as mentioned in section 3.5. Then the samples were aged for 16 hours and 48 hours to determine the corrosion performance of the alloy. The following is the data obtained from time lapse photography experiment.

SOLUTION TREATED ELEKTRON 21

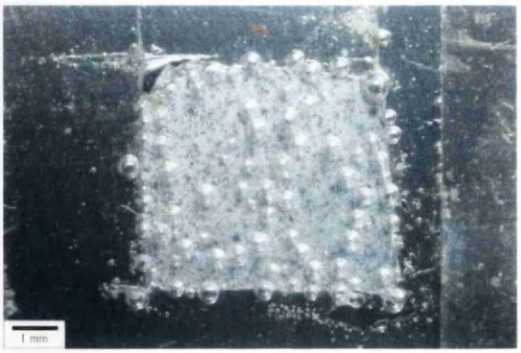

Figure 4.28 (a) At Time = 0 minutes

Figure 4.28 (b) At Time = 3.67 hours

Figure 4.28 (c) At Time = 6 hours

Figure 4.28 (d) At Time = 10 hours

Figure 4.28 (a) – (d) Time lapse images of solution treated Elektron 21

It can be seen that as soon as the sample is exposed to 5% NaCl solution (Figure 4.28(a)), a white oxide layer is formed which is much denser and visible to the sample without any heat treatment. The first surface breakdown occurs after about 3 hours and 40 minutes. (See Figure 4.28 (b)) From then on the corrosion of the sample occurs but at a much slower rate in comparison with the sample with no heat treatment. (See Figure 4.27 (a) – (e))

The following is the data obtained from time lapse photography experiment for 16 hours and 48 hours age hardened samples of Elektron 21.

16 HRS AGE HARDENED E21

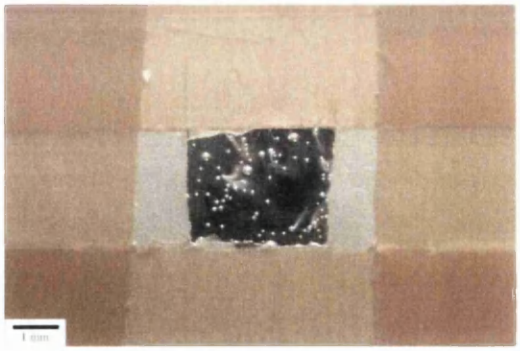

Figure 4.29 (a) At Time = 0 minutes

Figure 4.29 (b) At Time = 2 minutes

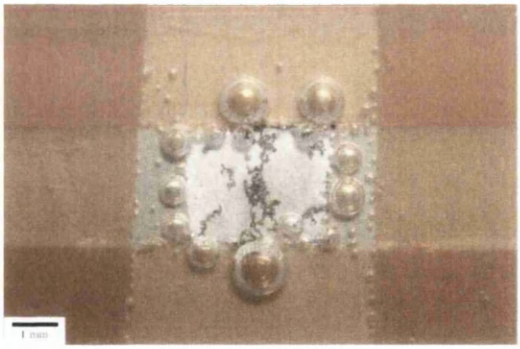

Figure 4.29 (c) At Time = 3 hours

48 HRS AGE HARDENED E21

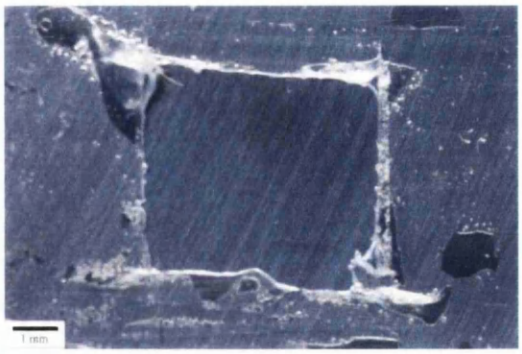

Figure 4.30 (a) At Time = 0 minutes

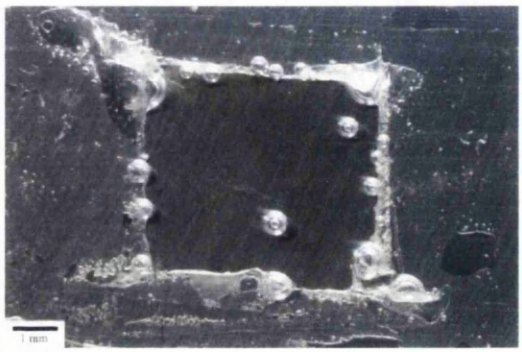

Figure 4.30 (b) At Time = 50 minutes

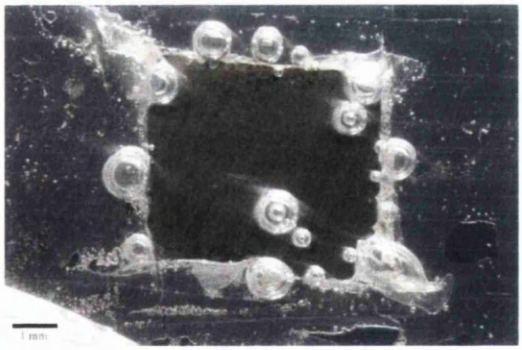

Figure 4.30 (c) At Time = 3 hours

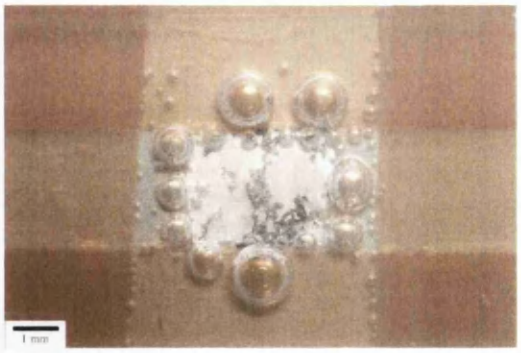

Figure 4.29 (d) At Time = 6 hours

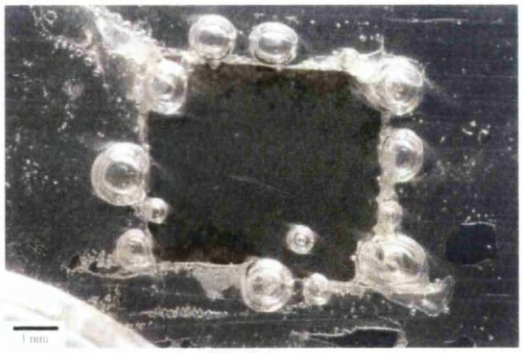

Figure 4.30 (d) At Time = 6 hours

Figure 4.29 (e) At Time = 10 hours

Figure 4.30 (e) At Time = 10 hours

Figure 4.29 (a) – (e) Time lapse images of 16 hours age hardened Elektron 21 alloy
Figure 4.30 (a) – (e) Time lapse images of 48 hours age hardened Elektron 21 alloy

It can be seen in Figure 4.29 (a) that as soon as the salt solution comes in contact with the 16 hours aged exposed alloy surface, the reaction starts with immediate surface breakdown. The next image taken within 2 minutes of initiation of the experiment shows various corroded spots all over the exposed surface. However, the surface breakdown of the 48 hours aged sample occurs around the 50^{th} minute of the start of the experiment. This shows that the corrosion performance of the 16 hours aged sample is very low in comparison with the 48 hours aged sample.

4.3.2.1 SIGMA PLOT EVALUATION OF ELEKTRON 21 ALLOY

A sigma plot evaluation of all the Elektron 21 sample images both with and without heat treatment can be represented graphically as follows,

Table 4.7 The corroded area of Elektron 21 with different heat treatments over a period of 10 hours evaluated using Sigma plot

Time in hours	Corroded area in $\times 10^{-6}$ m^2			
	E21 as received	E21 Solution treated	E21 16 hrs age hardened	E21 48 hrs age hardened
0	0	0	0.02	0
0.33	0.19			
0.83				0.11
1	0.98		2.86	0.16
2	1.54		3.53	2.62
3	2.64		4.66	3.12
3.67		0.01		
4	3.16	0.03	5.54	4.5
5	3.79	0.35	6.86	5.65
6	4.65	0.53	7.27	6.71
7	4.99	0.71	8.62	8.47
8	5.8	1.23	9.11	11.48
9	6.45	2.13	9.89	12.39
10	7.32	3.34	10.4	15.37

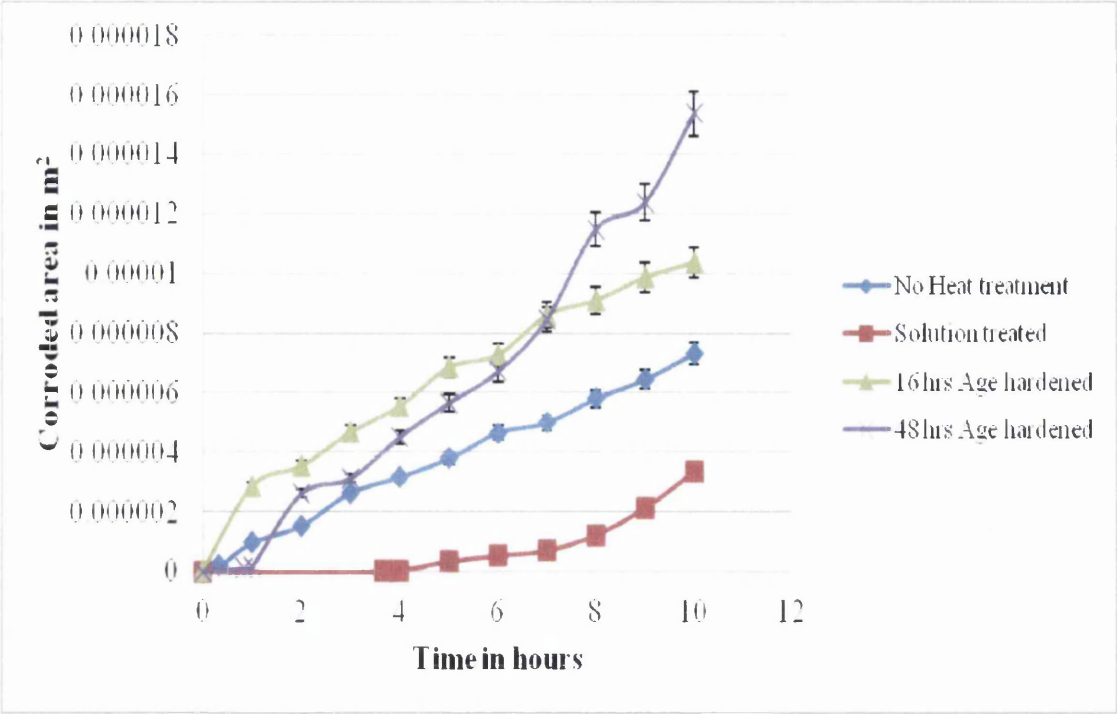

Figure 4.31 – Graph showing corroded area of Elektron 21 alloy under different heat treatment conditions in m^2 evaluated using Sigma plot

It can be seen from the data obtained after Sigma plot analysis (Table 4.7) that the solution treated alloy's corrosion performance is better than its counterparts.

4.3.3 HYDROGEN EVOLUTION EXPERIMENT

The hydrogen evolution experiment was carried out on all samples obtained with and without different heat treatment conditions. The following data was obtained from the experiment.

Table 4.8 Data obtained from hydrogen evolution experiment conducted on Elektron 21 alloy with and without heat treatment

Time in Hours	Hydrogen evolved in $\times 10^{-5}$ moles			
	E21 as received	E21 Solution treated	E21 16 hrs age hardened	E21 48 hrs age hardened
0	0	0	0	0
1	0.42	0.17	0.13	0
2	0.83	0.42	0.21	0.04
3	1.25	0.54	0.42	0.29
4	1.45	0.67	0.71	0.42
5	1.66	0.997	1.04	0.58
6	1.87	1.16	1.5	0.75
7	2.08	1.37	1.87	0.87
8	2.2	1.54	2.33	1.04
9	2.33	1.74	2.82	1.2
10	2.53	1.87	3.28	1.29
11	2.7	2.08	3.66	1.45
12	2.91	2.2	4.07	1.66
13	3.12	2.41	4.49	1.7
14	3.32	2.57	5.15	1.79
15	3.53	2.74	5.57	1.95
16	3.74	2.91	6.02	2.16

The data from hydrogen evolution experiment shows that the 16 hours age hardened Elektron 21 alloy evolves more hydrogen in comparison with other heat treatment

conditions and the 48 hours age hardened data is the lowest. The following is the graphical representation of the tabulated results found above.

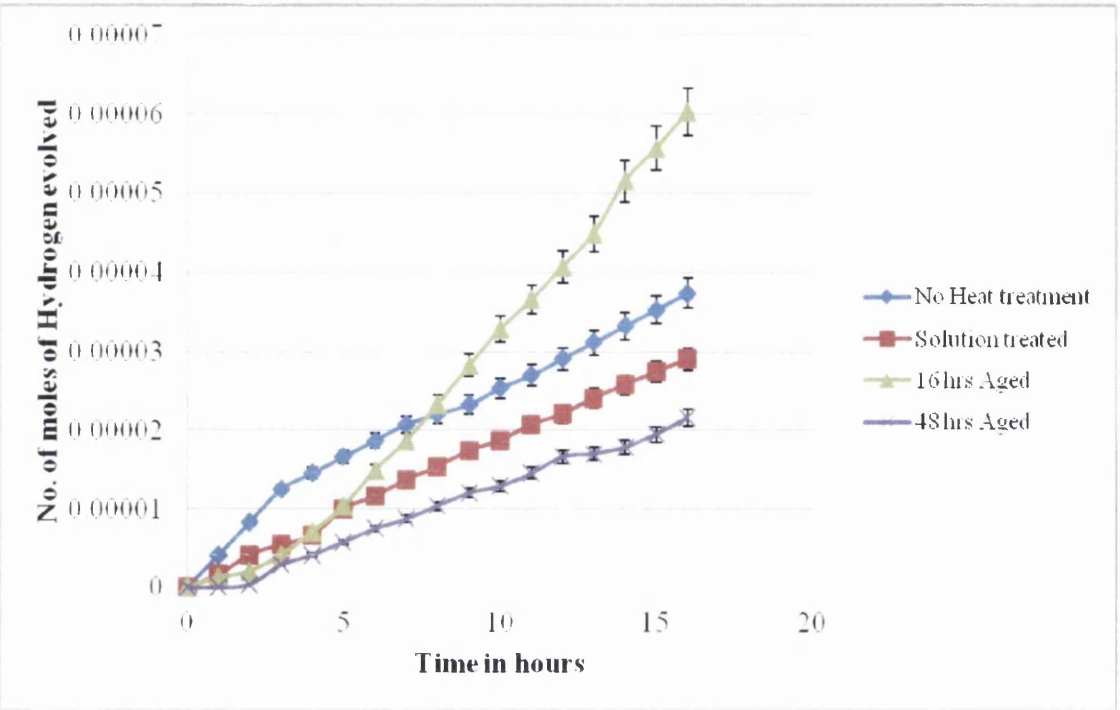

Figure 4.32 A graphical plot representing the number of moles of hydrogen evolved from an Elektron 21 sample with different heat treatment conditions.

4.3.4 SVET ANALYSIS

As per section 3.1.1 and 4.1.4, the surfaces of all the samples were polished and a 10mm × 10mm area was exposed to 5 % NaCl solution. Using the grid volume calculator in Surfer, the cut values were found from the data generated from SVET. The loss of magnesium metal over the period of the experiment was determined as mentioned in section 4.1.4 and following are the results obtained from the experiment for all heat treatment and non-treatment conditions of Elektron 21 sample.

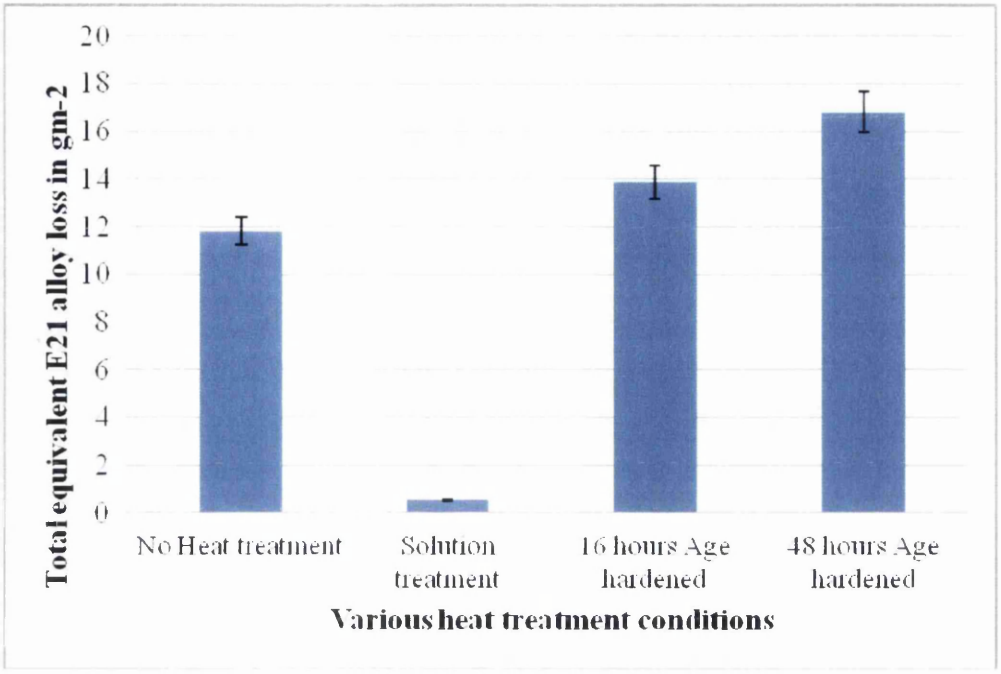

Figure 4.33 A bar chart showing the estimated loss of Elektron 21 in g/m^2

Table 4.9 The loss of Elektron 21 under all heat treatment conditions

Heat treatment condition	Loss of Elektron 21 in g/m^2
No Heat treatment	11.82
Solution treatment	0.55
16 hours Age hardened	13.88
48 hours Age hardened	16.8

It can be inferred from the above data (Figure 4.33 & Table 4.9) that the electrochemical reaction is quite slow and of lower intensity in case of solution treated Elektron 21 alloy. The 48 hours age hardened sample however yields the maximum loss of material suggesting that a Solution treatment is preferred for Elektron 21. The anodic activity of the alloy under different heat treatment conditions was also evaluated using Surfer and the following result was obtained, (Figure 4.34).

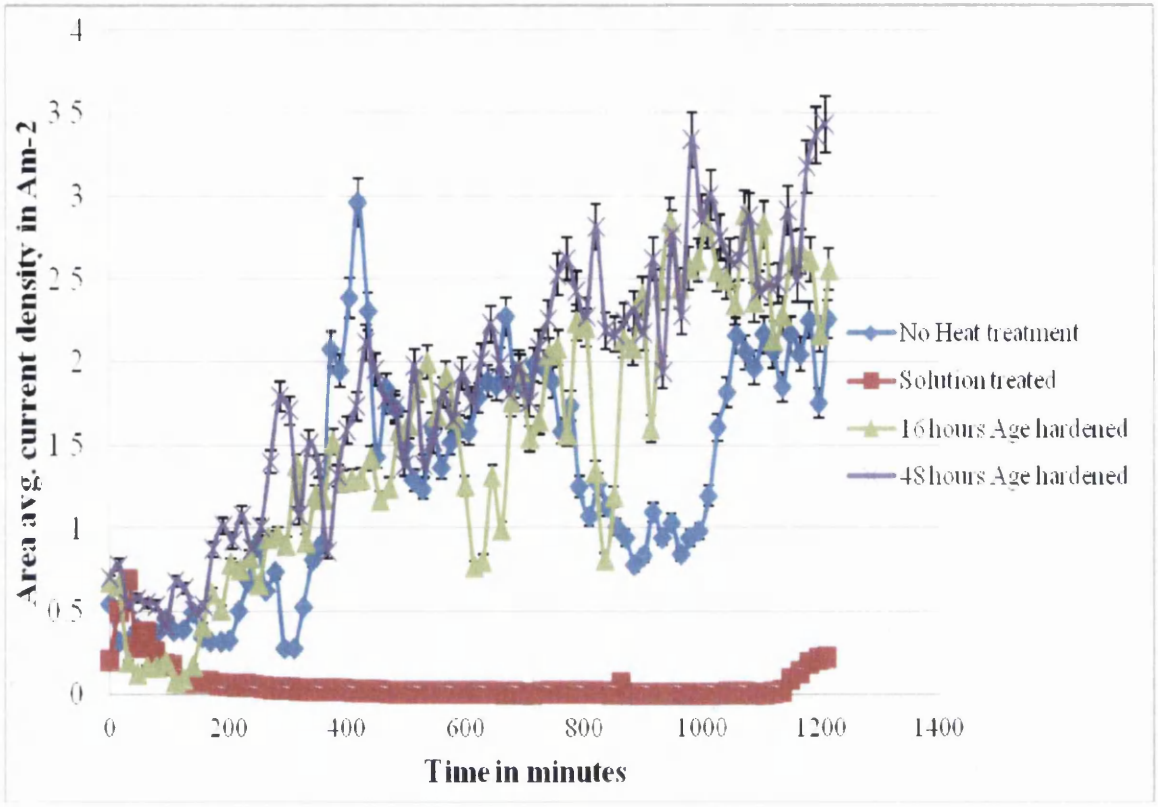

Figure 4.34 A graphical data of the anodic summary of Elektron 21 alloy under various heat treatment conditions obtained from SVET data evaluated using Surfer

The data obtained from SVET can be represented in the form of surface colour maps showing the anodic and cathodic activity using Surfer.

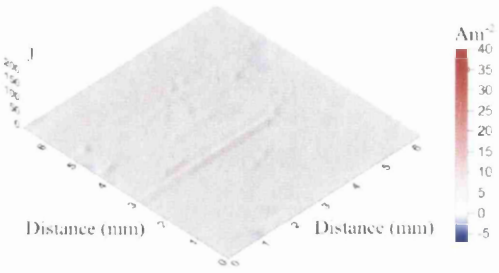

Figure 4.35 (a) At Time = 0 minutes

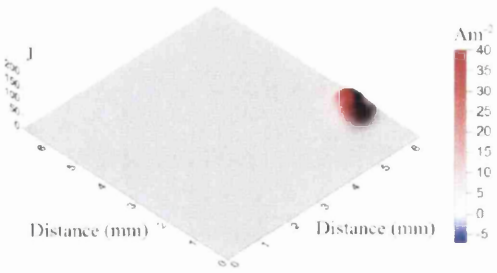

Figure 4.35 (b) At Time = 4 hours

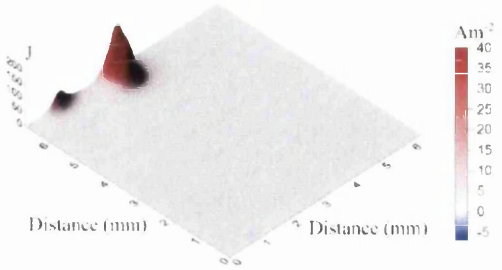

Figure 4.35 (c) At Time = 8 hours

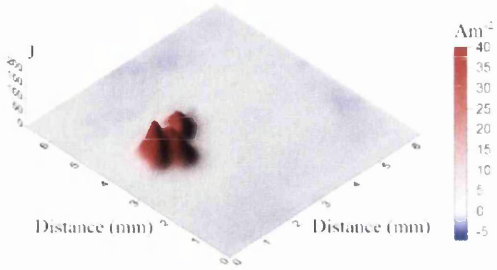

Figure 4.35 (d) At Time = 12 hours

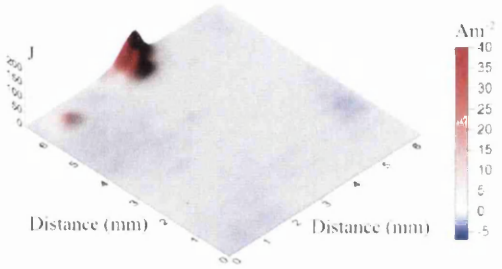

Figure 4.35 (e) At Time = 16 hours

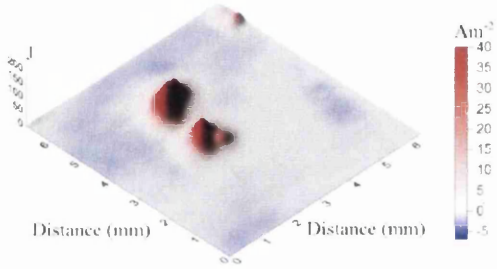

Figure 4.35 (f) At Time = 20 hours

Figure 4.35 (a) – (f) Surface plot images of Elektron 21 with no heat treatment.

The SVET analysis for Elektron 21 alloy with solution treatment and ageing was repeated and the data can be represented as surface maps as follows,

SOLUTION TREATED ELEKTRON 21 ALLOY

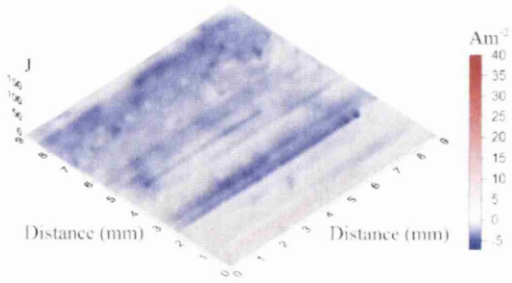

Figure 4.36 (a) At Time = 0 minutes

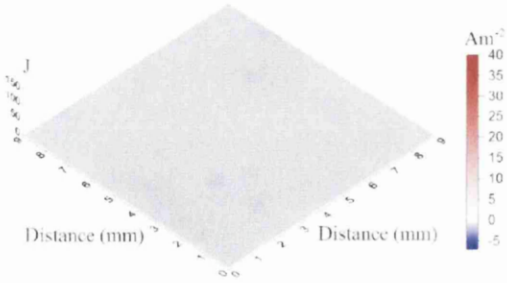

Figure 4.36 (b) At Time = 8 hours

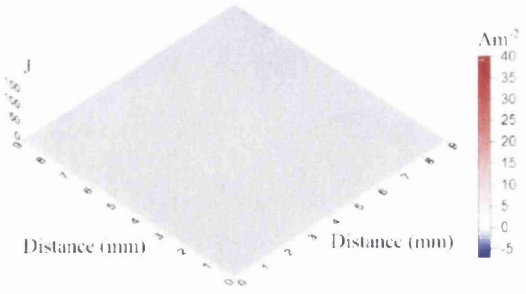

Figure 4.36 (c) At Time = 16 hours

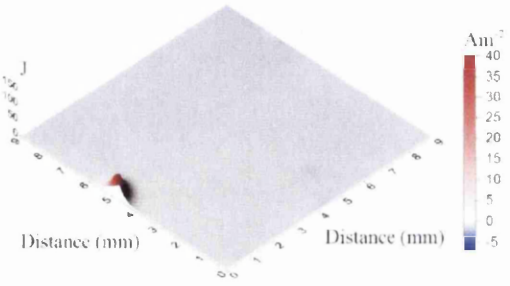

Figure 4.36 (d) At Time = 20 hours

Figure 4.36 (a) – (d) Surface images of Solution treated Elektron 21 obtained from SVET data

In case of the solution treated Elektron 21 alloy, it can be seen that the anodic activity is almost zero which can be inferred from the anodic summary (Figure 4.34). This is also seen in the SVET surface maps with lower or no active anodic centres.

16 HRS AGE HARDENED E21

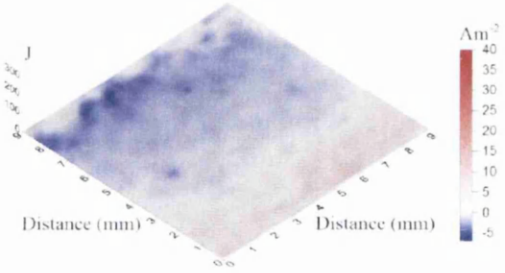

Figure 4.37 (a) At Time = 0 minutes

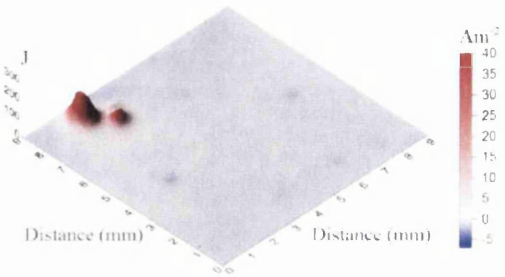

Figure 4.37 (b) At Time = 4 hours

48 HRS AGE HARDENED E21

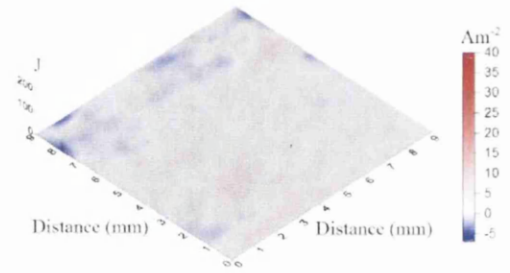

Figure 4.38 (a) At Time = 0 minutes

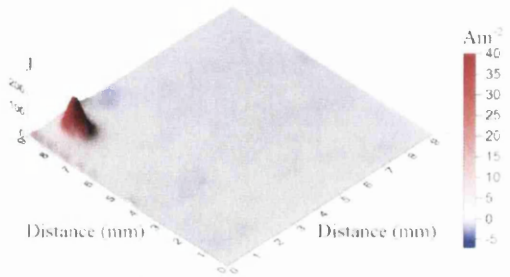

Figure 4.38 (b) At Time = 4 hours

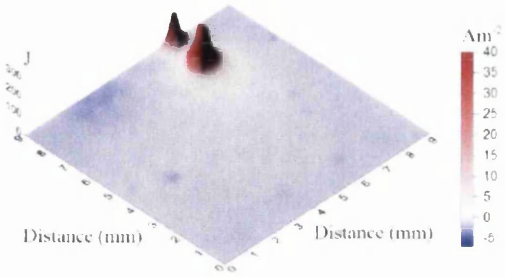

Figure 4.37 (c) At Time = 8 hours

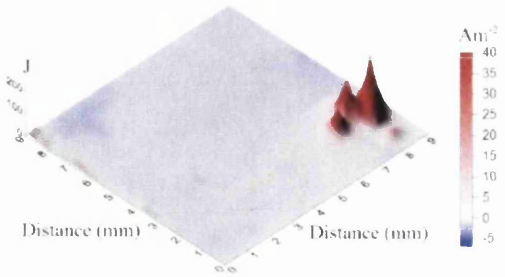

Figure 4.38 (c) At Time = 8 hours

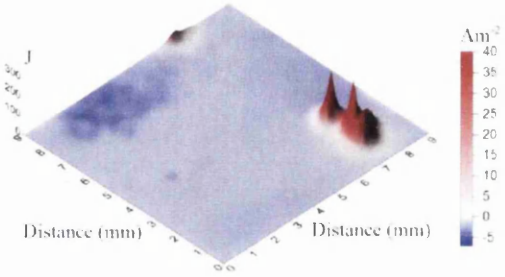

Figure 4.37 (d) At Time = 12 hours

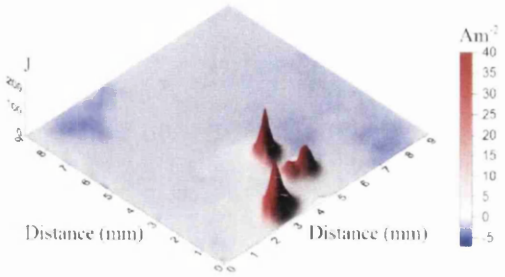

Figure 4.38 (d) At Time = 12 hours

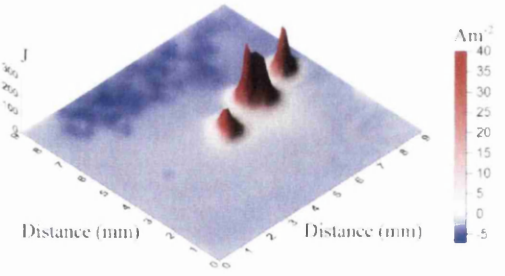

Figure 4.37 (e) At Time = 16 hours

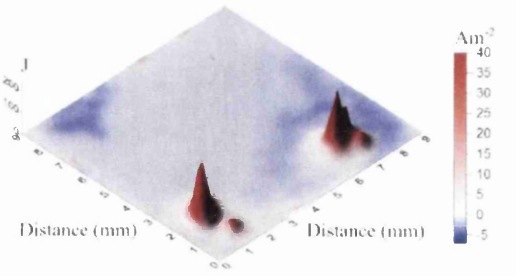

Figure 4.38 (e) At Time = 16 hours

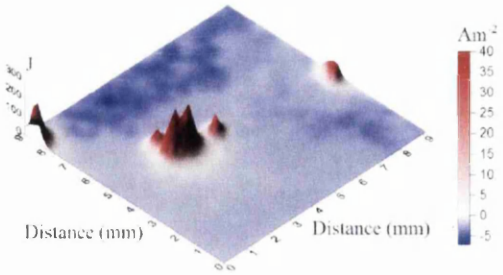

Figure 4.37 (f) At Time = 20 hours

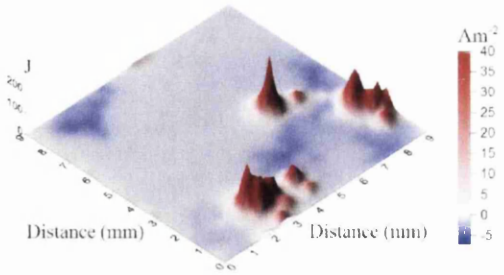

Figure 4.38 (f) At Time = 20 hours

Figure 4.37 (a) – (f) Surface images of 16 hrs aged Elektron 21 alloy from SVET data
Figure 4.38 (a) – (f) Surface images of 48 hrs aged Elektron 21 alloy from SVET data

It can be seen in the above images (Figure 4.37 & Figure 4.38) that the anodic activity is quite similar in both the aged samples. However it can be seen that the current density in case of 16 hrs aged sample of Elektron 21 alloy is higher in comparison with the 48 hrs aged sample. This data is in accordance with the actual anodic summary (Figure 4.34).

Further analysis is described in the following chapter. (Chapter 5)

5. DISCUSSION

The current research dealt with different heat treatment methods viz., homogeneous solution treatment and precipitation or age hardening treatment of some commercial and advanced magnesium alloys AZ31, AZ91 and ELEKTRON 21. The samples were first subjected to homogeneous solution heat treatment until the β-phase dissolved completely. It was quenched in cold water to achieve quick cooling rates. The homogenized samples were then aged according to the ageing times mentioned in Chapter 3. All the samples, both as received and heat treated samples were subjected to Time lapse photography experiment, Hydrogen evolution experiment and SVET experiment. The results were assessed using Sigma plot, Excel and Surfer and the results were compiled in the previous chapter (Chapter 4).

5.1 MAGNESIUM ALLOY AZ31 ANALYSIS

5.1.1 TIME LAPSE PHOTOGRAPHY & SIGMA PLOT ANALYSIS

It was seen from the images obtained from time lapse photography that the surface breakdown was instantaneous for solution treated AZ31 alloy where as it was 5 minutes and 10 minutes for the as received and fully aged sample of AZ31. (Refer Figures 4.3 (a) – (e), 4.5 (a) – (e) & 4.6 (a) – (e)). However it was noticed that once the surface breakdown occurred, the rate of corrosion was almost similar in both the solution treated and the fully aged sample. This can be inferred from the data obtained from sigma plot analysis (Figure 4.7). It should be noted that the time lapse photographic technique is purely subjective and the data obtained using Sigma plot is purely approximate as the Sigma plot analysis is scientifically less accurate.

These results show that there is definitely a change in the microstructural characterisitics of the AZ31 alloy on heat treatment as suggested in the literature which has resulted in above corrosion characteristics of the alloy. The area calculation is an approximation obtained from Sigma plot analysis. It was noticed that the first image showed a darker image in comparison with the subsequent images. It can be seen in the latter images that there is a formation of a thin white flim oxide layer as suggested by Roberts [16]. It should also be noted that the oxide film layer is more visible in the as received and fully aged sample of the alloy suggesting that this change in characteristics could be because of the presence of inter-dendritic β-phase.

In other words, during solution treatment, the elemental aluminium is completely dissolved which leads to better oxidation resistance. However, during ageing process, the aluminium reappears in the β-phase which inturn leads to poor oxidation resistance.

5.1.2 HYDROGEN EVOLUTION ANALYSIS

It can be seen the hydrogen evolution graph (Figure 4.8) that the age hardened sample evolved more hydrogen than its counterparts suggesting that the corrosion rate for the age hardening process is much higher than suggested in the previous test. It was also seen that the solution treated AZ31 alloy showed better performance than the age hardened sample. Though the surface breakdown of the sample occurs instantaneously, the amount of hydrogen evolved over a period of 5 hours was found to be much lower for the solution treated sample in comparison with other heat treated samples. Oxide layer formation was also noticed during the experiment.

5.1.3 SVET ANALYSIS

The SVET analysis was carried out on AZ31 samples with and without heat treatment. The anodic summary data obatined as a result of the test are present in Section 4.1.4.

As seen from the hydrogen evolution experiment, the solution treated alloy had the lowest current density plot which can be inferred from the above graph (Figure 4.10). Further it was noticed that the age hardened alloy exhibited the highest electrode potential difference resulting in a higher current density plot suggesting that the precipitate formation increases the corrosion rate considerably in comparison with the homogeneous solution treated sample.

The surface map images of the fully aged alloy (Figure 4.12 (a) – (e)) clearly show that the average current density over a period of time was found to be under 250 A/m^2 whereas the current density for the as received and solution treated alloy was well below 150 A/m^2. The red peaks represent the anodic activity and the blue surface represents the cathodic activity. It can be seen in the fully aged AZ31 sample surface plot images, that the anodic peaks are formed in once the reaction progresses, it leaves the surface more highly cathodic. The colour contrast clearly shows that the corrosion reactivity is quite high in comparison with the non heat treated and solution

treated sample. It was also noticed that localized corrosion centres were seen in all the samples of AZ31 except the age hardened sample.

On further evaluation of the data obtained from SVET experiment, it was found that the AZ31 alloy sample with age hardening treatment lost 6.56 g/m^2 over a period of five and a half hours where as the sample with solution treatment only lost 1.73 g/m^2 over the same time period of five and a half hours. The amount of material lost is depicted in the form of a bar chart in Figure 4.9.

The results clearly indicate that there are significant changes in the alloy due to heat treatment. According to Zeng *et al* [8], ageing of the sample caused the precipitation of aluminium atoms (due to diffusion) along the grain boundary forming the β-phase. It could be possible that the fine distribution of aluminium in the α-magnesium matrix reduced the average concentration from 3% aluminium to a lower concentration around the grain boundary. This seems to have accelerated the corrosion process suggesting that age hardening of AZ31 alloy is not desirable. Though the solution treated alloy seemed to react quickly, it can be found from the hydrogen evolution and SVET data that this could be superficial corrosion. Further literature proves that the corrosion performance of the alloy AZ31 is totally dependent on the concentration of aluminium rich β-phase [10][49]. It is also being found in the literature that during the solution treatment the secondary β-phase completely dissolves and during ageing the β-phase starts to reappear in a distributed fashion behaving as a corrosion inhibitor in this case [10][50]. This probably explains the lower corrosion rate of the solution treated alloy in comparison with the aged alloy sample.

It was noticed that the time lapse photography was merely a photographic technique which was carried out over a distance equal to the focal length of the camera lens. This experiment however could not consider the depth of attack and could not include the microscopic corrosion area. It was also noticed that though the exposed area was taped, there was corrosion activity closed to the cut ends of the tape which could be inferred from the time lapse images and were not considered for corroded area calculations. This could be one of the reasons as to why the data obtained from sigma plot did not resemble the ones from hydrogen evolution and SVET.

The hydrogen evolution data is obtained from experiment where the overall corrosion characteristics were considered. In other words, the complete corrosion activity was

considered to obtain the amount of hydrogen released. And in case of SVET only localized corrosion activity at height of 100μm is considered. This meant that any corrosion activity which occurs close to the alloy surface will not be picked up by the SVET probe and thus only localized corrosion centres were considered for analysing the results.

Thus the corrosion resistance in decreasing order can be written as:

AZ31 Solution treated > AZ31 as received > AZ31 Age hardened

5.2 MAGNESIUM ALLOY AZ91 ANALYSIS

5.2.1 TIME LAPSE PHOTOGRAPHY & SIGMA PLOT ANALYSIS

It was noticed from the images obtained from the time lapse photography experiment that the surface breakdown for the solution treated alloy occured instantaneously followed by rapid increase in corrosion of the surface (Refer Figure 4.16 (a) – (e)). Localized corrosion centres were formed which lead to rapid breakdown of the entire surface within hours of the start of the experiment. The surface breakdown for the as received and aged sample occured at 3 minutes and 10 minutes respectively from the start of the experiment. (Refer Figures 4.15 (a) – (e) & 4.17 (a) – (e)). It was also noticed that though the surface breakdown for the fully aged AZ91 alloy occured in 10 minutes, the rate of corrosion was much slower than it counterparts. This can be seen clearly in the following sigma plot analysis data (Figure 4.18).

It can be seen from Figure 4.18 that the solution treated and the as received AZ91 alloy samples corroded at a similar rate. And the fully aged AZ91 shows a much lower corrosion rate in comparison with its counterparts. It was noted that though the initial image was darker and later a thin white oxide film layer was formed due to the electrochemical reaction of the salt solution and exposed sample which is nothing but the passive film as stated in the literature [50].

5.2.2 HYDROGEN EVOLUTION ANALYSIS

The data from Figure 4.19 was obtained from the hydrogen evolution experiment conducted on all the samples of AZ91 alloy with and without heat treatment.

Again it can be noticed that the amount of hydrogen evolved in case of solution treated AZ91 alloy is much higher than its counterparts. And the AZ91 aged sample evolved the lowest amount of hydrogen over a period of 20 hours. This clearly shows that age hardening treatment is a desirable treatment and corresponds with the data obtained from sigma plot analysis.

5.2.3 SVET ANALYSIS

Figure 4.21 is the anodic summary data obtained from the SVET experiment and assessed using Surfer. It can be seen that the solution treated AZ91 shows a high

current density whereas the fully aged AZ91 sample shows the lowest. This data corresponds with the results obtained in the earlier tests, viz., Time lapse photography and Hydrogen evolution experiment.

Further surface images produced from SVET data using Surfer show that the maximum current density is under 400 A/m^2 for the solution treated sample (Figure 4.23 (a) – (e)) which was found to be quite high in comparison with other heat treatment conditions. Also it can be inferred from the surface plot images for solution treated AZ91 alloy that once the anodic reaction was completed a highly reactive cathodic region was noticed. This can be inferred from the thick blue colour scale on the surface map image. This clearly shows that solution treatment influences an increase in corrosion rate of the alloy.

The bar chart (Figure 4.20) shows that the loss of magnesium in the solution treated alloy was about 26.55 g/m^2 over a period of 20 hours where as the age hardened alloy only lost about 5.11 g/m^2 over the same time period of 20 hours. This clearly proves that a homogeneous solution phase increase the rate of corrosion and hence is not a desirable treatment for AZ91 alloy.

The data from all the three analysis suggests that the age hardened AZ91 alloy shows better and desirable corrosion resistance than its counterparts. It has already been demonstrated by Zeng *et al* [8] that heat treatment definitely changes the characteristics of the Magnesium alloy with change in microstructure. In their example, they reviewed that aluminium concentration in the α-Mg matrix decreased from 9% to 3% in the precipitation phase of the heat treatment process. Further they found that continuous distribution of the precipitate in the β-phase yielded better corrosion resistance for the alloy with ageing which clearly is in accordance with the results discussed above. Wan *et al*'s [50] research clearly showed that the β-phase precipitate obtained in the microstructure due to ageing improved the corrosion performance of AZ91 alloy. It has been previously proven that this precipitate was found to be rich in aluminium which acted as corrosion barriers slowing down the rate of corrosion [10][49]. This clearly proves the corrosion behaviour of magnesium alloy AZ91 found by the experimental methods in this research.

All the assumptions discussed in the previous section with reference to the discrepancies in the experimental techniques were considered.

Thus the corrosion resistance in decreasing order can be written as:

AZ91 Age hardened > AZ91 as received > AZ91 Solution treated

5.3 MAGNESIUM ALLOY ELEKTRON 21 ANALYSIS

The magnesium alloy Elektron 21 was first solutionized at 520°C for 12 hours and then aged for two different contiuous ageing times. The first homogeneous solution sample was aged for 16 hours continuously at 200°C and the other solutionized sample was aged for 48 hours continuously at 200°C and then both the sample were quenched in cold water to retain the precipitates. Different techniques were used to characterize the corrosion rates of the alloy with and without heat treatments.

The presence of rare earth materials seems have controlled the corrosion behaviour of Elektron 21. When the as received alloy is immersed in the salt solution, a thin oxide film is formed which adheres to the surface preventing corrosion. When the electrode potential increases the surface break down occurs. In the solution treated condition, the eutectic phase dissolves completely there by increasing the corrosion resistance. This clearly explains the impact of the secondary eutectic phase present in the alloy structure. The reappearance of precipitate along the grain boundary during ageing reduces the corrosion resistance as the grain size increases.

5.3.1 TIME LAPSE PHOTOGRAPHY AND SIGMA PLOT ANALYSIS

It can be seen from the time lapse photography images from Chapter 4 that the surface breakdown for 16 hours age hardened sample (Figure 4.29 (a) – (e)) is instantaneous where as the solution treated alloy (Figure 4.28 (a) – (d)) takes about 3.67 hours for the first surface breakdown. This clearly shows that the absence of β-phase has improved the corrosion resistance of Elektron 21 alloy. It was also noticed that the solution treated alloy readily reacted with the salt solution forming a thick white oxide film as suggested in the previously. There is a possibility that this oxide film acted as a protective layer in order to prevent the corrosion of the alloy.

It can be inferred from the graph (Figure 4.31) that the rate at which corrosion took place in case of age hardening was quite high in comparison with the solution treated alloy. It was seen that once the surface breakdown occurred, the rate of corrosion in case of solution treated alloy was slow. The ageing process definitely contributed to the increase in corrosion rate. It could further be noticed that though the initial corrosion rate for the 48 hours aged sample was slow in comparison with the 16 hours

aged sample, as time increased the corrosion activity seems to have accelerated due to the ageing process.

5.3.2 HYDROGEN EVOLUTION ANALYSIS

The data obtained from the hydrogen evolution experiment has been assesed and was represented in the form of a graph (Figure 4.32). It was noticed from the assessed data that 16 hours aged Elektron 21 sample released maximum amount of hydrogen in comparison with the 48 hours aged sample. This suggested that the corrosion process could be superficial in case of the 48 hours aged sample. It could also be noticed that the solution treated sample showed optimum corrosion performance with reduced corrosion rates.

5.3.3 SVET ANALYSIS

The following anodic summary data was obtained from the assessed SVET experiment using Surfer.

It can be seen from the data in Figure 4.34 that the solution treated alloy has the lowest average current density over a period of 20 hours. It can also be noticed that the 16 hours aged and the 48 hours aged sample showed similar current density profile. Further analysis showed that for a solution treated Elektron 21 alloy, a low anodic and cathodic activity was seen which could be interpreted in the form of surface images.

The bar chart (Figure 4.33) was obtained as a result of further analysis of the data obtained from the anodic summary. This data showed that the approximate amount of loss of hydrogen in case of a solution treated alloy was found to be 0.54689 g/m^2 where at the 16 hours and the 48 hours aged samples showed losses of 13.88 g/m^2 and 16.8 g/m^2 respectively, suggesting that the solution treatment is more desirable for Elektron 21 alloy. This also can be confirmed from the low current density value of 150 A/m^2 from the surface plot images. (Refer Figure 4.36 (a) – (d))

Thus it can be seen that heat treatment has definitely affected the corrosion characteristics of Elektron 21. As suggested in the literature [8][10][16], it is quite possible that the complete solubility of β-phase during solutionizing has improved the corrosion performance of the alloy. Also from the corrosion rates from the above

results, it is possible that the appearance of the β-phase precipitate during the age hardening process definitely increase the corrosion rate of the alloy[10]. And the more the ageing time, the more is the material loss which again can be inferred from the results obtained.

Thus the corrosion resistance in decreasing order can be written as:

E21 Solution treated > E21 as received > E21 16 hrs aged > E21 48 hrs aged

6. CONCLUSION

The current research dealt with different heat treatment methods viz., homogeneous solution treatment and precipitation or age hardening treatment of some commercial and advanced magnesium alloys AZ31, AZ91 and ELEKTRON 21. It was noticed that all the experimental techniques had some limitations or factors which were not considered in preparing the results. The results can be summarised as follows

1. AZ31 alloy with solution heat treatment at 395°C showed better corrosion resistance as the age hardening process accelerated the rate of corrosion.

2. AZ91 alloy with age hardening treatment at 200°C on the contrary showed better corrosion resistance than the solution treated alloy due to the discontinuous precipitation producing fine lamellar precipiates along the grain boundary.

3. The Elektron 21 alloy with solution treatment at 520°C increased the corrosion resistance of the alloy possibly due to the development of a protective oxide film layer and the absence of β-phase precipitate.

6.1 FUTURE WORK

It is a huge challenge to assess the corrosion characteristics of these advanced magnesium alloys. There is a need to determine the suitable methodologies to characterize the corrosion characteristics of these advanced light weight magnesium alloys in specific Elektron 21. Studies have suggested that the influence of alloying material greatly influences changes in both the mechanical and corrosion characteristics of alloys. Further work in assessing the entire characterization of the material under various environmental conditions is suggested.

BIBLIOGRAPHY

1. Haughton J. L., Prytherch W. E., *'Magnesium and its alloys'* (1937) p1-6
2. Wikipedia, *http://en.wikipedia.org/wiki/Magnesium*, accessed on 19-12-2009,
3. Emley E. F., *'Principles of Magnesium Technology'*, Pergamon Press, (1966) p1-12, 25-156, 126-130,
4. Committee on Science, Engineering, and Public Policy (COSEPUP), 'Materials *and Man's Needs: Materials Science and Engineering – Vol. I, The History, Scope, and Nature of Materials Science and Engineering*' (1975) p3-9
5. Kielbus A., *'Microstructure and mechanical properties of Elektron21 alloy after heat treatment'*, Journal of Achievements in Materials and Manufacturing Engineering, Vol. 22 Issue 1 (2007) p127-130
6. Kielbus A., *'Corrosion resistance of Elektron21magnesium alloy'*, Journal of Achievements in Materials and Manufacturing Engineering, Vol. 22 Issue 1 (2007) p29 – 32.
7. Ravi Kumar N.V., Bladin J.J., Desrayaud C., Montheillet F., Suery M., *'Grain refinement in AZ91 magnesium alloy during thermomechanical processing'*, Material Science and Engineering A359, (2003) p150 – 157.
8. Zeng Rong-Chang, Zhang Jin, Huang Wei-jiu, Dietzel W., Kainer K.U., Blawert C., Ke Wei, *'Review of studies on corrosion of magnesium alloys'*, Transactions of Nonferrous Metals Society of China 16 (2006), p s763-s771.
9. Joachim Gröbner, Andres Janz, Artem Kozlov, Djordje Mirković, Rainer Schmid-Fetze, *'Phase Diagrams of Advanced Magnesium Alloys Containing Al, Ca, Sn, Sr, and Mn'*, Journal of the Minerals, Metals and Materials Society, Vol 60, No. 12, (2008), p32 – 38
10. Federica Zanotto, *'Corrosion behaviour of the AZ31 magnesium alloy and surface treatments for its corrosion protection'*, PhD Thesis submitted to Università degli Studi di Ferrara, Italy, 2007/2009, p1 – 63
11. Guangling Song, *'Recent progress in corrosion and protection of magnesium alloys'*, Advanced Engineering Materials, 7, No. 7 (2005), p563 – 586
12. Guangling Song, Andrej Atrens, *'Corrosion mechanism of magnesium alloys'*, Advanced Engineering Materials, 1, No. 1, (1999), p11 – 33

13. Guangling Song, Andrej Atrens, *'Understanding magnesium corrosion – A framework for improved alloy performance'*, Advanced Engineering Materials, 5, No. 12, (2003), p837 – 858
14. Davies D.J., Oelmann L.A., *'The Structure, Properties and Heat Treatment of Metals'* Pitman Bokls Ltd, (1983), p100 – 128, 162, 163
15. Grossmann M.A., Bain E.C., *'Principles of Heat Treatment'*, American Society for Metals, (1935), p1 – 54, 209 – 228
16. Owen W.S., *'Theory of Heat Treatment'*, Heat Treatment of Metals – Lectures delivered at the Institution of Metallurgists Refresher Course 1963, (1963), p1 – 28.
17. Martin J.W., *'Precipitation Hardening'*, Pergamon Press, (1968), p 1 – 24, 87 – 111.
18. Porter D.A., Easterling K.E., *' Phase Transformations in Metals and Alloys'*, Second Edition, Chapman & Hall, (1992), p1 – 184, 263 – 317
19. Roberts C.S., *'Magnesium and Its Alloys'*, John Wiley & Sons Inc, (1960), p42 – 45, 194 – 205.
20. James H. Richardson, *'Specimen preparation methods for microstructural analysis'*, Microstructural Analysis: Tools and Techniques, Edited by McCall J. L., Mueller W.M., Plenum Press, (1973), p23 – 34.
21. James L. McCall, *'Scanning electron microscope for microstructural analysis'*, Microstructural Analysis: Tools and Techniques, Edited by McCall J. L., Mueller W.M., Plenum Press, (1973), p93 – 96.
22. Einar Mattsson, *'Basic Corrosion Technology for Scientists and Engineers'*, The Institute of Materials, Second Edition, (1996), p11 – 63.
23. Cáceres C.H., Davidson C.J., Griffiths J.R., Newton C.L., *'Effects of solidification rate and ageing on the microstructure and mechanical properties of AZ91 alloy'* Materials Science and Engineering A325, (2002), p344 – 355.
24. Aung N.N., Zhou W., *'Effect of heat treatment on corrosion and electrochemical behaviour of AZ91D magnesium alloy'* Journal of Applied Electrochemistry, Vol. 32, (2002), p1397 – 1401.

25. Vesling F., Ryspaev T., *'Effect of heat treatment on the superplasticity of magnesium alloys'*, Russian Journal of Non-Ferrous metals, Vol. 48, No. 1, (2007), p57 – 62.
26. Ming-Chung Zhao, Yun-Lai Deng, Xin-Ming Zhang, *'Strengthening and improvement of ductility without loss of corrosion performance in a magnesium alloy by homogenizing annealing'*, Scripta Materialia, Vol.58, No.7, (2008), p560 – 563.
27. Bialobrzeski A., Czekaj E., *'An attempt to use alloy synthesis in evaluating the corrosion behaviour of Al- and Mg-based alloys'*, Journal of Materials Processing Technology, 175, (2006), p27 – 32.
28. Shigematsu I., Nakamura M., Saitou N., Shimojima K., *'Surface treatment of AZ91D magnesium alloy by aluminium diffusion coating'*, Journal of Materials Science Letters, Vol.19, (2000), p473 – 475.
29. Gray J.E., Luan B., *'Protective coatings on magnesium and its alloys – a critical review'*, Journal of Alloys and Compounds, 336, (2002), p88 – 113.
30. Fan Z., Liu G., Wang Y., *'Microstructure and mechanical properties of rheo-diecast AZ91D magnesium alloy'*, Journal of Material Science, Vol. 41, (2006), p3631 – 3644.
31. Stanford N., Barnett M., *'Effect of composition on the texture and deformation behaviour of wrought Mg alloys'*, Scripta Materialia, Vol. 58, (2008), p179 – 182.
32. Dobrzanski L.A., Tanski T., Cizek L., Brytan Z., *'Structure and properties of magnesium cast alloys'*, Journal of Material Processing Technology, 192 – 193, (2007), p567 – 574.
33. Lun Sin S., Dube D., Tremblay R., *'An investigation on microstructural and mechanical properties of solid mould investment casting of AZ91D magnesium alloy'*, Material characterization, Vol. 59, (2008), p178 – 187.
34. Han L., Hu H., Northwood D.O., Li N., *'Microstructure and nano-scale behaviour of Mg-Al and Mg-Al-Ca alloys'*, Material Science and Engineering, Vol. 473, (2008), p16 – 27.
35. El-Amoush A.S., *'Effect of aluminium content on the mechanical properties of hydrogenated Mg-Al magnesium alloys'*, Journal of Alloys and Compounds, Vol. 463, Issue 1-2, (2008), p475 – 479.

36. Lindemann A., Schmidt J., Todte M., Zeuner T., *'Thermal analytical investigations of the magnesium alloys AM60 and AZ91 including the melting range'*, Thermochimica acta, Vol. 382, (2002) p269 – 275.
37. Kubota K., Mabuchi M., Higashi K., *'Review: Processing and mechanical properties of fine-grained magnesium alloys'*, Journal of Material Science, Vol. 34, (1999), p2255 – 2262.
38. Lyon P, Syed I, Heaney S, *'Elektron 21 – An aerospace magnesium alloy for sand cast and investment cast applications'*, Advanced Engineering Materials, Vol. 9, No. 9, (2007), p793 – 798.
39. Riontino G., Lussana D., Massazza M., Zanada A., *'DSC investigation on WE43 and Elektron 21 Mg alloys'*, Journal of Material Science Letters, Vol. 41, (2006), p3167 – 3169.
40. Fidel Guadarrama-Munoz, Juan Mendoza-Flores, Ruben Duran-Romero, Genesca J., *'Electrochemical study on magnesium anodes in NaCl and $CaSO_4$–$Mg(OH)_2$ aqueous solutions'*, Electrochimica Acta, Vol. 51, (2006), p1820 – 1830.
41. Kurze P., *'Corrosion and corrosion protection of magnesium'*, Magnesium – Alloys and Technologies, Edited by Kainer K.U., Wiley-VCH GmbH & Co. KGaA, (2003), p218 – 225.
42. Bobby Kannan M., Dietzel W., Blawert C., Atrens A., Lyon P., *'Stress corrosion cracking of rare-earth containing magnesium alloys ZE41, QE22 and Elektron 21 (EV31A) compared with AZ80'*, Material Science and Engineering, Vol. 480, (2008), p529 – 539.
43. Song G, Bowles A.L., StJohn D., *'Corrosion resistance of aged die cast magnesium alloy AZ91D'*, Material Science and Engineering, A366, (2004), p74 – 86.
44. Andrej Atrens, Wolfgang Dietzel, *'The negative difference effect and unipositive Mg^+'*, Advanced engineering materials, 9, No.4, (2007), p292 – 297
45. Edward Ghali, Wolfgang Dietzel, Karl-Ulrich Kainer, *'General and localised corrosion of magnesium alloys: A critical review'*, Journal of Materials engineering and performance, Vol. 13 (1), (2004), p7 – 23

46. Edward Ghali, Wolfgang Dietzel, Karl-Ulrich Kainer, *'Testing of general and localised corrosion of magnesium alloys: A critical review'*, Journal of Materials engineering and performance, Vol. 13 (5), (2004), p517 - 529
47. Guang-Ling Song, ZhenQing Xu, *'The surface, microstructure, and corrosion of magnesium alloy AZ31 sheet'*, Electrochimica Acta, Vol. 55, (2010), p4148 – 4161
48. Xian-bin Liu, Da-yong Shan, Ying-wei Song, En-hou Han, *'Effects of heat treatment on corrosion behaviours of Mg-3Zn magnesium alloy'*, Transactions of Nonferrous Metals Society of China, Vol. 20, (2010), p1345 – 1350
49. Lunder O., Lein J. E., Aune T. Kr., Nisancioglu K., *'The role of $Mg_{17}Al_{12}$ phase in the corrosion of Mg alloy AZ91'*, Corrosion, Vol. 45, No. 9, (1989), p741 – 748
50. Lei Wang, Bo-Ping Zhang, Tadashi Shinohara, *'Corrosion behaviour of AZ91 magnesium alloy in dilute NaCl solutions'*, Materials and Design, Vol. 31, (2010), p857 – 863
51. Zhi-min Zhang, Hong-yan Xu, Qiang Wang, *'Corrosion and mechanical properties of hot extruded AZ31 magnesium alloys'*, Transactions of Nonferrous Metals Society of China, Vol. 18, (2008), ps140 – s144
52. Jonathon Elvins, John Spittle, David Worsley, *'Microstructural changes in zinc aluminium alloy galvanising as a function of processing parameters and their influence on corrosion'*, Corrosion Science, Vol 47, Issue 11, (2005), p2740 – 2759
53. David Penney, James Sullivan, David Worsley, *'Investigation into the effects of metallic coating thickness on the corrosion properties of Zn-Al alloy galvanising coatings'*, Corrosion Science, Vol 49, Issue 3, (2007), p1321 – 1339
54. Jonathon Elvins, John Spittle, James Sullivan, David Worsley, *'Short term predictive testing for cut edge corrosion resistance in zinc-aluminium alloy galvanised steels'*, Corrosion Engineering, Science and Technology, Vol 40, No 1, (2005), p45 – 50

55. Böhm S., McMurray H.N., Powell S.M., Worsley D.A., *'Photoelectrochemical investigation of corrosion using scanning electrochemical techniques'*, Electrochimica Acta, Vol. 45, Issue 14, (2000), p2165 – 2174

56. James Sullivan, Chris Weirman, Jon Kennedy, David Penney, *'Influence of steel gauge on the microstructure and corrosion performance of zinc alloy coated steel'*, Corrosion Science, Vol. 52, Issue 5, (2010), p1853 – 1862.

57. *Magnesium and Magnesium Alloys*, ASM Speciality Handbook, ASM International, The Materials Information Society (1999).

58. Hiroyuki Watanabe, Masao Fukusumi, *'Mechanical properties and texture of a superplastically deformed AZ31 magnesium alloy'*, Material Science and Engineering A, Vol. 477, (2008), p153 – 161.

59. Yizhen Lü, Qudong Wang, Xiaoqin Zeng, Wenjiang Ding, Chunquan Zhai, Yanping Zhu, *'Effects of rare earths on the microstructure, properties and fracture behaviour of Mg – Al alloys'*, Material Science and Engineering A, Vol. 278, (2000), p66 – 76.